

FRAGMENT BASED DRUG DEVELOPMENT BASED ON 6,7
DIMETHOXYQUINAZOLINE AS A CORE SCAFFOLD

CODY ORAHOSKE

Bachelor of Science in Chemistry

Cleveland State University

May 2018

Bachelor of Business Administration

Cleveland State University

May 2018

Submitted in partial fulfillment of requirements for the degree

DOCTOR OF PHILOSOPHY IN CLINICAL-BIOANALYTICAL CHEMISTRY WITH
SPECIALIZATION IN CELLULAR AND MOLECULAR MEDICINE

OF CHEMISTRY DEPARTMENT

at the

CLEVELAND STATE UNIVERSITY

MAY 2023

We hereby approve this dissertation for

Cody Orahoske

Candidate for the Doctor of Philosophy in Clinical-Bioanalytical Chemistry degree

for the Department of Chemistry

and the CLEVELAND STATE UNIVERSITY'S

College of Graduate Studies by

Committee Chairperson, Dr. Bin Su

Department & Date

Committee Member, Dr. Michael Kalafatis

Department & Date

Committee Member, Dr. David Anderson

Department & Date

Committee Member, Dr. Bibo Li

Department & Date

Committee Member, Dr. Crystal Weyman

Department & Date

Student's Date of Defense: April 26, 2023

ACKNOWLEDGMENT

I am thankful for all the experiences at Cleveland State University that have shaped me into the person I am today, including my time spent on sports, student organizations, studying on courses, and performing experiments in the laboratory. I am grateful for all the resources and support that I received along the way, and I thank all the people who motivated me to work harder and to prove that I can achieve remarkable things.

As a blue-collar worker at the age of twelve, I learned the true value of time and the importance of having an unobstructed vision of my future. Despite facing numerous challenges along the way, I remained committed to my goals and never lost sight of my dreams. For me, obtaining my Ph.D. represents much more than just a degree; it is a testament to my determination and willingness to push myself to pursue my dream. I am proud of myself for staying on the course and never giving up, and I sincerely appreciate all the help I received to keep me moving forward.

I am deeply grateful to the individuals who have supported me throughout my academic journey. Primarily, I owe a tremendous debt of gratitude to Dr. Bin Su, my Ph.D. mentor and also my undergraduate research adviser, whose mentorship and guidance have had a profound impact on both my personal and professional growth. Over the past six years, Dr. Su's insights and encouragement have motivated me to strive for excellence and become the best version of myself. Dr. Michael Kalafatis deserves special thanks for his enthusiastic attitude that has instilled in me a deep sense of drive and a determination to become a more productive researcher. His guidance throughout my Ph.D. has helped me develop a systematic approach to problem-solving and enabled me to ask the right questions to obtain relevant information. Furthermore, I am grateful to Dr. Bibo Li, whose

positive energy and dedication to science and her laboratory has provided great resources that made my research efficient and productive. I also want to thank Dr. David Anderson for introducing me to Clinical Chemistry and providing valuable guidance that helped me secure a Clinical Chemistry Fellowship position and transition smoothly into professional life. And finally, I would like to express my sincere gratitude to Dr. Crystal Weyman, whose ability to provide biologically relevant knowledge in systematic processes that are fundamental to cellular mechanisms is invaluable.

Finally, I would like to extend my heartfelt gratitude to my family, friends, and colleagues, whose unwavering support has been a constant source of motivation and inspiration. Without their encouragement and assistance, I would not have been able to achieve as much as I have. Their love, guidance, and unwavering support have been a crucial factor in my success, and I am eternally grateful for their presence in my life.

Thank you all for being a part of my academic journey and supporting me in every conceivable way. I could not have done it without you, and I look forward to continuing to make a positive impact in the future.

P.S. Chen Guanmin always yours

FRAGMENT BASED DRUG DEVELOPMENT BASED ON 6,7
DIMETHOXYQUINAZOLINE AS A CORE SCAFFOLD

CODY ORAHOSKE

ABSTRACT

The work entitled “Fragment Based Drug Design based on 6,7-Dimethoxyquinazoline core structure” presents a unique approach to drug discovery, specifically focusing on the pharmacophore 6,7-dimethoxyquinazoline. This study explores the structural diversity of 6,7-Dimethoxyquinazoline derivatives to identify other pharmacologically relevant targets, with evidence indicating that this core structure possesses intrinsic properties that make it suitable as a base structure of small molecule drugs. Furthermore, this pharmacophore has been observed in various approved therapeutics or drug candidates under investigation, highlighting its importance in drug discovery. My research showcases of 6,7-dimethoxyquinazoline core structure been derivatized to generate an anti-trypanosomiasis drug candidates and anti-cancer drug candidates. In the first project, the pharmacophore was identified through a high-throughput screen as having the potential to function as an anti-parasitic drug. A protein pulldown assay was subsequently performed, and the molecular mechanism of action was explored. A compound library was synthesized to check the efficiency of the pharmacophore, leading to a more detailed structure-activity relationship (SAR) analysis for future lead optimization. In the second project, the molecular docking approach identified the 6,7-dimethoxyquinazoline core as the interacting partner with EPH receptor A2 (ephrin type-A receptor 2) that is involved in cellular adhesion and growth. A series of analogs were synthesized and evaluated to determine whether they could inhibit tumor cell

growth. Overall, the study demonstrated the potential of the 6,7-dimethoxyquinazoline pharmacophore as a versatile platform for drug discovery. The work also built a foundation for further structural modification to improve the absorption, distribution, metabolism, and excretion (ADME) of small molecule drugs based on a well-documented core structure. By exploring the pharmacophore 6,7-dimethoxyquinazoline reveals its potential for drug discovery for different diseases.

In conclusion, the study demonstrates the potential of the 6,7-dimethoxyquinazoline pharmacophore as core structure for small molecule drugs. The work emphasizes the importance of understanding the SAR of compounds in the development of novel therapeutics. Overall, this study has the potential to contribute to the development of new small molecule drug candidates to combat trypanosomiasis and brain cancer.

TABLE OF CONTENTS

	Page	
ABSTRACT.....	v	
LIST OF TABLES.....	xi	
LIST OF FIGURES	xii	
CHAPTER		
I. QUINAZOLINE, A PRIVILEGED SCAFFOLD IN SMALL MOLECULE		
DRUG DISCOVERY	1	
1.1 Introduction to Fragment Based Drug Design	1	
1.2 Biological Activities of Quinazolines	3	
1.3 Pharmacology of Adrenoreceptor	7	
1.3.1 Signaling cascade of adrenoreceptor	7	
1.3.2 Ligands for alpha-1a adrenergic receptors.....	10	
1.4 Epidermal Growth Factor Receptor (EGFR)	14	
1.4.1 Signaling cascade of EGFR	14	
1.4.2 Quinazoline derivatives targeting EGFR.....	19	
1.5 Conclusion	20	
II. IDENTIFICATION OF PRAZOSIN AS A POTENTIAL FLAGELLUM		
ATTACHMENT ZONE 1(FAZ1) INHIBITOR FOR THE TREATMENT OF		
HUMAN AFRICAN TRYPANOSOMIASIS		22
2.1 Introduction.....	22	

2.1.1 Trypanosoma brucei.....	22
2.1.2 Clinical significance and treatment.....	26
2.1.3 Current outlook and direction of research	29
2.2 Results and Discussion.....	32
2.2.1 Identification of new lead compounds.....	32
2.2.2 Prazosin analogs showed improved activity against T.b. brucei cell growth	37
2.2.3 Biotinylated molecular probe design	41
2.2.4 Affinity purification and identification of 2-piperazinyl-4-amino-6,7- dimethoxyquinazoline bound proteins.....	43
2.2.5 FAZ1 as a potential molecular target of prazosin analogs in trypanosome cells	47
2.2.6 FAZ1 co-localization with prazosin fluorescent probe in trypanosome cells	51
2.2.7 Introduction of the carbothioamide moiety reduces the adrenoceptor activity	53
2.3 Conclusion	55
2.4 Methods.....	55
2.4.1 Chemistry.....	55
2.4.2 Procedure of biotin linked compounds	56
2.4.3 Procedure of fluorescein isothiocyanate (FITC) analog	56
2.4.4 Procedure of prazosin analogs	56
2.4.5 Cell culture.....	56

2.4.6	<i>T.b. brucei</i> cell viability analysis	57
2.4.7	Mammalian cell viability analysis	57
2.4.8	Protein pulldown assay	58
2.4.9	Proteomics analysis.....	58
2.4.10	Plasmid construction and design.....	59
2.4.11	<i>T.b. brucei</i> cell lysate preparation and western blot assay.....	60
2.4.12	Immunofluorescence assay	61
III.	DIMERIC SMALL MOLECULE AGONISTS OF EPHA2 RECEPTOR INHIBIT GLIOBLASTOMA CELL GROWTH	62
3.1	Introduction.....	62
3.2	Results and Discussion.....	64
3.2.1	Development of an EphA2 overexpressed glioblastoma cell line ...	64
3.2.2	Lead optimization and biological evaluation.....	65
3.2.3	EphA2 activation	70
3.2.4	Log P value	71
3.3	Conclusion	72
3.4	Methods.....	73
3.4.1	Chemistry.....	73
3.4.2	Organic compounds synthesis and identification	73
3.4.3	Log P measurement.....	84
3.4.4	Cell culture and antibodies.....	85
3.4.5	Mammalian cell viability analysis	85
3.4.6	EphA2 activation.	86

IV. CONCLUSION AND FUTURE DIRECTION	87
BIBLIOGRAPHY.....	90

LIST OF TABLES

Table	Page
I. Alpha Blockers.....	13
II. Approved EGFR Inhibitors.....	20
III. Pharmacological treatments	29
IV. The 38 identified Hits from the HTS assay, the common name followed by their mechanism of action are listed.....	35
V. Prazosin analogs showed improved activity and selectivity against trypanosome cells over mammalian cells.....	41
VI. Inhibition of the cell proliferation of U251/U251 EphA2 cells	70
VII. Log P values.....	72

LIST OF FIGURES

Figure	Page
1. Quinazoline pharmaceuticals and derivatives.....	6
2. Signal transduction pathways activated by α 1-ARs	8
3. Family Portrait: this figure was adapted from The ERBB network: At last, Cancer therapy meets system biology.....	15
4. Phylum tree: A tree map of the kinetoplast	23
5. Three cell lines were used in the HTS, (A) HEK 293 and (B) Raw 267.4 were used as control cell lines for toxicity, while the bloodstream form cells of the (C) T.b. brucei Lister 427 strain was used as the parasite model	33
6. Conformation of unique pharmacophore.....	37
7. Biotin Pulldown and Potency of The Positive and Negative Probe.....	42
8. Affinity isolation of compound 2-binding proteins	46
9. PCR plasmid for F2H tag.....	49
10. Production of tagged cell and its corresponding effect on viability. Construction of an F2H-FAZ1 T.b. brucei strain	50
11. Fluorescent probe interaction with FAZ1	52
12. c-FOS expression is correlated with alpha adrenoceptor activity in MCF-7 cells	54
13. Dimer scaffold synthesized to target EphA2 receptor	63
14. Construction of U251/EphA2 cell line based on U251 wild type cells	65
15. Synthesis of dimers based on 6,7-dimethoxy-2-(piperazin-1-yl) quinazolin-4-amine as the monomer	66
16. Monomers with a benzamide moiety form dimer.....	67

17. EphA2 activation of the new derivatives	71
18. Schemes for drug discovery based on 6,7 dimethoxyquinazoline.....	89

CHAPTER I
QUINAZOLINE, A PRIVILEGED SCAFFOLD IN SMALL MOLECULE DRUG
DISCOVERY

1.1 Introduction to Fragment Based Drug Design

Combinatorial chemistry is based on active pharmacophores to develop small molecule drugs, which is a branch of Medicinal Chemistry in drug discovery [1-10]. The field combines knowledge from molecule pharmacology of structural fragment in the database of approved drugs or drug candidates to create new drug candidates, and hope to target the corresponding receptors or enzymes to treat diseases and improve human health [11-18]. My study will focus on fragment-based drug design (FBDD) and the concept of using several pharmacophores of clinical approved drugs to increase the drug likelihood of the newly designed small molecules [19-23]. To emphasize this practice, the pharmacophore quinazoline will be the focus of this review [11, 24-27]. Quinazoline is a heterocyclic compound containing a fused benzene and pyrimidine ring [28-32]. This pharmacophore historical use, structural diversity, biological activity, and clinical applications will be discussed. This review will launch a foundation of my major research

projects based on this structure as the core scaffold to perform fragment-based drug design, synthesis, and pharmacological evaluation [19, 33-37].

The concept of combinatorial chemistry is a highly documented in the field of drug discovery, and various small molecular drugs were discovered based on this strategy [19, 22, 23, 38, 39]. This approach is based on the concept that certain organic compound cores possess the ability to bind specifically to certain domains of receptors or enzymes or important proteins. The advantage of FBDD lies in its ability to identify novel chemical scaffolds and optimize binding affinity and selectivity based on information gained during the drug development process in the past [19-24, 38-55]. The fragments serve as the small ligands for certain molecular targets, and by combining them together to generate new fragments and hope maintaining the activity as well. The ligand-based optimization sometimes even doesn't need clear molecular targets, new structures can be design and synthesized based on existing ligand structure for certain diseases. On the other hand, computational chemistry could be explored in FBDD, if the binding domain of the ligands is well defined and there are accurate crystal structures of the targets to perform docking study. Molecular docking, for example, is a widely used computational technique that predicts the binding affinity of a ligand to a protein by modeling their interactions at the atomic level. This method has proven highly effective in identifying and prioritizing potential fragments for experimental screening, predicting their binding affinity and mode of binding, and guiding the design of new compounds. As the crystal structures of more and more proteins are deposited in the Protein Data Bank, combined with the binding ligands, computational chemistry has demonstrated a more powerful role in drug discovery. Nevertheless, both FBDD and computational chemistry based virtual screening then

docking for new ligands design and synthesis are crucial approaches in the field of medicinal chemistry. They are effective approaches in the design and optimization of small molecules that interact with specific biological targets. Through a systematic process of SAR studies, these ligands are modified and optimized to enhance their binding affinity, selectivity, and pharmacological properties. This iterative process involves design and prediction, synthesis, and evaluation of various analogs guided by either SAR from the known structures of ligands or computational modeling and experimental assays.

1.2 Biological Activities of Quinazolines

Quinazoline is a heterocyclic compound that was first synthesized in 1869, but its discovery as a therapeutic drug did not occur until 1903. Modifications to the structure, including the addition of nitrogen bound to carbon, led to the development of quinazoline derivatives that exhibit various pharmacological activities. The quinazoline pharmacophore consists of two fused aromatic rings, a carbonyl group, and a nitrogen atom in the 2- or 4-position, which are essential for the biological activity of these compounds.

Quinazoline derivatives have been extensively studied and have demonstrated promising therapeutic potential in the treatment of cancer, inflammation, hypertension, and infections [18, 28-37, 55-67]. These derivatives can bind to multiple receptors within the cellular space and exert their effects through various mechanisms of action. For example, some quinazoline derivatives have been identified as potent inhibitors of protein kinases such as epidermal growth factor receptor (EGFR), platelet-derived growth factor receptor (PDGFR), and vascular endothelial growth factor receptor (VEGFR). They bind to the adenosine triphosphate (ATP)-binding pocket of the kinases, blocking their activity and preventing cell proliferation and angiogenesis. Other quinazoline derivatives function as

alpha-adrenoreceptor blockers, inhibiting the action of adrenaline on smooth muscle cells and leading to the relaxation of blood vessels blockers, inhibiting the action of adrenaline on smooth muscle cells, and leading to the relaxation of blood vessels. This activity makes them useful in the treatment of hypertension.

Quinazoline derivatives have also been reported to exhibit anti-inflammatory and analgesic activities, through the inhibition of enzymes involved in the production of prostaglandins and leukotrienes, which are mediators of inflammation and pain. The versatility of the quinazoline scaffold provides a scaffold for the development of derivatives with improved potency and selectivity for specific targets [21, 33-37, 41-45, 54, 55, 59, 63, 64, 68-74]. These derivatives have shown improved pharmacokinetic properties and biological activity, such as good bioavailability and metabolic stability and selectivity. The quinazoline core is a privileged scaffold that has found clinical utility in treating many different diseases.

The chemistry behind the synthesis has been excellently reviewed by many, with various schemes designed to synthesis new drug candidates [33, 34, 36, 37, 42, 43, 45, 53]. The core quinazoline can undergo simple processing via hydrolysis, oxidation, and reduction to allow for sites of modification for fragments to be added onto the core to build new drug candidates [42, 45]. Thus the discovery of drugs is through the combinatorial chemistry approach. The synthesis of quinazoline and quinazolinone derivatives is a complex and multifaceted field that has been extensively reviewed in the literature [33-36, 45, 53, 55, 64, 73-86]. More advanced synthetic methods developed in the past decades combined with combinatorial chemistry accelerated the process to generate large libraries of quinazoline derivatives for drug discovery purposes. More biological assays applied in

high-throughput screening make the biological testing of large scales of compounds easy to perform. These advances in science offer an efficient means of identifying promising drug candidates through the screening of vast numbers of compounds in a short amount of time.

It is evident that the chemistry behind the synthesis of quinazoline derivatives plays a critical role in drug discovery efforts. The ability to manipulate the core structure of these compounds with ease and precision, and to synthesize diverse libraries of derivatives, provides an excellent platform for the development of new drugs to treat a variety of diseases (Figure 1).

The advantages of quinazoline as a pharmacophore lie in its structural diversity and versatility. The quinazoline scaffold can be modified with various substituents at multiple positions, allowing for the development of structural diverse derivatives with improved potency and selectivity for specific targets. Moreover, quinazoline derivatives have shown good pharmacokinetic properties, such as good bioavailability and metabolic stability. Overall, the quinazoline core is critical for functional use and can bind to multiple receptors, making it a promising target for drug development.

My research mainly focuses on two targets of quinazoline analogs, i.e., Adrenoceptors and Tyrosine kinases, therefore I will detailly discuss what has been done in this regard and launch a foundation of rationale for my research projects.

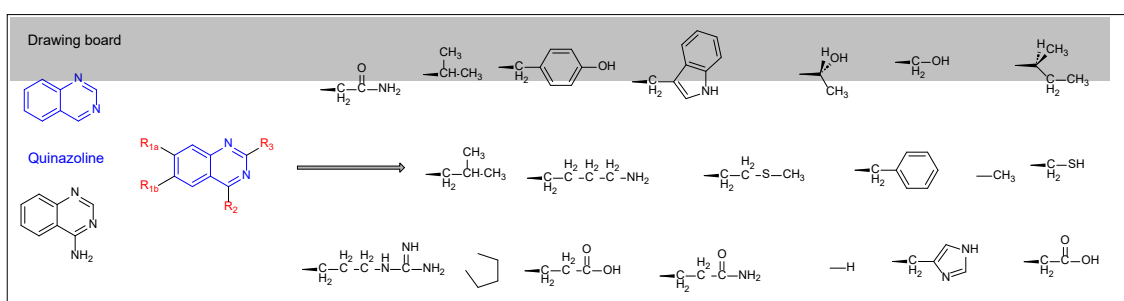
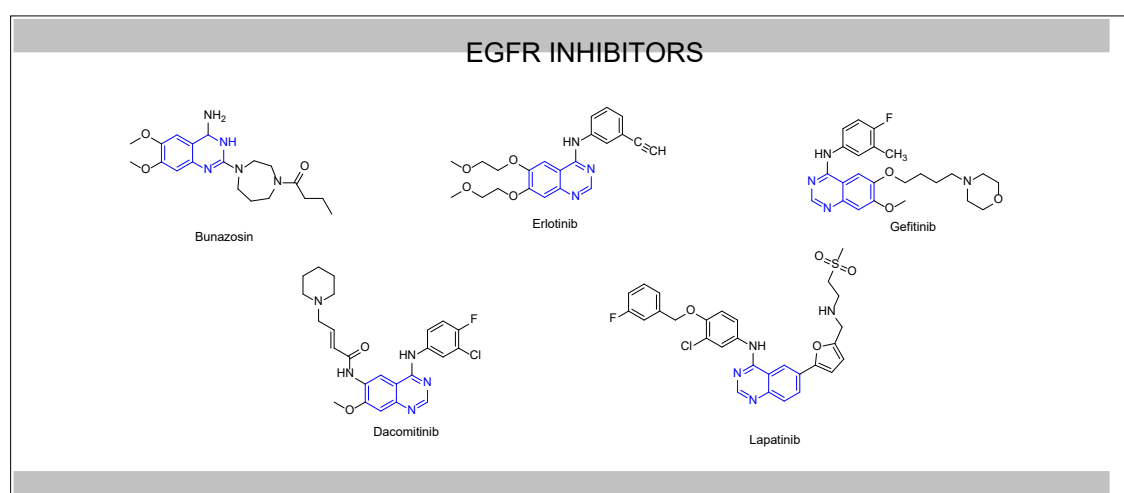
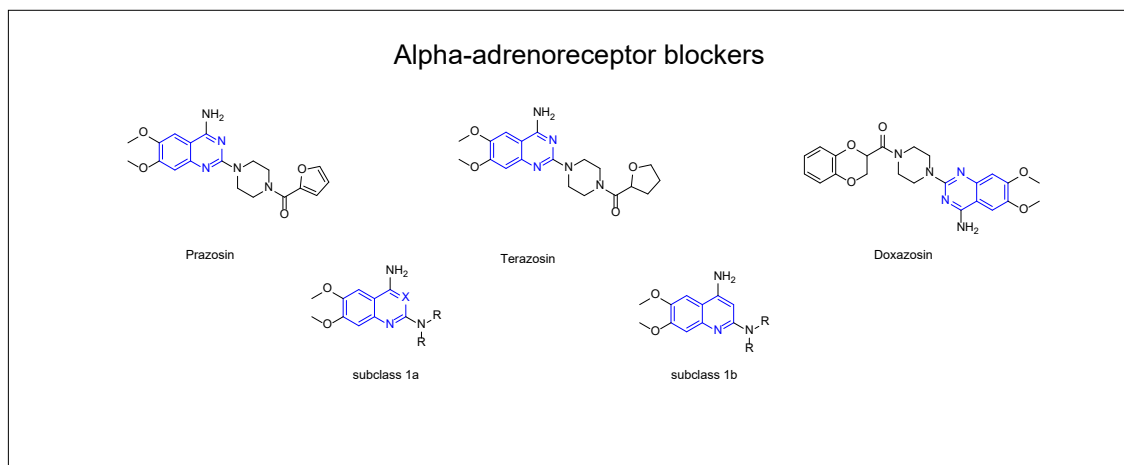


Figure 1. Quinazoline pharmaceuticals and derivatives

The top figure displays a list of 3 alpha 1 blockers and their corresponding synthesized derivatives. The bottom figure lists a small amount of EGFR inhibitors, with the quinazoline core highlighted in blue to emphasize its pharmacophore significance. The drawing board displays fragment-based design concepts that can be included at R1, R2, or R3 depending on the chosen synthetic path. This design approach allows for flexibility and customization in drug development.

1.3 Pharmacology of Adrenoreceptor

1.3.1 Signaling cascade of adrenoreceptor

The adrenergic receptors (ARs) are a family of G protein-coupled receptors (GPCRs) that are widely expressed throughout the body and play a key role in the regulation of various physiological processes such as blood pressure, heart rate, smooth muscle contraction, and metabolic rate [67, 87-89]. The alpha and beta subtypes of ARs were initially identified based on their affinity for specific sympathomimetic amines, such as epinephrine and norepinephrine.

The alpha subtype is further divided into two subclasses, alpha-1, and alpha-2, based on the differences in their second messenger signaling pathways. Alpha-1 receptors activate phospholipase C (PLC) and generate inositol triphosphate (IP3) and diacylglycerol (DAG), which in turn activate intracellular calcium and protein kinase C (PKC), respectively. Alpha-2 receptors, on the other hand, inhibit adenylate cyclase (AC) activity and reduce cyclic AMP (cAMP) levels.

The beta subtype is also divided into two subclasses, beta-1, and beta-2, based on their anatomical distribution and second messenger signaling pathways. Beta-1 receptors are found in the heart, stimulate AC activity, and increase cAMP levels, which in turn activate protein kinase A (PKA) and enhance cardiac contractility and heart rate. Beta-2 receptors are found in smooth muscle cells and activate AC activity, leading to increased cAMP levels and relaxation of smooth muscles.

Recent studies have revealed that there are several subtypes of alpha and beta ARs, including alpha-1a, alpha-1b, alpha-1d, alpha-2a, alpha-2b, alpha-2c, beta-1, beta-2, beta-

3, and beta-4, each with distinct physiological functions and signaling mechanisms (Figure 2).

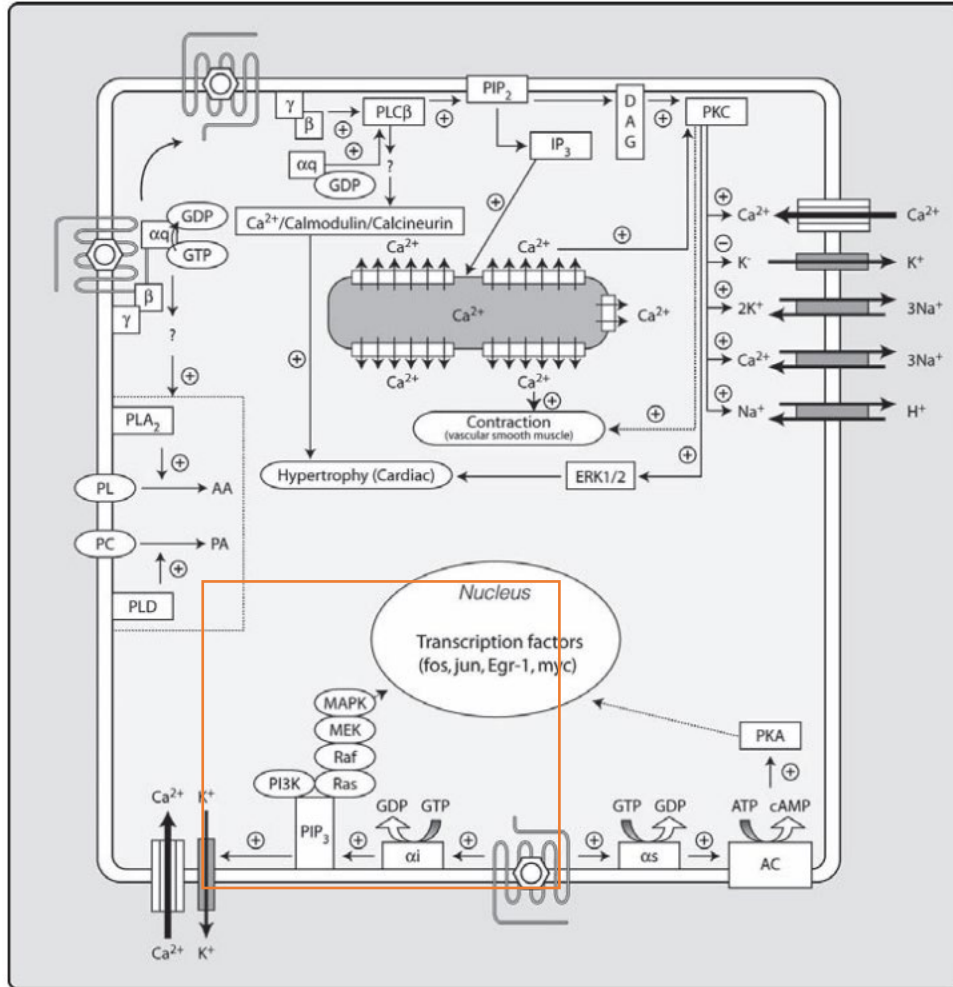


Figure 2. Signal transduction pathways activated by α 1-ARs

This figure was adapted from The Adrenergic Receptors with modification[90] The upper portion of the figure shows the classical receptor-linked phosphoinositide pathway and secondary effector activation. The lower portion shows additional α 1-AR-linked pathways, which include modulation of ion channels and activation of MAPK pathways via Gi-mediated PI3K stimulation. α 1-AR-mediated activation of adenylyl cyclase via G α s has also been reported. The area circled in red indicates a part of the downstream signaling which will be used as a biomarker of the receptor activation in my research.

Initially, the binding of the alpha 1 subclass of adrenergic receptors was thought to be determined by a hypothesis theory based on the interactions of the natural ligand with the receptor's H-bond acceptor, H-bond donor, hydrophobic, and positive ionizable sites [90, 91]. However, with advancements in computational modeling and experimental techniques, the binding site was later modeled more accurately. Studies have identified that the interacting amino acids are located on domain 3, 5, and 6 of the alpha 1 adrenergic receptor. The interacting amino acids include serine 192, serine 188, serine 296, threonine 111, and asparagine 106 [93]. These amino acids form a hydrogen binding capability as well as ionized association with distinct parts of the prazosin which are essential for the receptor's activity and signaling cascade.

Understanding the molecular structure and binding site of the alpha 1 adrenergic receptor has led to the development of new therapeutics that target this receptor. Various selective alpha blockers have been designed based on the 2,4-diamino-6,7-dimethoxyquinazoline core, which is a bio isosteric replacement for norepinephrine [94]. These compounds bind to the receptor and cause a cascade of signaling events that release intracellular calcium, allowing for selective processing and expression within the cell. On the other hand, the detailed interaction of the binding could provide valuable information to design molecules that don't interact with the binding site.

In addition to their role in cardiovascular diseases, recent studies have focused on the role of alpha 1 adrenergic receptor in the pathophysiology of other diseases, including cancer and neurodegenerative diseases [90, 95]. These studies have identified new signaling pathways and potential therapeutic targets that may lead to the development of novel treatments for these diseases.

One area of active research in the field of adrenergic receptors is the mapping of their distribution throughout the body and their role in various physiological processes. While the expression of AR subtypes has been well documented in many organs and tissues, their distribution and functional significance in the brain is still poorly understood.

Recent studies have suggested that adrenergic signaling in the brain plays a crucial role in modulating a range of cognitive and emotional processes, including attention, learning, memory, anxiety, and depression. Moreover, dysregulation of adrenergic signaling has been implicated in various neuropsychiatric disorders, including attention deficit hyperactivity disorder (ADHD), post-traumatic stress disorder (PTSD), and major depressive disorder (MDD) [87, 88, 96-110].

Given the importance of adrenergic signaling in the brain and its potential implications for neuropsychiatric disorders, further research is needed to elucidate the specific roles of different AR subtypes in different brain regions and under different physiological and pathological conditions. This could pave the way for the development of novel therapeutic strategies for the treatment of these disorders. Overall, the study of the alpha 1 adrenergic receptor and its role in physiological and pathological processes has been a key area of research in pharmacology and continues to offer exciting opportunities for the development of new drugs and treatments.

1.3.2 Ligands for alpha-1a adrenergic receptors

The study of adrenergic receptors, particularly the alpha-1 receptor subtype, has been an important area of research in pharmacology for several decades [52, 90, 95, 111-116]. Alpha-1 blockers have been developed to modulate the effects of norepinephrine on this receptor and have been used to treat hypertension, benign prostatic hyperplasia, and

other conditions. The identification of the binding site for small molecules on the alpha-1 receptor has allowed for the rational design of more selective and potent drug candidates. Various selective alpha-1 blockers, including doxazosin, terazosin, tamsulosin, alfuzosin, and silodosin, have been developed and used to treat different patient populations. These compounds interact with different transmembrane parts of the receptor and cause a cascade of signaling events that release intracellular calcium.

Besides hypertension management, recent studies have also identified the roles of alpha-1 receptors in the pathophysiology of various other diseases including cancer, diabetes, and neurodegenerative diseases. These studies have identified new signaling pathways and potential therapeutic targets that may lead to the development of novel treatments for these diseases.

Prazosin is a chemical compound with the chemical name 2-[4-(2-furoyl)piperazin-1-yl]-6,7-dimethoxyquinazolin-4-amine. Has been shown to bind to the alpha-1a receptor, initiating a cascade of signaling that leads to a reduction in blood pressure by inhibiting the vasoconstrictive action of norepinephrine. Prazosin was originally developed by Pfizer in the 1960s to help people with hypertension and has since been found to be effective in treating benign prostatic hyperplasia by blocking norepinephrine and relaxing the muscles in the prostate, making it easier to urinate [117]. Through various structural activity relationship studies many conclusion have been drawn but mainly it is thought that the 2,4-diamino-6,7-dimethoxyquinazoline core is a bio isosteric replacement for norepinephrine. Additionally, disruption of the quinazoline core by replacement with a diaminoisoquinoline results in poorer receptor activity. Other selective alpha blockers have been developed consequently, which have various selectivity and activity and are listed in

Table 1. The list of alpha blockers in the table all share the same 6,7 dimethoxyquinazoline core scaffold including Doxazosin, Terazosin, Tamsulosin, Alfuzosin, and Silodosin.

Prazosin was the first alpha-1 adrenergic receptor blocker to be developed and used therapeutically for the treatment of hypertension, and later found to be effective in reducing the symptoms of benign prostatic hyperplasia (BPH). However, subsequent pharmaceuticals were synthesized and evaluated, and found to act similarly to prazosin, but with some advantages over the parent compound. One of the advantages of the newer alpha-1 adrenergic receptor blockers is their selectivity for specific alpha-1 receptor subtypes. For instance, tamsulosin is highly selective for the alpha-1a receptor subtype, which is predominantly found in the prostate, thereby reducing the side effects [100]. Other pharmaceuticals such as alfuzosin and silodosin have a higher selectivity for the alpha-1d receptor subtype, which is also found in the prostate, but with less affinity for the alpha-1a and alpha-1b subtypes.

Pharmacokinetic properties are also important considerations in the selection of alpha-1 adrenergic receptor blockers. Some of the newer pharmaceuticals have a longer duration of action, such as doxazosin, which has an extended half-life compared to prazosin, leading to a reduced dosing frequency and improved patient compliance. Lastly, newer analogs of alpha-1 adrenergic receptor blockers have a safer profile with fewer side effects, such as cardiovascular events and orthostatic hypotension. Moreover, these newer analogs have demonstrated improved efficacy in the treatment of BPH symptoms. Nevertheless, prazosin is still used clinically, particularly for the treatment of hypertension and post-traumatic stress disorder (PTSD). Prazosin is sufficiently lipophilic to cross the blood-brain barrier and antagonize the alpha-1 receptors in the CNS, blocking these stress

responses. Through this mechanism, it can improve sleep and reduce nightmares associated with PTSD.

In conclusion, alpha-1 adrenergic receptor blockers based on 6,7 dimethoxyquinazoline as the core scaffold are a group of important medications for various disease treatment. The success of these drugs demonstrates the potential of this structure as a base for new drug development, because human body seems have a good tolerance of this structure. In addition, these drugs all show good oral bioavailability, suggesting that the scaffold is a unique moiety for orally active drug development.

<u>Alpha Blocker</u>	<u>Use</u>	<u>Type</u>	<u>Mechanism of Action</u>	<u>Dose (oral)</u>
Doxazosin (Cardura)	Hypertension, BPH	Selective alpha-1 blocker	Relaxes smooth muscle in the prostate and bladder neck, reducing urinary obstruction	Initial dose of 1 mg daily, can be increased to 8 mg daily
Prazosin (Minipress)	Hypertension	Selective alpha-1 blocker	Decreases peripheral vascular resistance, reducing blood pressure	Initial dose of 1 mg 2-3 times daily, can be increased up to 20 mg daily
Terazosin (Hytrin)	Hypertension, BPH	Selective alpha-1 blocker	Dilates blood vessels, reducing peripheral vascular resistance and blood pressure; also relaxes smooth muscle in the prostate and bladder neck, reducing urinary obstruction	Initial dose of 1 mg at bedtime, can be increased up to 10 mg daily
Tamsulosin (Flomax)	BPH	Selective alpha-1A blocker	Relaxes smooth muscle in the prostate and bladder neck, reducing urinary obstruction	Initial dose of 0.4 mg daily
Alfuzosin (Uroxatral)	BPH	Selective alpha-1 blocker	Relaxes smooth muscle in the prostate and bladder neck, reducing urinary obstruction	Initial dose of 10 mg daily
Silodosin (Rapaflo)	BPH	Selective alpha-1A blocker	Relaxes smooth muscle in the prostate and bladder neck, reducing urinary obstruction	Initial dose of 8 mg daily

Table I. Alpha Blockers

A small list of Alpha blockers with 6,7 dimethoxyquinazoline as the core scaffold.

1.4 Epidermal Growth Factor Receptor (EGFR)

1.4.1 Signaling cascade of EGFR

Growth factor receptors (GFRs) are a family of transmembrane proteins that play important roles in various physiological and pathological processes in the human body [68, 118-129]. GFRs are characterized by their enormous size, with a molecular weight of approximately 170 kDa, and contain extracellular domains that are responsible for ligand binding. The ligand-binding pocket of GFRs is formed by a specific set of amino acid residues in the receptor's N-terminal lobe, which can vary depending on the specific GFR subtype and ligand.

Epidermal Growth Factor Receptor (EGFR) is a transmembrane receptor protein that is activated by binding to epidermal growth factor (EGF) and other related growth factors. EGFR is a member of the ErbB family of receptor tyrosine kinases and plays a crucial role in regulating various cellular processes such as cell proliferation, differentiation, and survival. The EGFR protein is composed of several distinct domains, including an extracellular ligand-binding domain, a single transmembrane domain, and an intracellular tyrosine kinase domain. The extracellular domain of EGFR contains four subdomains (I-IV) that are responsible for ligand binding. The ligand-binding pocket is formed by a cleft between subdomains I and III (Figure 3).

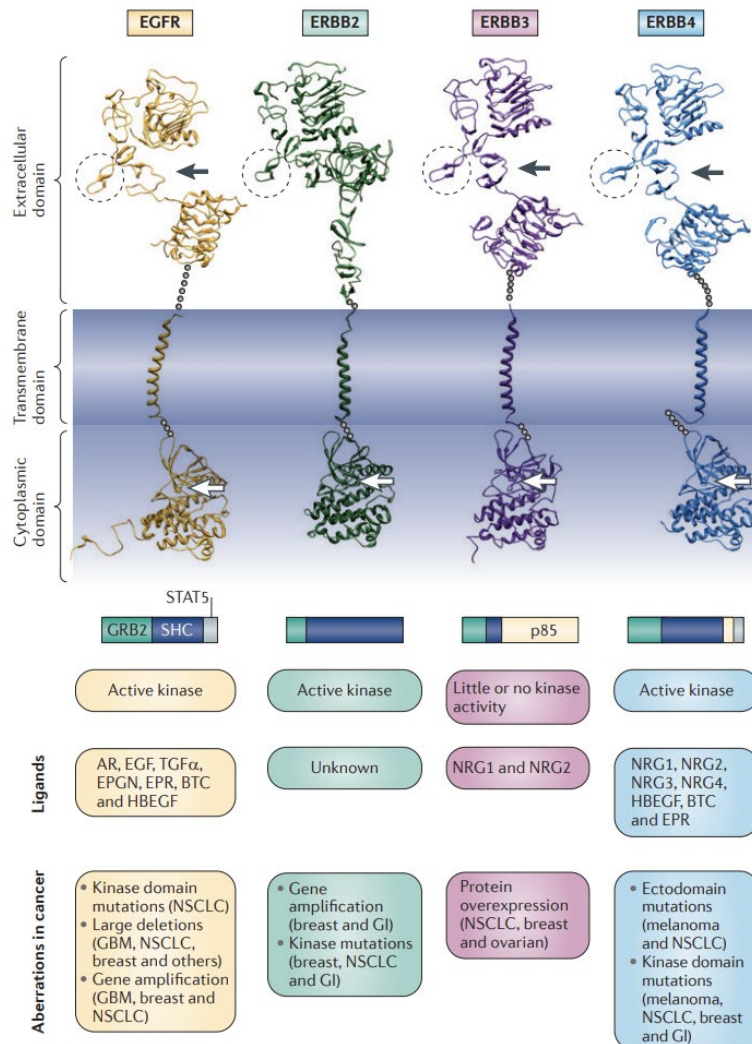


Figure 3. Family Portrait: this figure was adapted from The ERBB network: At last, Cancer therapy meets system biology

Functional and structural features that are unique to each receptor. The four family members are represented by the crystal structures of their three major domains, which have been solved separately (the unstructured carboxy-terminal tails are not shown). The domains are the ligand-binding domain (Protein Data Bank (PDB) accession numbers 1NQL, 1N8Z, 3P11 and 2AHX, respectively), the transmembrane domain (2KS1 (chain B), 2KS1 (chain A), 2L9U and 2L2T) and the kinase domain (1M17, 3PP0, 3KEX and 3BCE). Molecular models were made using Chimera161. The ligand-binding clefts are marked by black arrows and the dimerization loops by dashed circles. The membrane-proximal extracellular segments of both ERBB1 and ERBB4 were omitted to expose the otherwise buried dimerization loops. Note that ERBB2 harbors no ligand-binding cleft, but its dimerization loop is nevertheless extended. White arrows mark the ATP-binding clefts. The sizes of the colored rectangles below the protein structures represent the fractions of docking site specificities; that is, the number of binding sites for each indicated protein normalized to the total number of phosphotyrosine docking sites of each receptor [122].

Upon ligand binding, EGFR undergoes conformational changes that lead to dimerization or oligomerization with other ERBB family members, such as ERBB2, ERBB3, or ERBB4. This dimerization allows the activation of the intrinsic tyrosine kinase activity of EGFR, resulting in autophosphorylation of specific tyrosine residues within the receptor's cytoplasmic domain.

GFRs are widely distributed throughout the human body, being present in many different cell types and tissues. They play crucial roles in various normal cellular processes, such as cell growth, differentiation, and survival. However, aberrant activation of GFRs has been linked to the development and progression of various diseases, including cancer and developmental disorders. Growth Factor Receptor Activation.

Activation of EGFR by ligands, such as EGF, triggers a conformational change that leads to the formation of receptor dimers, resulting in the activation of the kinase domain. The activation of the kinase domain leads to autophosphorylation of specific tyrosine residues, which creates binding sites for downstream signaling molecules such as growth receptor-bound protein 2 (Grb2) and SHC-transforming protein 1 (Shc). These signaling molecules then recruit other proteins, including rat sarcoma (Ras) and phosphatidylinositol 3-kinase (PI3K), which further propagate downstream signaling cascades, leading to changes in cellular behavior.

There are multiple downstream signaling pathways that can be activated by EGFR, including the mitogen-activated protein kinase/extracellular signal-regulated kinase (MAPK/ERK) pathway, phosphatidylinositol 3-kinase/protein kinase B (PI3K/Akt) pathway, and the Janus kinase/signal transducer and activator of transcription pathway (JAK/STAT) pathway. The MAPK/ERK pathway plays a crucial role in cell proliferation,

differentiation, and survival. This pathway is activated by the binding of growth factors or cytokines to their receptors, including GFR. The activation of the MAPK/ERK pathway leads to the phosphorylation of downstream targets, including transcription factors, which induce changes in gene expression that promote cell proliferation, differentiation, and survival. The PI3K/Akt pathway regulates another critical downstream signaling pathway activated by GFR. This pathway regulates cell growth and survival by inhibiting apoptotic pathways. The binding of ligands to GFR leads to the activation of PI3K, which phosphorylates membrane lipids, resulting in the recruitment and activation of Akt. Akt promotes cell survival by phosphorylating and inhibiting pro-apoptotic proteins and promoting the expression of anti-apoptotic genes. The JAK/STAT pathway is a third critical downstream signaling pathway activated by GFR. This pathway regulates cytokine and growth factor signaling. Upon ligand binding to GFR, the JAK family of kinases are activated, which phosphorylates and activates the transcription factor STAT. STAT then translocates to the nucleus and activates the transcription of target genes involved in cell growth, proliferation, and differentiation.

Overall, these downstream signaling pathways activated by GFR play critical roles in regulating cellular processes, including cell proliferation, differentiation, and survival, as well as the response to cytokines and growth factors. Understanding these pathways and their dysregulation in diseases, such as cancer, is essential for the development of effective therapies targeting GFR signaling.

Understanding the role of GFR in regulating cell growth and proliferation is crucial for developing effective anti-cancer therapies. GFRs are widely distributed throughout the human body, being present in many different cell types and tissues. They play crucial roles

in various normal cellular processes, such as cell growth, differentiation, and survival. However, aberrant activation of GFRs has been linked to the development and progression of various diseases, including cancer and developmental disorders. Mutations in EGFR genes have been implicated in several diseases, with activating mutations in the EGFR gene being identified in several types of cancer. Drugs that target EGFR, such as erlotinib and gefitinib, have been developed and are used as cancer treatments. Similarly, mutations in genes encoding other GFRs, such as FGFR3, have been linked to skeletal dysplasia and other developmental disorders. These findings highlight the importance of GFRs in human health and disease, and the potential for targeting GFRs as a therapeutic strategy. Autophosphorylation, ATP phosphorylation, and the interplay between them are critical biological processes involved in various cellular signaling pathways, including GFR. Drug discovery efforts have focused on developing compounds that can modulate the activity of GFR through these processes.

Developing compounds that can selectively inhibit the activity of EGFR by targeting the ATP-binding site of the receptor, called EGFR tyrosine kinase inhibitors (TKIs), can block autophosphorylation of EGFR and downstream signaling cascades. On the other hand, enhancing ATP phosphorylation of EGFR, either by increasing the activity of the receptor or promoting the binding of ATP to EGFR, can be useful in certain disease states where GFR activity is reduced or compromised, such as in some forms of cancer.

Overall, the interplay between ATP phosphorylation and EGFR activity is a complex and key area of drug discovery, with potential applications in a wide range of diseases and conditions.

1.4.2 Quinazoline derivatives targeting EGFR

Overexpression of EGFR is associated with various cancers, including non-small cell lung cancer (NSCLC). Therefore, EGFR has become an attractive target for anticancer therapy. Quinazoline derivatives have been developed as a group of important kinase inhibitors that bind to the ATP-binding site of the EGFR tyrosine kinase domain, thereby inhibiting its activity. Some examples of quinazoline-based EGFR inhibitors include gefitinib, erlotinib, and afatinib.

Gefitinib was the first EGFR inhibitor approved by the US Food and Drug Administration (FDA) in 2003 for the treatment of locally advanced or metastatic NSCLC. Erlotinib was approved in 2004 for the same indication. Afatinib is a newer EGFR inhibitor that was approved by the FDA in 2013 for the treatment of metastatic NSCLC with EGFR mutations. Gefitinib is a small molecule with a molecular weight of 446.9 g/mol and a low solubility in water (0.01 mg/mL at 25°C). The bioavailability of Gefitinib is about 60%, indicating that a significant amount of the drug is metabolized and/or excreted before reaching the systemic circulation.

Erlotinib was approved in 2004 for the same indication as Gefitinib. It is a small molecule with a molecular weight of 429.9 g/mol and a moderate solubility in water (0.42 mg/mL at 25°C) (Table 2).

Overall, these kinase inhibitors based on quinazoline show oral bioavailability, that has a similarity to the ligands in the adrenoceptor ligands based on the same pharmacophore. The bioavailability, absorption, distribution, metabolism, and elimination related to this core structure seems share similarity, which gives us a rationale to design new analogs that could have similarity to the know drugs in market.

<u>Drug Name</u>	<u>Use</u>	<u>Type</u>	<u>Mechanism of Action</u>	<u>Dose</u>
Gefitinib (Iressa)	Treatment of locally advanced or metastatic non-small cell lung cancer (NSCLC)	Tyrosine kinase inhibitor	Binds to the ATP-binding site of the EGFR tyrosine kinase domain, inhibiting its activity	250 mg orally once daily
Erlotinib (Tarceva)	Treatment of locally advanced or metastatic NSCLC and pancreatic cancer	Tyrosine kinase inhibitor	Binds to the ATP-binding site of the EGFR tyrosine kinase domain, inhibiting its activity	150 mg orally once daily
Afatinib (Gilotrif)	Treatment of metastatic NSCLC with EGFR mutations	Tyrosine kinase inhibitor	Irreversibly binds to EGFR and other ErbB family receptors, inhibiting their activity	40 mg orally once daily
Dacomitinib (Vizimpro)	Treatment of metastatic NSCLC with EGFR mutations	Tyrosine kinase inhibitor	Irreversibly binds to EGFR and other ErbB family receptors, inhibiting their activity	45 mg orally once daily
Lapatinib (Tykerb)	Treatment of advanced or metastatic breast cancer	Dual kinase inhibitor of EGFR and HER2	Inhibits the kinase activity of EGFR and HER2, leading to cell growth inhibition	1250 mg orally once daily

Table II. Approved EGFR Inhibitors

The list is not comprehensive, but it highlights inhibitors which share the Quinazoline pharmacophore.

1.5 Conclusion

The main idea of FBDD is to break down a small molecule into smaller fragments and explore the potential biological binding domain of those fragments to re-design new drug candidates. This approach starts with identifying the scaffold of the small molecule, which is then constructed in numerous ways to develop new testing libraries. These libraries are subjected to *in vitro* testing and further refined to move into *in vivo* testing.

The 6,7-dimethoxyquinazoline core has been extensively explored in small molecule drug development. Various medications are currently in clinic usage to greatly benefit the patients. Despite the extensive research that has been done on the 6,7-dimethoxyquinazoline core, it has not yet reached its full potential. There is still a vast chemical space in which this pharmacophore exists that has not been exhausted. In

addition, the potential therapeutic effects of the compounds in other diseases could be explored as well.

In conclusion, the findings of the two research papers demonstrate that the 6,7-dimethoxyquinzalone core has enormous potential as a therapeutic agent, and that the chemical space in which this pharmacophore exists is vast and still unexplored. The idea of fragment-based drug design is an innovative approach to drug discovery that has the potential to revolutionize the field. By exploring the structural diversity of small fragments and their ability to target other molecular targets within the cell, new pharmaceuticals can be created to treat various disease states.

CHAPTER II

IDENTIFICATION OF PRAZOSIN AS A POTENTIAL FLAGELLUM
ATTACHMENT ZONE 1(FAZ1) INHIBITOR FOR THE TREATMENT OF
HUMAN AFRICAN TRYPANOSOMIASIS

2.1 Introduction

2.1.1 Trypanosoma brucei

Kinetoplast is an order of flagellated protozoans belonging to the phylum Protozoa [130-136]. They are characterized by the presence of a kinetoplast, which is a unique structure located in their mitochondria that contains extranuclear DNA (Figure 3) [130-132, 134, 135, 137]. Kinetoplastea is further divided into a family called trypanosomatidae. This family contains this many parasitic species, including *Trypanosoma brucei*, *Trypanosoma cruzi*, and various species of *Leishmania* [138, 139].

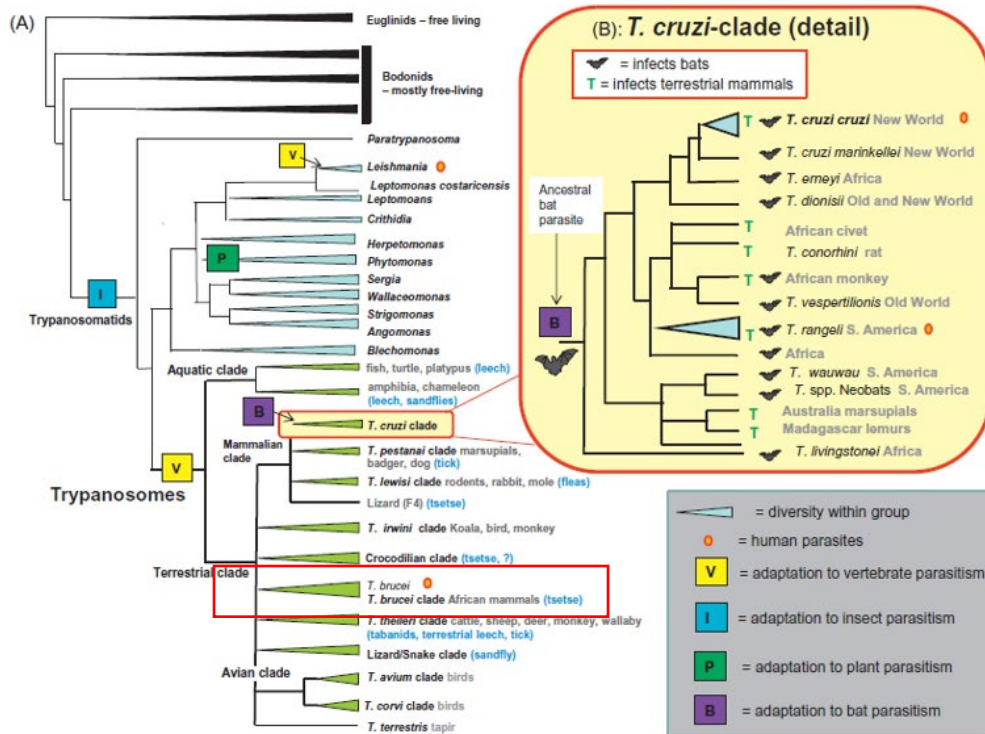
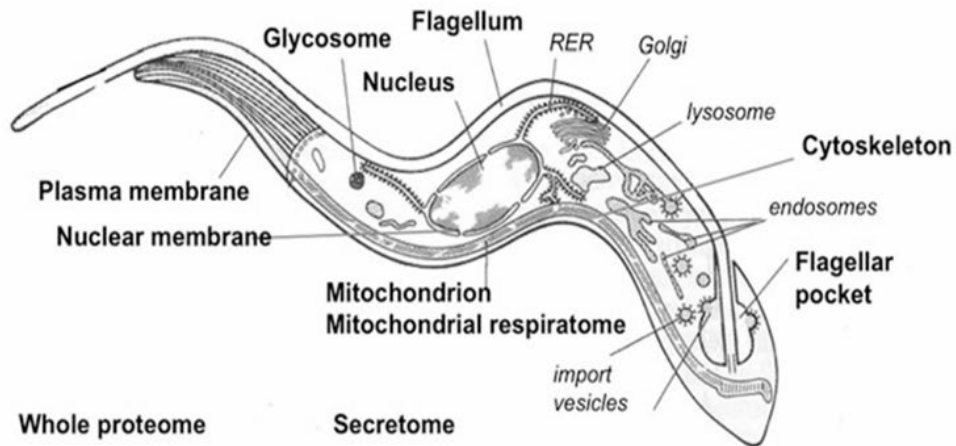


Figure 4. Phylum tree: A tree map of the kinetoplast

This figure was adapted from American Trypanosomiasis 100 years of Research and Trypanosomes and trypanosomiasis [130, 140].

Trypanosoma brucei inhabits Africa primarily located within eastern, western, and central Sahara locations [140]. Depending on the location, acute or chronic infections can occur. The current medication suffers from pharmaceutical imperfections due to these key issues; they include time of stay in hospital, geographical accessibility, fatal side effects, and cost of administration. This neglected tropical diseases (NTD) has shown the ability to gain resistance to current medication and its economic burden hinders the local communities. A cost-analysis model demonstrated that the disease has an overall cost of 400 million to 1.2 billion dollars for elimination, these areas would have to sacrifice 80% of their national income to combat this alone. Making the removal of the HAT impracticable [141, 142].

Genus *Glossina* is a fly who can carry the HAT infection by acting as a vehicle for the parasite and is commonly named the tsetse fly. Transmission of HAT by the fly happens during a blood meal. Two distinctive *Trypanosoma* parasites can cause a HAT infection they are *Trypanosoma brucei rhodesiense* (*T. b. rhodesiense*) and *Trypanosoma brucei gambiense* (*T. b. gambiense*). While a third strand *Trypanosoma brucei brucei* (*T. b. brucei*) only infects nagana and other livestock is often the model strand studied in laboratories for research. *T. b. brucei* is non-infectious to humans due to innate immunity by trypanosome lytic factor 1 (TLF1). This phenomenon has led to the identification of apolipoprotein-L1 (Apol1) and haptoglobin-related protein (Hpr). These two factors synchronize then bind to the surface of the parasite by a haptoglobin-hemoglobin receptor (HpHbR) thus enabling endocytosis of TLF1. The exact mechanism of lysis is debatable, but most recently, a group has shown that Apol1 causes an ionic imbalance that stimulates thiol oxidation leading to osmotic swelling followed by cell lysis. Both *T.b. rhodesiense*

and *T. b. gambiense* have evolved to resist this innate immunity allowing them to be infectious. The life cycle of this protozoa is highly dependent on evading the host immune system. To achieve this, a variant surface glycoprotein (VSG) which is the parasite major surface antigen disguises the parasite from the host immune system by cycling expression of new VSG to the host [131, 134]. The mechanism in which the VSG switches occurs by transcription sites known as bloodstream-form expression sites. How the VSG switch occurs is under investigation but currently the type of switching includes, an in-situ switch, DNA rearrangements via gene conversion or telomere exchange, and homologous recombination. The new VSG variant parasite survives by immune evasion and repopulates the life pool allowing the parasite to cause harm to the host. Many biologists are attempting to decipher VSG switching allowing for immune system evasion, but no drugs or vaccines can target this switching mechanism.

T. b. gambiense and *T. b. rhodesiense* belong to the distinctive group of protozoans characterized by the presence of a kinetoplast. The third strain is *T. b. brucei* which is only infectious to nagana and other livestock as mentioned earlier are non-infectious to humans due to innate immunity. The parasite can be classified based on its lifestyle. *T. b. gambiense* and *T. b. rhodesiense* are dixenous parasites who live in the extracellular space of the host and share similar morphological behavior as well as disease manifestation. The genome size is 26,075,396 base pairs that consists of 11 mega base-sized chromosomes creating 9068 genes and 904 pseudogenes [135, 136]. From research examining the genome it is apparent that all genes lack introns constitutively transcribed as polycistronic. The main distinguishing feature between *T. b. gambiense* and *T. b. rhodesiense* is the presence of the serum resistance associated (SRA) protein. This is a member of the VSG gene family. It is

a glycosylated cell surface protein bound to the membrane by a glycosylphosphatidylinositol lipid anchor. This SRA protein is responsible for the resistance of *T. b. rhodesiense* to TLF-1 by binding the TLF-1 and neutralizing the lysis factor [143-146]. SRA gene also is a diagnostic tool to distinguish the parasite from *T. b. gambiense*. As for *T. b. gambiense* resistance arises from a separate mechanism, this strand gains resistance from TLF-1 by the expression of *T.b. gambiense*-specific glycoprotein (TgsGP) and a mutation in the HpHbR at L210S [136, 144-147]. Unlike the SRA protein TgsGP does not act alone to provide complete immunity to TLF-1 the mutation in the binding site for tlf-1 must also be present [134, 148]. Demonstrated is the ability of both strands to have resistance to TLF-1 and it is only time before selective pressure cause a mutation to make the Trypanosoma resistant to treatment.

2.1.2 Clinical significance and treatment

The disease's clinical significance is well-understood, and its clinical symptoms can be characterized into two distinct phases. In stage one of the disease, haemolympathic conditions occur and are characterized by fever, headaches, joint pain, and itching [141, 149-151]. Once the infection has invaded the central nervous system and passed through the blood brain barrier it is then classified as stage two. During stage two, encephalitic conditions occur and are characterized as impaired function, sleep disturbances, and neurological disfunctions [152]. Depending on the infecting parasite the symptoms could be acute or chronic. Distinguishing clinical signs for HAT are inconclusive and can commonly be misinterpreted as malaria, HIV, tubercular meningitis, and enteric fever. It is critical to identify which stage of HAT the patient is currently diagnosed with to allow correct medical intervention.

The medications available for HAT dates to the early nineteen hundred. Over the century a small list of different treatments became available, they include Suramin (1916), Pentamidine (1942), melarsoprol (1959), nifurtimox (1967), eflornithine (1981), and most recently approved fexinidazole (2018) (Table 3) [151, 153]. Treatment for stage 1 of HAT is suramin and pentamidine and as the disease advances to the second stage melarsoprol and nifurtimox- eflornithine combination therapy (NECT) are used. Recently approved and still under investigation as a first-line treatment, fexinidazole can clear both stage 1 and stage 2 of HAT caused by *T.b. gambiense* with an overall success rate of 90% with minimal setbacks. Suramin, is a poly sulphonated naphthalene derivative it is speculated that the drug interferes with glycolysis and enters the parasite by endocytosis thus starving the parasite from glucose [149, 154]. Pentamidine is classed as a diamidine which has a distinctive path of entry by uptake via the P2 aminopurine permease, but once inside the parasite it is unclear how the drug obtains its trypanocide activity. Melarsoprol a melaminophenyl based arsenical compound also is up taken by the P2 aminopurine transporter as well as the P1 purine nucleoside transporter, the drug target is not clear, but it is speculated that either glycerol-3-phosphate dehydrogenase or trypanothione is the target; nevertheless, research has shown both mechanisms demonstrating a multi-targetable ability inside the parasite. Nifurtimox, a nitrofurane, can passively diffuse across the membrane, once inside reduction of the nitro group generates a potent free radical, the assumption is these leads to generation of oxygen radicals and oxygen metabolites causing death to the parasite. Eflornithine, an analog of the amino-acid ornithine is transported into the parasite by the amino acid/auxin permease specifically TbAAT6 sub-type, where it covalently binds to ornithine decarboxylases an essential pathway for trypanosomes

causing a proline deficiency leading to increased methylation of cell components [155]. Fexinidazole, a nitroimidazole was just released and the uptake and mechanism of action is poorly understood, although it is speculated that it generates reactive amine species causing mutagenesis and result in the trypanocide activity [156]. As for the administration of medicine, it depends on the infecting parasite for *T.b. gambiense* in a stage one condition the first-line medication is pentamidine. The administration is as followed an IM injection at a dosage of 4 mg/kg once a day for 7 days. Once the infection enters stage 2 the current medication is NECT. Due to the combination, two different administration routes occur they are oral and IV infusions. For orally active nifurtimox the dosage is 5 mg/kg three times a day for 10 days and for Eflornithine the dosage is 200 mg/kg twice daily as an IV infusion over 2 hours for 7 days. For *T.b. rhodesiense* the medication changes and for the first stage, Suramin is administered through an IV. The dosage begins with a test dose of 4-5 mg/kg followed by a waiting period of one day then five injections of 20 mg/kg every 7 days. As the disease enters the second stage the medication of choice is melarsoprol given through IV injections at the dosage of three 3.6 mg/kg injections over the span of seven days. In table 3 a summary of the administration, as well as the adverse side effects, are listed. The research for a new medication has led to two tolerable drugs NECT and fexinidazole, but the parasite can gain resistance as demonstrated in an extensive review of transporter-related resistance due to point mutations of the genome [154, 157].

drug	Strain	Indication	Dosing	Mechanism of action	Side effects
Suramin	T.b. Rhodesiense	Stage 1	IV, Test does 5 mg/kg for one day, then 20 mg/kg every 7 days	speculated that the drug interferes with glycolysis	Hypersensitivity, albuminuria, hematuria, neuropathy
Pentamidine	T.b. Gambiense	Stage 1	IM, 4 mg/kg once a day for 7 days	N/A	Hypoglycemia, diarrhea, nausea, vomiting
Melarsoprol	T.b. Rhodesiense T.b. Gambiense	Stage 2	IV, 2 mg/kg once a day for 10 days	speculated that either glycerol- 3-phosphate dehydrogenase	Encephalopathic syndromes, neuropathies, thrombophlebitis
*Nifurtimox	T.b. Gambiense	Stage 2	Oral ,5 mg/kg three times daily for 10 days	speculated generation of oxygen radicals	Tremors, gastrointestinal disturbances,
Eflornithine	T.b. Gambiense	Stage 2	IV Infusion > 30 min, 100 mg/kg every 6 hours for 14 days	ornithine decarboxylases causing proline deficiency	Convulsions, anemia, leucopenia, thrombocytopenia
Fexinidazole	T.b. Gambiense	Stage 1/2	Oral, 1200mg twice a day for 4 days followed by 600 mg once a day for 6 days	speculated generation of reactive amine species	Insomnia, Qt interval prolongation, mental disorder, anemia

*Only given in combination with Eflornithine as NECT.

Table III. Pharmacological treatments

The clinical used agents for African Sleeping Sickness and their side effects

2.1.3 Current outlook and direction of research

Neglected tropical diseases (NTDs) include Chagas disease, Dengue fever, Leishmaniasis, and Human African Trypanosomiasis (HAT), and more information on other NTDs can be viewed from the World Health Organization (WHO) report [132, 158]. HAT is still considered a health threat to sub-Saharan Africa residents and impacts

economic growth [134, 159, 142, 141]. The current treatment suffers from inconvenient administration, high toxicity, and drug resistance [154, 149, 160]. WHO and Bayer have established a coalition for drug discovery against HAT, and the first oral active drug fexinidazole was developed [161, 156, 162]. The release of this drug in 2018, along with the efforts to control the parasite vector tsetse fly population, have resulted in a dramatic decrease in the number of cases of HAT. The reported number of instances was around 1,000 in 2018, but it varies in different seasons [161, 163]. It is still considered a neglected disease and remains un-erasable due to various reasons including wild animals as the parasite reservoirs [164, 165]. In continuing effort, development of new anti-HAT drugs will help the global eradication of this NTDs.

Small molecule drugs often have off-target effects besides their originally approved usage [166, 167]. Repurposing drugs used in the clinic for off labeled indications is a common medical practice. Therefore, it is plausible to find potential treatments for HAT from the current medications in the market. The Library of Pharmaceutically Active Compounds (LOPAC) contains 1280 compounds, with the majority being FDA approved drugs [168, 169]. The compound library was screened by using three cell lines to determine the selectivity and potency of the compounds, each cell line was tested independently and they are as followed; the lister 427 strain of *T.b. brucei*, a mouse macrophage cell line RAW267.4, and human kidney cell line HEK293. Among the 38 hits, our screen identified Prazosin and doxazosin, both alpha-adrenoceptor antagonist, showing prominent activity towards the parasite [112, 117, 87]. Furthermore, we determined the activity of a series of Prazosin analogs that resulted in improved activity and selectivity, suggesting Prazosin is the lead compound for optimization. To date *T.b. brucei* has undergone extensive

characterization of its proteome by various institutions yet, identification of the adrenoceptor is absent [170-175]. Therefore, Prazosin cannot use the original attended molecular target in *T.b. brucei* cells. It is speculated that new molecular targets are involved to selectively inhibit the growth of *T.b. brucei* cells. To identify the novel molecular targets of Prazosin in trypanosome cells, a biotin conjugated molecular probe was synthesized based on the structure of Prazosin by modifying the furan ring to instead incorporate biotinamidohexanoic acid N-hydroxysuccinimide ester. Using this probe, we performed a protein pulldown assay combined with a proteomic analysis to identify protein interactions with the probe. Flagellum attachment zone 1 (FAZ1) filament was found to be a potential target of this novel class of compounds, and Prazosin treatment resulted in flagellum dysfunction in trypanosome cells as well. To confirm the targeting effect as well as examine the drug distribution, a fluorescent probe was synthesized based on Prazosin. Additionally, to be able to identify FAZ1 a trypanosome strain expressing a F2H-FAZ1 tag was also established. We observed a partial colocalization of the probe and FAZ1 in the immunofluorescence assay. Based on the analog library a Structural Activity Relationship (SAR) was summarized, which is critical for further lead optimization to improve the selectivity and potency of the compounds to inhibit trypanosome cell growth. In brief, our findings provide a class of novel FAZ1 inhibitors to treat trypanosomiasis.

Elimination of this disease must be tackled to elevate the area of detrimental side effects hindering society. Prestigious organizations are combining together to push the elimination of HAT they include; International Glossina Genome Initiative (IGGI), World health organization (WHO), Sanofi Aventis, Bayer and other non-governmental organizations such as Bill & Melinda gates foundation.³⁹ Current medication lacks the

ability to coexist with the economic environment and the occurrence of resistances pressures the need for an oral medication to elevate the burden. In attempt to find an effective cure for *T.b. brucei* our work will be an important part of the ongoing effort of many organizations to rid the earth of this disease.

2.2 Results and Discussion

2.2.1 Identification of new lead compounds

The *T.b. brucei* lister 427 strain, mouse macrophage cell line RAW267.4, and human kidney cell line HEK293 were used for three independent high throughput screening (HTS) cell proliferation assays. LOPAC was assessed at 10 μ M for 48 h, and the HTS identified 38 different compounds that satisfy the cutoff of activity and selectivity (Figure 1). The molecular mechanism of action of these 38 compounds was diverse, but Prazosin and Doxazosin, two adrenoceptor antagonists, cultivated our interest because of their shared core structure containing 2-piperazinyl-4-amino-6,7-dimethoxyquinazoline, and similar mechanism (Figure 2). Amongst the hits identified by the HTS an approved treatment for HAT, suramin, was also identified under our criteria (Table 4). Within this work the 38 hits are listed in Table 4, in attempt to identify a lead compound the structures were compared for similarity. Of these compounds only the two-adrenoceptor antagonist shared a similar core structure, therefore our attention in this work focused on exploring why these compounds were active against the parasite. Although, the original intended target for Prazosin and Doxazosin is absent in the parasite because there is no expression of adrenoceptors [170, 171, 176]. Therefore, exploring why Prazosin and Doxazosin cause activity towards *T.b. brucei* could lead to new molecular targets to inhibit cell proliferation.

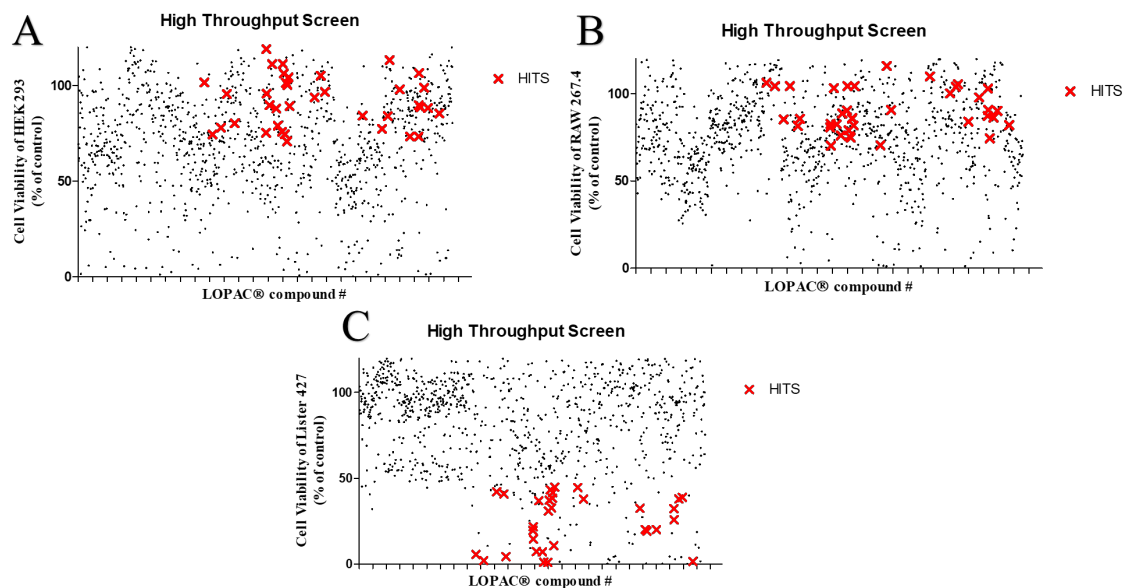


Figure 5. Three cell lines were used in the HTS, (A) HEK 293 and (B) Raw 267.4 were used as control cell lines for toxicity, while the bloodstream form cells of the (C) *T.b. brucei* Lister 427 strain was used as the parasite model

The criteria are setup as: at 10 μ M, compounds that result in >70% viability in mammalian cells and <40% viability in *T.b. brucei* cells. There are 38 hits meeting this criterium.

Name	Mechanism of Action	Name	Mechanism of Action
<u>Doxazosin mesylate</u>	<u>alpha 1 adrenoceptor blocker</u>	Loratadine	H1 Histamine receptor antagonist
5,7-Dichlorokynurenic acid	Potent inhibitor of gastric H ⁺ and K ⁺ -ATPase.	Loxapine succinate	Dibenzoxazepine antipsychotic agent
Rofecoxib	Selective cyclooxygenase-2 (COX-2) inhibitor.	cis (+/-)-8-OH-PBZI hydrobromide	D3 dopamine receptor agonist
Felbamate	Anticonvulsant; glutamate receptor antagonist	Minocycline hydrochloride	Basement membrane protease inhibitor; inhibits endothelial cell proliferation and angiogenesis.
Flutamide	Non-steroidal anti-androgen	Methysergide maleate	Serotonin receptor antagonist; antimigraine
FPL 64176	Potent L-type Ca ²⁺ channel activator	S-(4-Nitrobenzyl)-6-thioinosine	Potent adenosine uptake inhibitor
Ifenprodil tartrate	Blocks the polyamine binding site associated with the NMDA glutamate receptor; neuroprotective	<u>Prazosin hydrochloride</u>	<u>Peripheral alpha 1 adrenoceptor antagonist</u>
Isotharine mesylate	beta-Adrenoceptor agonist; bronchodilator	Candesartan cilexetil	Candesartan cilexetil is the prodrug form of the potent angiotensin II receptor antagonist, candesartan
Isoliquiritigenin	Soluble guanylyl cyclase activator and aldose reductase inhibitor	Ribavirin	Antiviral agent: its metabolite, ribavirin 5'-phosphate, is an inhibitor of inosine monophosphate (IMP) dehydrogenase
Isoxanthopterin	Product of xanthine oxidase oxidation of pterin, an enzyme involved in reactive oxygen formation.	Ro 41-0960	Specific, reversible, orally active COMT-inhibitor
Stevioside	Noncaloric natural sweetener; inhibits transepithelial transport of para-aminohippurate (PAH) by interfering with the organic anion transport system.	SCH-202676 hydrobromide	Allosteric agonist and antagonist of G protein coupled receptors (GPCRs)
3-(1H-Imidazol-4-yl) propyl di(p-fluorophenyl) methyl ether hydrochloride	H3 Histamine receptor antagonist	Suramin sodium salt	P2X and P2Y receptor antagonist; antiparasitic; anti-tumor agent
Ketoconazole	Potent inhibitor of cytochrome P450c17 enzyme; antifungal agent	Trimipramine maleate	Serotonin reuptake inhibitor that also blocks norepinephrine reuptake; antidepressant

Name	Mechanism of Action	Name	Mechanism of Action
LY-310,762 hydrochloride	Potent, selective 5-HT 1D serotonin receptor antagonist.	Oltipraz metabolite M2	Oltipraz metabolite M2 acts as a potent inhibitor of LXRA transcriptional activity, and AMPK activator inducing the phosphorylation of AMPK.
Lomefloxacin hydrochloride	DNA gyrase inhibitor	TTNPB	Selective and highly potent retinoic acid analog with affinity for retinoic acid receptors (RAR) alpha, beta, and gamma
Lonidamine	Inhibits the energy metabolism of neoplastic cells by interfering with mitochondrial hexokinase, cellular respiration, and glycolysis; damages cell and mitochondrial membranes	KB-R7493	KB-R7943 inhibits the reversed Na (+)/Ca (2+) exchanger, NCX. In cardiomyocytes
Lidocaine hydrochloride	Anti-arrhythmic; local anesthetic	Entecavir	Entecavir is an antiviral guanine analog that inhibits reverse transcription, DNA replication and transcription in the viral replication process.
Lansoprazole	Gastric proton pump inhibitor	Tyrphostin 23	Protein tyrosine kinase EGFR inhibitor.
Ro 90-7501	Inhibits amyloid beta42 (Abeta42) fibril formation.	U-74389G maleate	Free radical lipid peroxidation inhibitor

Table IV. The 38 identified Hits from the HTS assay, the common name followed by their mechanism of action are listed

These hits satisfied our criteria by compounds that having >70% viability in mammalian cells and <40% viability in *T.b. brucei* parasites.

Based on the HTS results two alpha adrenoceptor antagonists were able to significantly reduce *T.b. brucei* cell proliferation at 10 µM. Therefore, our hypothesis is that other alpha adrenoceptor antagonists will retain or have improved activity. Four other FDA approved alpha adrenoceptor antagonist were assessed as well, these compounds include, Tamsulosin, Silodosin, Alfuzosin and Terazosin (Figure 5). Alfuzosin and Terazosin share a similar 6,7-dimethoxyquinazoline pharmacophore to Prazosin and

Doxazosin, whereas Tamsulosin and Silodosin have vastly different structural scaffolds but still bind to the adrenoceptor [112, 177, 178]. The compounds IC₅₀ values of *T.b. brucei* cell proliferation inhibition was determined with three independent repeats and the results are reported as a mean ± standard deviation. We found that Prazosin, Doxazosin, Alfuzosin, and Terazosin that all share the 6,7-dimethoxyquinazoline pharmacophore showed IC₅₀s of 3.32 ± 1.62 μM, 4.11 ± 1.91 μM, 11.97 ± 7.86 μM, and 20.98 ± 11.47 μM, respectively. Tamsulosin and Silodosin exhibited much higher IC₅₀s above 50 μM. The results suggest that the 6,7-dimethoxyquinazoline pharmacophore is responsible for the anti-trypanosome activity, and the alpha adrenoceptor antagonizing effect has no correlation to this activity. To further confirm whether adrenoceptor engages in the biological activity of Prazosin in the parasite, we treated the cells with Prazosin along with adrenoceptor endogenous ligand epinephrine (Figure 5C). The result indicates that epinephrine did not rescue the cell viability of trypanosome cells, nor did it attenuate the activity of Prazosin, which further supported the conclusion that the alpha adrenoceptor is not involved in the process.

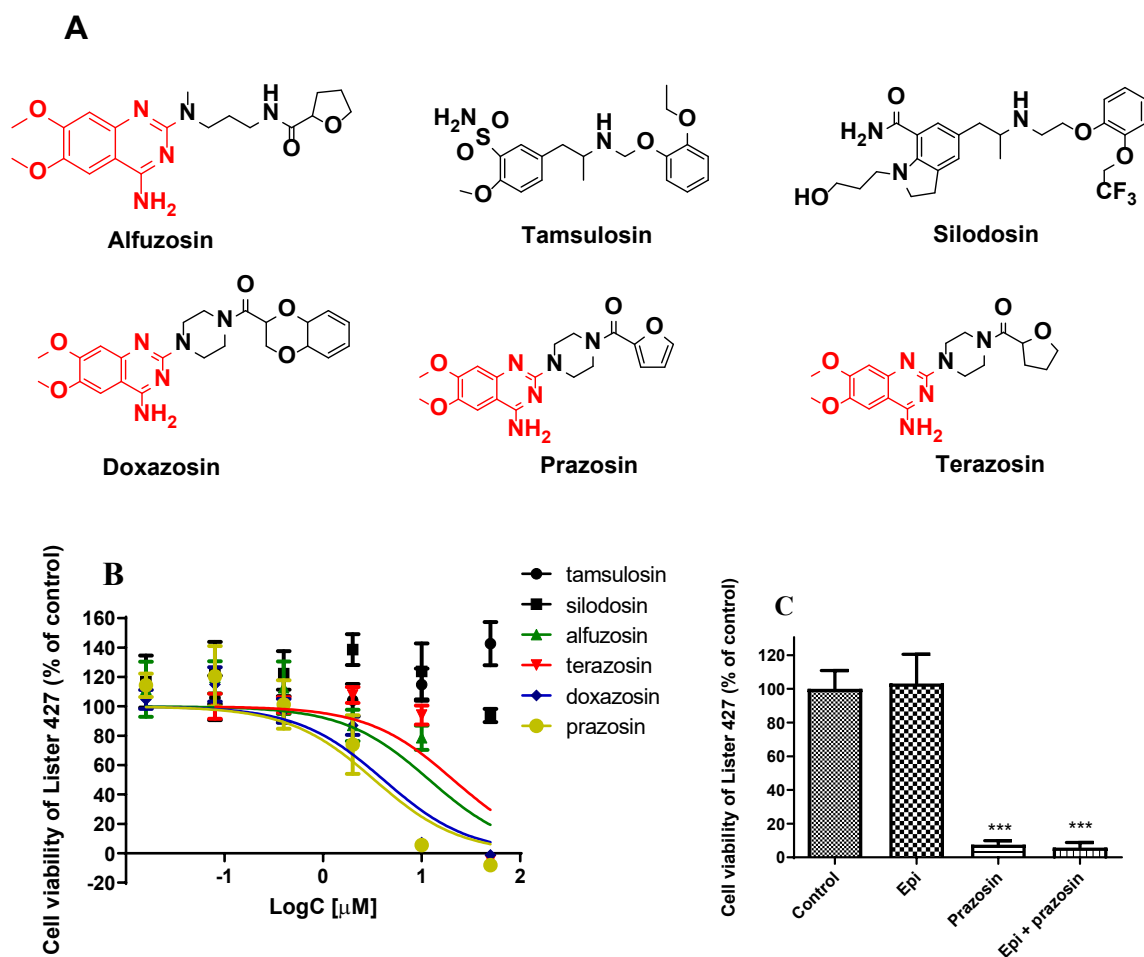


Figure 6. Conformation of unique pharmacophore

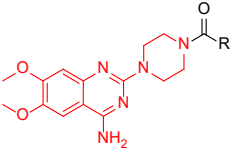
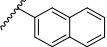
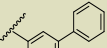
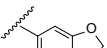
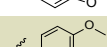
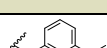
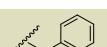
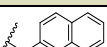

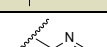
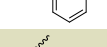
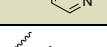
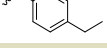
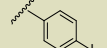
Alpha adrenoceptor antagonist showed different activities against the proliferation of *T.b. brucei* cells. (A) structures of the alpha adrenoceptor antagonists. (B) Compounds with a 2-piperazinyl-4-amino-6,7-dimethoxyquinazoline moiety exhibited better potency with lower IC_{50} s. (C) Epinephrine (50 μ M) did not attenuate the cytotoxicity of Prazosin at 5 μ M to *T.b. brucei* cells. *** $p < 0.001$, unpaired t test.


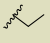
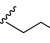
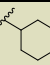
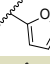

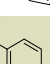
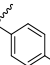


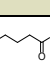
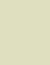
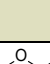
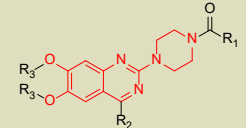
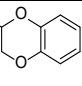
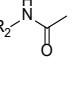
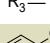
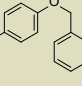
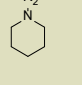
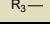
2.2.2 Prazosin analogs showed improved activity against *T.b. brucei* cell growth

A compound library of Prazosin derivatives previously developed for drug development of cancer treatment will be repurposed towards HAT [179]. The majority of these compounds held 2-piperazinyl-4-amino-6,7-dimethoxyquinazoline constant with a

few modifications to the aniline position as well as the dimethoxy position (Table 5). The main structural modifications focused on the right side of the structure at the secondary amine of the piperazine ring to form various benzamides. As previously described in the HTS the same three cell lines were treated with various doses of these compounds, and the IC₅₀s and selectivity index are summarized in Table 5. Five analogs of the lead Prazosin generated IC₅₀s below 1 μM with varying selectivity for the parasite over RAW 267.4 and HEK 293 cells. Particularly, compound 28 showed an IC₅₀ of 0.220 ± 0.091 μM and a selectivity of ~380 times over both mammalian cell lines, whereas compound 27 with a similar dimer structure showed an improved potency to the parasite, but a reduced selectivity index indicates compound 28 potentially will have a safer *in vivo* profile. Overall, the dimeric structure is an interesting new scaffold and worth further lead optimization in the future. For the benzamide moiety, bulky benzamide substituted piperazine shows better activity, compounds 1, 2, 7 all have IC₅₀ at low micromolar levels. An interesting observation is that compounds 7 and 8, only difference is a methyl group inserted between the aromatic ring and the ketone in compound 8, which resulted in loss of activity, suggesting that the amide bond or the methylene between the bulky aromatic region is critical for the activity. Anything bulkier than hydrogen on the methylene bridge will harm the activity as indicated by compound 8. The substitution on the benzamide moiety also affects the activity, with para substitution giving the best results, indicated by compounds 4, 11, 12, 22 and 24 which showed IC₅₀s at low micromolar levels. Compounds 25 and 26 do not have the 2-piperazinyl-4-amino-6,7-dimethoxyquinazoline scaffold and showed no activity. Compounds 30-33 are derivatives of compound 24. Any modification on the aniline group of the 6,7-dimethoxyquinazoline harms the activity, and when the

aniline is acylated, compound 29 activity is lost. Compound 33 contains ethoxy groups in the R₃ position showing significantly decreased activity compared to compound 24, suggesting the importance of the methoxy groups. Overall, the diversely substituted Prazosin analogs allowed us to summarize a detailed SAR to pave a good foundation for future lead optimization.

						
#	R group	Raw 267.4	HEK 293	<i>T.b.</i> <i>brucei</i>	Selectivity Raw/ <i>T.b.</i> <i>brucei</i>	Selectivity of HEK/ <i>T.b.</i> <i>brucei</i>
1		7.44 ±	6.93 ±	2.15 ±	3.5	3.2
		4.76	4.75	1.06		
2		2.53 ±	2.67 ±	1.37 ±	1.9	2.0
		1.83	1.56	0.079		
3		36.73 ±	1.77 ±	20.05 ±	1.8	0.1
		13.01	1.03	8.83		
4		70.78 ±	17.79 ±	4.41 ±	16.1	4.0
		46.35	12.22	1.52		
5		56.09 ±	28.11 ±	4.07 ±	13.8	6.9
		34.48	19.58	1.52		
6		53.2 ±	75.64 ±	16.2 ±	0.5	0.8
		25.5	54.52	8.87		
7		14.22 ±	5.65 ±	0.94 ±	15.2	6.0
		12.49	3.78	0.93		
8		> 100	> 100	> 100	N/A	N/A
9		> 100	48.27 ±	17.4 ±	N/A	2.8
			39.29	2.95		
10		> 100	53.89 ±	46.64 ±	N/A	1.2
			36.71	31.4		
11		9.98 ±	19.74 ±	1.97 ±	5.1	10.0
		4.42	6.18	0.42		
12		1.43 ±	4.25 ±	0.25 ±	5.7	16.9
		0.44	2.92	0.02		
13		13.9 ±	11.91 ±	16.24 ±	0.9	0.7
		5.73	6.18	3.58		

#	R group	Raw 267.4	HEK 293	<i>T.b.</i> <i>brucei</i>	Selectivity Raw/ <i>T.b.</i> <i>brucei</i>	Selectivity of HEK/ <i>T.b. brucei</i>
14		> 100	> 100	83.51 ± 5.24	N/A	N/A
15		> 100	39.32 ± 13.57	30.45 ± 6.11	N/A	1.3
16		> 100	> 100	12.56 ± 4.64	N/A	N/A
17		7.88 ± 4.94	13.69 ± 5.68	4.92 ± 1.51	1.6	2.8
18		11.14 ± 4.83	17.88 ± 12.32	3.32 ± 1.67	3.4	5.4
19		5.80 ± 3.83	23.76 ± 22.35	3.52 ± 2.67	1.7	6.8
20		> 100	59.96 ± 35.48	59.53 ± 28.98	N/A	1.0
21		> 100	71.73 ± 53.19	12.65 ± 2.33	N/A	5.7
22		5.84 ± 5.29	32.22 ± 26.72	2.11 ± 1.68	2.8	15.3
23		35.41 ± 16.23	48.27 ± 15.15	2.32 ± 0.70	15.3	20.8
24		14.79 ± 10.1	19.74 ± 19.05	0.086 ± 0.073	171.8	229.3
27		4.38 ± 2.36	11.91 ± 7.80	0.057 ± 0.032	77.0	209.7
28		> 100	85.23 ± 78.16	0.220 ± 0.091	N/A	380.7
						
29	  	5.3 ± 2.34	83.18 ± 62.74	> 100	N/A	N/A
30	  	52.07 ± 16.69	48.09 ± 19.22	14.68 ± 3.11	3.6	3.3

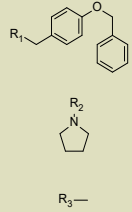
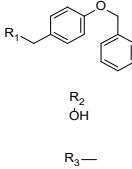
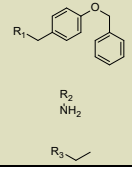
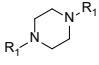
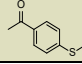
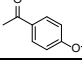
#	R group	Raw 267.4	HEK 293	<i>T.b.</i> <i>brucei</i>	Selectivity Raw/ <i>T.b.</i> <i>brucei</i>	Selectivity of HEK/ <i>T.b. brucei</i>
31		42.53 ± 36.24	>100	76.16 ± 11.47	0.6	N/A
32		10.21 ± 3.85	>100	5.21 ± 2.25	2.0	N/A
33		47.58 ± 34.48	96.54 ± 56.86	21.91 ± 1.91	2.2	47.6
						
25		> 100	> 100	> 100	N/A	N/A
26		> 100	> 100	> 100	N/A	N/A

Table V. Prazosin analogs showed improved activity and selectivity against trypanosome cells over mammalian cells

IC₅₀ values reported in μM with mean ± SD (n=4), and the selectivity index is calculated with IC₅₀s from different cell lines.

2.2.3 Biotinylated molecular probe design

Trypanosome cell growth was inhibited by Prazosin and its derivatives independent of alpha adrenoceptor, and novel targets are responsible for this current activity. Evaluating a series of alpha adrenoceptor antagonists revealed that the 2-piperazinyl-4-amino-6,7-dimethoxyquinazoline moiety plays a critical role of the current activity (Figure 6). To elucidate the detailed molecular mechanisms, it is necessary to identify the targets of

Prazosin in the parasite. A biotinylated molecular probe based on 2-piperazinyl-4-amino-6,7-dimethoxyquinazoline was designed and synthesized (Figure 6). The biotin moiety will allow the immobilization of the probe with neutravidin beads and subsequently retainment of the interacting proteins. To minimize the nonspecific binding proteins, a negative probe designed without biological activity used the same biotin linker to function as a control.

The probe was first examined for its anti-trypanosome activity. Treating *T.b. brucei* cells with either biotinylated 2-piperazinyl-4-amino-6,7-dimethoxyquinazoline or 2-piperazinyl-4-amino-6,7-dimethoxyquinazoline alone resulted in similar cell proliferation inhibition (Figure 6B), indicating that the biotin moiety did not attenuate the activity of the parental compound, and the probe was able to bind to their targets therefore inhibiting trypanosome cell proliferation.

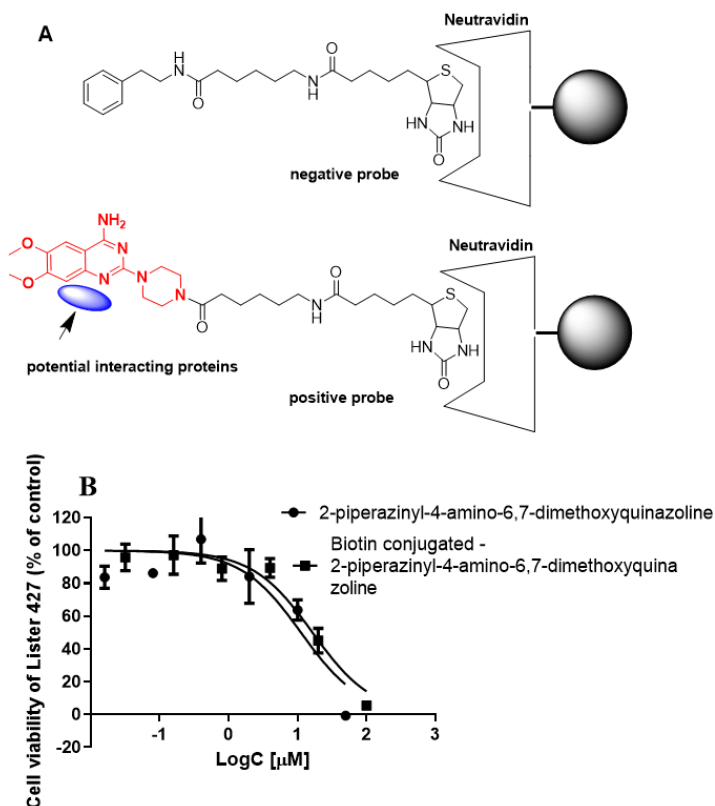


Figure 7. Biotin Pulldown and Potency of The Positive and Negative Probe

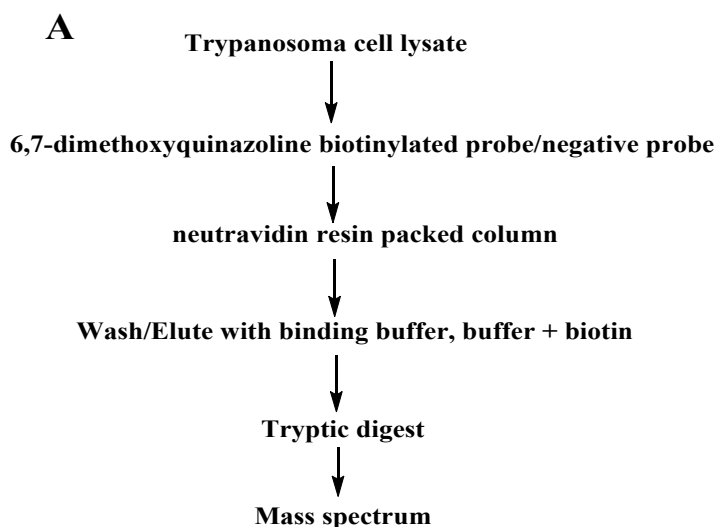
A) Structures of 2-piperazinyl-4-amino-6,7-dimethoxyquinazoline (highlighted in red) probe and a negative control probe. (B) Biotinylated probe and 2-piperazinyl-4-amino-6,7-dimethoxyquinazoline dose dependently inhibits trypanosome cell proliferation with similar activity (IC50s of $11.21 \pm 8.58 \mu\text{M}$ and $16.50 \pm 8.13 \mu\text{M}$ for 2-piperazinyl-4-amino-6,7-dimethoxyquinazoline, and probe respectively).

2.2.4 Affinity purification and identification of 2-piperazinyl-4-amino-6,7-dimethoxyquinazoline bound proteins

We hypothesize that Prazosin analogs bind to certain cellular proteins resulting in inhibition of trypanosome cell growth. Therefore, the probes were incubated with parasite cell lysates to allow binding of cellular proteins to the 2-piperazinyl-4-amino-6,7-dimethoxyquinazoline moiety of the probe. For protein isolation, the biotin moiety of the probe was bound to the neutravidin resin to immobilize the probe. Nonspecific binding proteins were minimized by extensive washing with the binding buffer. Biotin was then used as a competing agent to elute proteins bound to the neutravidin beads. For comparison of the active pharmacophore versus a negative control, the pulldown was performed in parallel with a negative probe without any biological activity. The major steps are shown in Figure 7A. The samples were subjected to tryptic digestion *in situ*. The resulting peptide mixture was identified with mass spectrometry. The molecular weight of the peptide mass fingerprint was used to determine the protein identity via the AB Sciex Analyst QS. Proteins with the best score and selectivity (positive probe/negative probe) are listed in Figure 7B. Eight hits were identified with a cutoff of three-fold difference between the two probes, they include; antigenic protein, calmodulin, flagellar attachment zone protein 1, translational controlled tumor protein, kinetoplastid membrane protein 11 (KMP-11), cytoskeleton-associated protein 15, microtubule-associated repetitive protein, and protein

disulfide isomerases. Three proteins, antigenic protein, translational controlled tumor protein, and protein disulfide isomerases are all putative and would need further confirmation before being treated as a target. Calmodulin, an interesting target belonging to the transmembrane to regulate calcium flux within the parasite but, based on the localization of the fluorescent probe this target was disregarded due to the positioning of the probe near the flagellum pocket. Kinetoplastid membrane protein 11, is a critical small molecular weight protein involved in cytokinesis and the cell cycle as well as contribution to nuclei size [180, 181]. Due to the involvement of this protein in the FAZ assembly we decided to first evaluate FAZ1 because KMP-11 protein functions as a potential binding partner with the FAZ1 portion of the FAZ filament complex therefore, we will investigate this protein in future studies [182]. Microtubule associated repetitive protein interestingly is the first protein recognized by the immune system in both human and bovine hosts, this cytoskeleton protein main function is to help maintain structural integrity, but it also has microtubule-binding motifs and was identified as a microtubule binding partner [183]. Therefore based on this protein being located in the cytoskeleton and its function as a microtubule binding partner our group did not consider this to be a target. Last, Cytoskeleton associated protein 15 is associated with the subpellicular corset and aids with kinetoplast segregation and cytokinesis (CAP15) [184]. It was shown that overexpression of the CAP15 protein produced phenotypes of two kinds, one with a loss of mitosis and cytokinesis coordination producing parasites with abnormal kinetoplast to nucleus ratios, while the other leads to polynucleated cells [184]. From our data we do see both of these phenotypes but the location of the immunofluorescence assay does not localize to the subpellicular corset, making this target less likely. Therefore, from our binding partner

results FAZ1, along with KMP-11 and CAP15 could potentially be the interacting partners of the probe and will be explored, respectively.



Comparison of proteins identified in LC-MS/MS analysis.	Gene ID	Ratio (binding to positive probe/negative probe)	Location	Function
Antigenic protein, putative	Tb927.4.2070	3.24	cytoplasm	N/A
Calmodulin	Tb11.01.4621	3.93	cytoplasm	Calcium binding
Flagellar attachment zone protein 1	FAZ1	6.09	Flagellum attachment zone	Flagellum attachment
translationally-controlled tumor protein homolog, putative	Tb927.8.6760	12.19	cytoplasm	cell growth and development, the cell cycle, apoptosis a
Kinetoplastid membrane protein KMP-11	Tb09.211.4511	3.67	FAZ, basal body, flagellum, nucleus, cytosol	FAZ assembly and cytokinesis
cytoskeleton-associated protein 15	Tb11.01.3805	3.75	anterior	Stabilize Microtubules
Microtubule-associated repetitive protein	Tb10.406.0560	5.99	cytoplasm	Stabilize Tubulin
protein disulfide isomerase, putative	Tb927.7.5790	5.52	ER lumen	Complexes with Ero1, oxidoreductase

Figure 8. Affinity isolation of compound 2-binding proteins

(A) Procedure for the purification of probe binding proteins. The digestion generated peptides that were subjected to an electrospray ionization quadrupole time-of-flight tandem mass spectrometry, and the resulting peptide sequences were searched using the AB Sciex Analyst QS, and the proteins identified in the elute with higher selectivity to the positive probe are listed.

2.2.5 FAZ1 as a potential molecular target of prazosin analogs in trypanosome cells

Among the proteins identified, flagellar attachment zone protein 1 (FAZ1) was explored first due to its high selectivity of interaction with the 2-piperazinyl-4-amino-6,7-dimethoxyquinazoline probe. Flagella, a critical macrostructure important for the trypanosome locomotion, is essential for trypanosome survival [182, 185, 186]. The *T.b. brucei* cell body is cylindrical in shape with tapered anterior and posterior ends. A single flagellum emerges from the basal body near the posterior end of the cell. Within the flagellum is a canonical “9 + 2” microtubule axoneme that drives the flagellar movement [187]. Any interference with the locomotion function of flagellum could lead to cell death eventually [188]. Apparently, flagella serve as a potential target for anti-*T.b. brucei* drug development [131]. FAZ1 is one protein of a complex structure of the FAZ filament, knockdown of FAZ1 by RNA interference (RNAi) results in the assembly of a compromised FAZ domain and results in defects in flagellum attachment, which affects the locomotion of the parasite [189]. Interestingly, we observed that the trypanosome cell movement was dramatically affected by the Prazosin analogs, suggesting that FAZ1 might be affected. Combined with the proteomic results, it is highly likely that FAZ1 is a direct molecular target of the Prazosin analogs. It has been reported that knockdown of FAZ1 by RNAi compromised flagellum attachment in about ~30% of the parasites [190]. However, not all parasites have detached flagella after FAZ1 depletion, suggesting that FAZ1 may be only partially responsible for the biological activity of the filament complex. It is likely that knockdown of FAZ1 results in an unstable FAZ filament, which leads to improper assembly of all the necessary components in a certain percentage of the parasites. Regardless, inhibiting the function of FAZ1 with small molecules is a new discovery, and

might provide a new direction for eradication of HAT as well as be applied to other kinetoplastid infections due to the structure similarity among these pathogens [189].

To further confirm that FAZ1 directly binds to Prazosin analogs, it is necessary to use specific antibody to check if FAZ1 was part of the elute from the pulldown assay. Unfortunately, there is no commercially available antibody for FAZ1. A new *T.b. brucei* strain expressing an N-terminal FLAG-HA-HA (F2H)-tagged FAZ1 (*T.b. brucei* F2H) was established (Figure 8). These cells grow normally, and the tag allowed us to detect FAZ1 using the corresponding secondary antibody. First, we used western blotting assay to confirm expression of F2H-FAZ1 in these cells (Figure 9A). Subsequently, we examined the growth of wild type and F2H-FAZ1 strain, found that the newly constructed cells maintain a similar growth rate as the wild type (Figure 9B). Furthermore, when treated with Prazosin, the IC_{50} s mean and standard deviation (n=4) for the two strains were very close, i.e., IC_{50} of $3.32 \pm 2.39 \mu M$ for *T.b. brucei* and $4.75 \pm 4.40 \mu M$ for the new strain, indicating that the F2H tag didn't affect the function of FAZ1, and Prazosin activity was not affected (Figure 9C). We then examined the location of the FAZ1 protein using immunofluorescence to visualize and confirm we tagged the correct structure, FAZ1 is located the cytoplasm region near the membrane of *T.b. brucei* and is stained green (Figure 9E) [191]. Variant surface glycoprotein (VSG) is the coat of this special pathogen that was stained in red, which gives the out layer including the flagella of the cell surface. In addition, we observed that some Prazosin treated cells show similar flagella de-attachment phenotypes as FAZ1-depleted cells (Figure 9F) [189]. The flagella of the treated cells were split from the cell body, and the cells were not moving in the normal rate, which led to the cell aggregation in clusters. We proceeded to repeat the pulldown assay using the

biotinylated probe with F2H *T.b. brucei* cell lysate, and the F2H-FAZ1 was detected in the pull-down product when assayed by western blotting using an F2H antibody (Figure 9D). The positive probe pulled down an incremental amount of F2H-FAZ1 compared to the negative probe, which is consistent with the results from the proteomic identification.

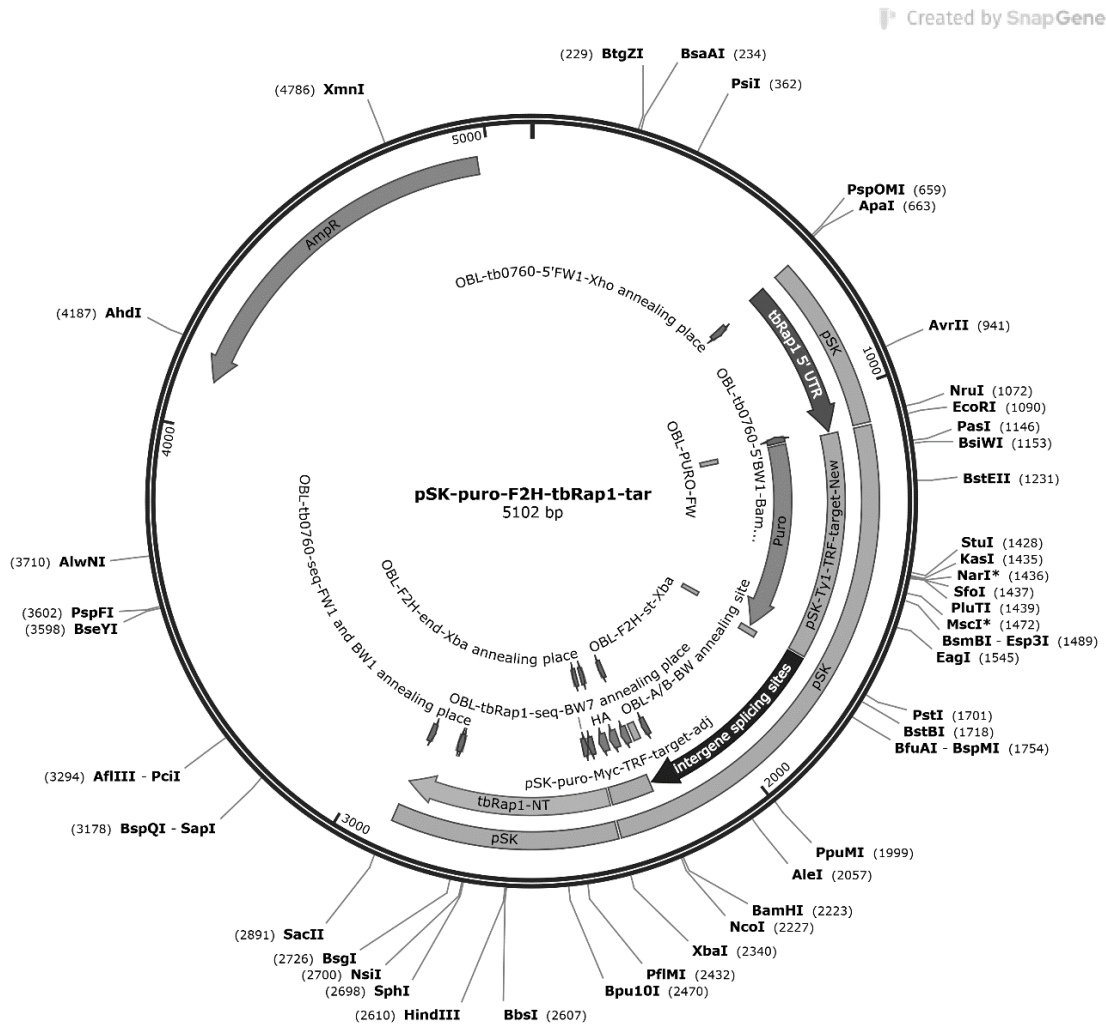


Figure 9. PCR plasmid for F2H tag

The basic construction map for transient transfection using DNA. FLAG-HA-HA (F2H) tag into one endogenous allele of FAZ1 was performed in the SM strain. PCR amplified the N-terminal FLAG-HA-HA FAZ1 fragment with primers OBL-Tb3740-N-term-PURO-FW(5'GGAAAAAATAAAATAGCACTTCCGCAAGGATATAGGGATTTCGCGAACTCCGATTAAGTCGCTTTAGAAGTGCTCCAATTATGACCGAGTACAAGCCCAC3") and OBL-Tb3740-Nterm-F2Hend-BW (5'CTCCGTTTGCCAAATGATCGAATGCAATAACTTGGCCAGGCTGTAAGTTAG TGGGTTTTCACTGATAACATTCAGAAGAGCTCTAGATGCCTCGAGGGC

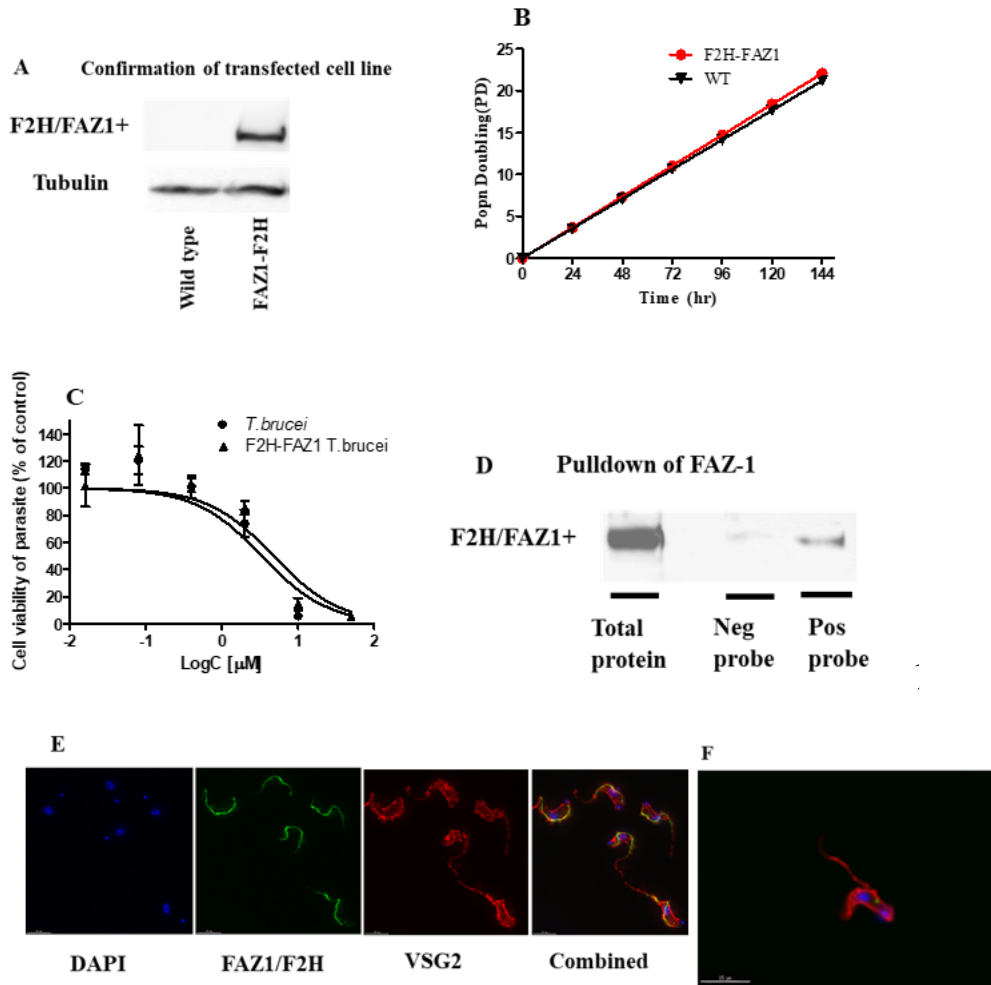


Figure 10. Production of tagged cell and its corresponding effect on viability. Construction of an F2H-FAZ1 *T.b. brucei* strain

Production of tagged cell and its corresponding effect on viability. Construction of an F2H-FAZ1 *T.b. brucei* strain. (A) An F2H antibody could be used to detect F2H-FAZ1 in the established strain in western blotting. (B) New strain showed a similar growth rate compared to wild type. (C) Prazosin showed similar dose-dependent inhibition of the growth of wild type and F2H-FAZ1 strain. (D) Pulldown using the biotinylated probe and F2H-FAZ1 cell lysate. An F2H antibody was used to determine the FAZ1 protein. (E) Immunofluorescent imaging of the F2H-FAZ1 expressing cells. Variant surface glycoprotein (VSG) was stained in red to show the cell surface; F2H-FAZ1 was in green and showed FAZ1 in the cells. (F) Prozosin treatment resulted in partial detachment of the flagella, which makes it not along with the cell body, indicating the dysfunction of the flagella.

2.2.6 FAZ1 co-localization with prazosin fluorescent probe in trypanosome cells

FAZ1 is part of the FAZ filament and forms complex structures in the flagella attachment zone. It will be helpful to find out how these compounds interact with FAZ1 assembled in the whole structure in live cells. To obtain evidence of the drug co-localization with FAZ1, we designed and synthesized a fluorescent probe based on 2-piperaziny1-4-amino-6,7-dimethoxyquinazoline (Figure 10A) following a published method [192]. First, the probe was examined in a cell proliferation assay using the F2H-FAZ1 strain (Figure 10B). Unexpectedly, the fluorescent probe showed 66 times more activity (IC_{50} of $0.050 \pm 0.043 \mu\text{M}$) than Prazosin to inhibit trypanosome cell proliferation, which is consistent to the SAR summarized with the Prazosin analogs that bulky substitutes enhance the activity. Interestingly, the amide bond was replaced with a carbothioamide (blue moiety in Figure 10A) in the probe and this change could contribute to the activity too. Therefore, carbothioamide could potentially act to optimize the structure and function as a new moiety in the future drug development. Second, considering the activity of the probe, we speculated that this compound might be able to affect the stability of FAZ1 in the cells. Therefore, a western blotting assay was performed after treatment of the probe and Prazosin with F2H *T.b. brucei* cells for 24h and 48h at $0.25 \mu\text{M}$ and $5 \mu\text{M}$, respectively. The results indicate FAZ1 expression to be downregulated, suggesting that these compounds reduce FAZ1 protein level, but the mechanism for this phenomenon is still under investigation (Figure 10C). Third, a time-dependent immunofluorescent experiment was performed to observe the probe interaction with FAZ1 in live cells. We found that the probe was localized between the kinetoplast and the nucleus after 6hr. Partial co-localization of the probe and FAZ1 was observed, but the overlapping of the probe and the

FAZ1 was not as significant as we expected (Figure 10D). It is possible that in the FAZ filament complex, FAZ1 protein could be hidden inside and not fully exposed in the complex structure, which might reduce the interaction with the probe. Whereas in the pulldown assay, it was fully exposed in the cell lysate for the biotinylated probe to interact with the FAZ1 binding site.

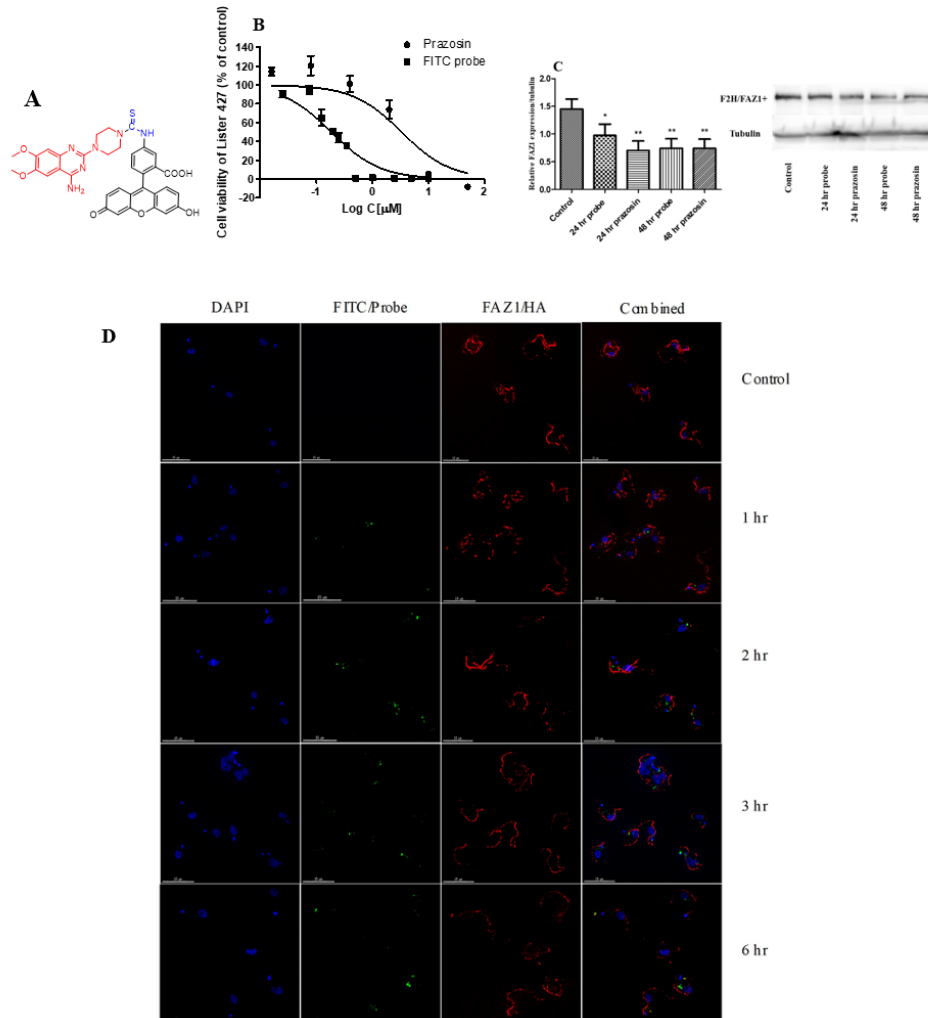


Figure 11. Fluorescent probe interaction with FAZ1

(A) Structure of the fluorescent probe. (B) The probe showed better activity than Prazosin to inhibit trypanosome cell growth. (C) The probe (0.25µM) and Prazosin (5 µM) decreased the FAZ1 protein level. The proteins were analyzed by western blot with specific antibodies, and the results are the representative images and quantification. Data are expressed as Means ± SD (n=3). *p < 0.05, **p < 0.01 compared to DMSO treatment group by unpaired *t* test. (D) Visualizing the probe and FAZ1 in cells in the immunofluorescence assay.

2.2.7 Introduction of the carbothioamide moiety reduces the adrenoceptor activity

Prazosin was identified as the lead compound for the novel FAZ1 inhibitory activity in the parasite, and the analogs showed improved activity. However, the analogs also showed alpha adrenoceptor binding activity in our previous study [179]. For HAT treatment, the adrenoceptor binding activity could affect blood pressure and cause unintended side effects [112]. It has been reported that adrenoceptor activation could lead to increased c-FOS expression in MCF-7 breast cancer cells and other cells as well, which could be used as a method to examine the adrenoceptor activity [193-195]. Prazosin has been found to significantly decrease c-FOS protein level as an adrenoceptor antagonist (Figure 11A). Interestingly, the fluorescent probe with a carbothioamide moiety didn't show adrenoceptor antagonizing activity and did not affect c-FOS level (Figure 11B). This finding suggests that the carbothioamide moiety could reduce the adrenoceptor binding while also improving the anti-trypanosome activity (Figure 10B). Therefore, this bioisotere is a new structural moiety to be used to optimize derivatives in future studies to target trypanosomiasis. To further verify this is an effective method to determine adrenoceptor activity, three Prazosin analogs compounds 28, 27, 24 in Table 5 with good anti-trypanosome activity were evaluated for c-FOS as well. Due to their cytotoxicity to MCF-7 cells, they could only be assessed at 2.5 μ M as the highest dose. Compounds 27 and 24 showed slight activity but not statistically significant to reduce c-FOS, which is consistent with the results in previous study [179]. Taking together, c-FOS measurement could serve as an assay in the future for the analog development to rule out any new derivatives with adrenoceptor binding activity.

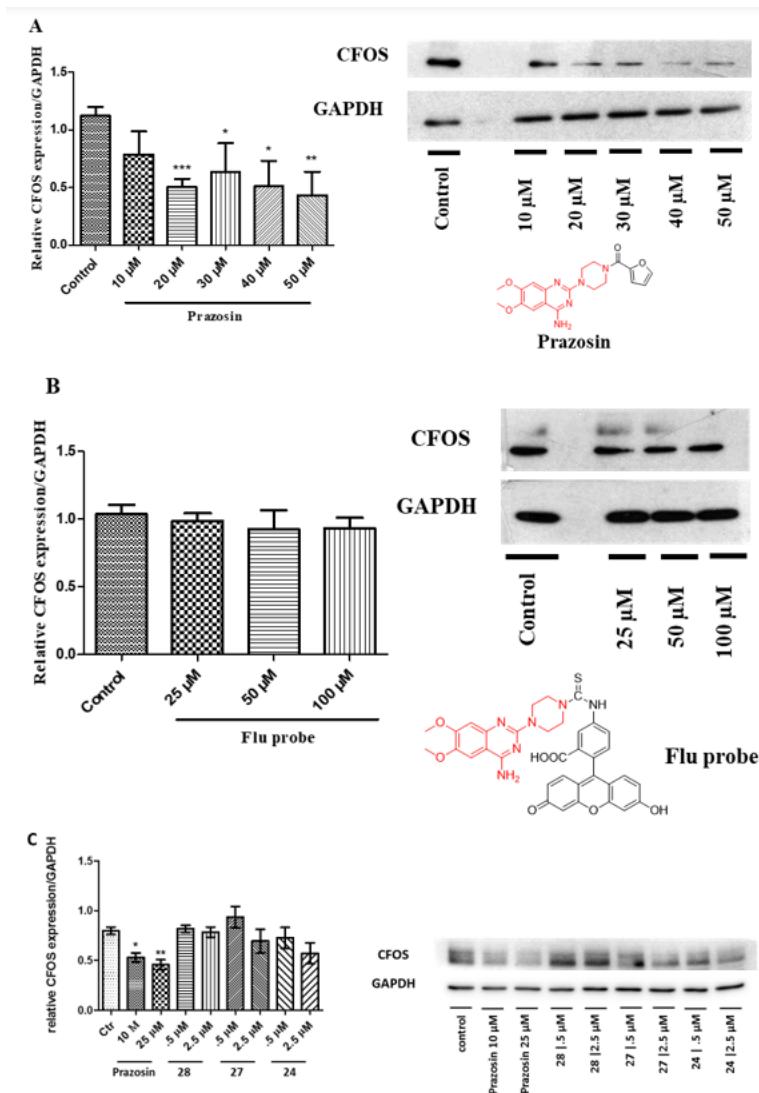


Figure 12. c-FOS expression is correlated with alpha adrenoceptor activity in MCF-7 cells

(A) Prazosin significantly decreased c-FOS protein. (B) The probe with a carbothioamide moiety did not affect c-FOS even at 100 μM, suggesting it did not affect alpha adrenoceptor. (C) Three Prazosin analogs compounds 28, 27, 24 in Table 5 with good anti-trypanosome activity were tested for c-FOS as well. The proteins were analyzed by western blot with specific antibodies, and the results are the representative images and quantification. Data are expressed as Means ± SD (n=3). **p* < 0.05, ***p* < 0.01, *** *p* < 0.001 compared to DMSO treatment group by unpaired *t* test.

2.3 Conclusion

HAT is still a NTDs that affects both the people and economic growth of the sub-Saharan Africa region. It is highly desirable to develop orally active and effective new treatments for this disease. In this study, the HTS of the LOPAC library led to a new discovery of a lead compound, Prazosin as a selective and potent anti-trypanosome agent. A protein pulldown and proteomic approach revealed that FAZ1 could be a potential new molecular target of Prazosin in the parasite, and Prazosin treatment caused cellular flagella dysfunction. More importantly, we found that introduction of the carbothioamide moiety to Prazosin could reduce adrenoceptor binding activity, which paves a new lead optimization direction to improve anti-trypanosome activity while reducing potential toxicity to the host. Future work will focus on the *in vivo* testing of this class of compounds, and further lead optimization to improve the absorption, distribution, metabolism, and elimination (ADME) of this novel class of compounds as potential anti-trypanosomiasis agents.

2.4 Methods

2.4.1 Chemistry

Chemicals were commercially available and used as received without further purification unless otherwise noted. Moisture-sensitive reactions were conducted under a dry argon atmosphere in flame-dried glassware. Solvents were distilled before use under argon. Thin-layer chromatography was performed on precoated silica gel F254 plates (Whatman). Silica gel column chromatography was performed using silica gel 60Å (Merck, 230-400 Mesh). Mass spectra were obtained on the electrospray mass spectrometer

at Cleveland State University MS facility Center. The molecular weight of the compounds was examined with LC-MS. All the NMR spectra were recorded on a Bruker 400 MHz in DMSO-d⁶. Chemical shifts (δ) for ¹H NMR and ¹³C NMR spectra are reported in parts per million to residual solvent protons.

2.4.2 Procedure of biotin linked compounds

The synthesis of the biotin linked compound followed a slightly modified procedure [196]. Full details of the procedure and characterization can be found in the supplementary materials.

2.4.3 Procedure of fluorescein isothiocyanate (FITC) analog

The synthesis followed the procedure by Li et al. [197]. Full details of the procedure and characterization can be found in the supplementary materials.

2.4.4 Procedure of prazosin analogs

The synthesis followed the previously published work by our lab, the compounds were prepared with the same procedure, full details can be referenced to our previous work [179].

2.4.5 Cell culture

HEK293 kidney cells and mouse macrophage RAW264.7 cells were obtained from ATCC (Rockville, MD) and maintained in RPMI1640 medium supplemented with 10% fetal bovine serum (FBS), 2 mM L-Glutamine, 1 mM sodium pyruvate, and 100 U/mL penicillin-streptomycin. FBS was heat inactivated for 30 min at 56 °C. Mammalian cells were grown at 37 °C in a Heraeus water-jacketed incubator with 5% CO₂. In addition,

bloodstream *T.b. brucei* Lister 427 cells, and transfected cell line F2H-TbFAZ1/+ were cultured in HMI-9 medium supplemented with 10% FBS and appropriate antibiotics at 37 °C in a Heraeus water-jacketed incubator with 7.5% CO₂.

2.4.6 *T.b. brucei* cell viability analysis

MTS assay was used to examine the effect of the compounds on *T.b. brucei* cell viability. 2000 *T.b. brucei* cells were seeded in 96 well plates and exposed to 10 µM concentration of 1280 compounds of LOPAC (Sigma-Aldrich) or various concentrations of Prazosin analogs dissolved in DMSO (final concentration 0.1%) in the medium for 48 h at 37 °C. Controls received DMSO at the same concentration as that in drug-treated cells. Subsequently, 20 µL of MTS (5% PMS) from the CellTiter Cell Proliferation Assay (Promega) was added to 200 µL of *T.b. brucei* cells in each well and incubated at 37 °C for 3 h. Soluble formazan, produced by viable cells due to reduction of MTS, was measured at 490 nm with a SpectraMax Plus384 spectrophotometer (Molecular Devices). Statistical and graphical information was determined using GraphPad Prism software. IC₅₀s values were determined using nonlinear regression analysis.

2.4.7 Mammalian cell viability analysis

MTT assay was used to examine the effect of the compounds on the growth of RAW 264.7 and HEK293 cells. 5000 Cells were seeded with RPMI1640 medium in 96-well flat-bottomed plates for 24 h. Then, cells were exposed to 10 µM concentration of 1280 compounds or various concentrations of Prazosin analogs for 48 h. Controls received DMSO at the same concentration as that in drug-treated cells. Next, cells were incubated in 200 µL of 0.5 mg/mL of MTT reagent diluted in fresh media at 37 °C for 3 h.

Supernatants were removed from the wells, and the reduced MTT dye was solubilized with 200 μ L/well DMSO. Absorbance at 570 nm was determined on a SpectraMax Plus384 spectrophotometer (Molecular Devices). Statistical and graphical information was determined using GraphPad Prism software. IC₅₀s values were determined using nonlinear regression analysis.

2.4.8 Protein pulldown assay

The pulldown assay was performed according to the protocol of neutravidin (Thermo Scientific, 29204). *T.b. brucei* and F2H-TbFAZ1/+ cell lines were used to examine how the small molecule biotin complex interacts with a total protein lysate. The cells (1×10^8) were disrupted in NP-40 lysis buffer with protease inhibitors cocktail (Thermo Scientific, 1861278) and ultrasonication on ice. The lysate was incubated with the biotin probe at 100 μ M for 2 h at 4°C, and then incubated with neutravidin resin for 2 h. Then, the resin was collected by centrifuge, and washed with binding buffer 5 times. Then, biotin (100 μ M) was added to release the bound proteins. Followed by centrifugation at 10,000g for 5 mins, and the supernatant was collected. The supernatant was subjected to SDS page and analyzed with blue silver [198], which was used determined that the protein amount by the pulldown was minimal enough to run in-solution digestion for the proteomic analysis.

2.4.9 Proteomics analysis

The samples (1-10 μ g protein) were constituted in 50 μ L of 6 M urea buffer. Then, proteins were reduced and alkylated with DTT and iodoacetamide (IAA). After reduction and alkylation, 50 mM ammonium bicarb was added to adjust pH. Next, the proteins were

digested by adding Trypsin (Promega # V5111) for initial overnight digestion followed by an additional 4-hour digestion. Next, the peptide samples were desalted using a PepClean C₁₈ spin column (Thermo Scientific #89870). The samples were then reconstituted in 30 μ L of 1% acetic acid for LC-MS/MS analysis. The LC-MS system was a Thermo Scientific Orbitrap Fusion Lumos spectrometer system. The HPLC column was a Dionex 15 cm x 75 μ m id Acclaim Pepmap C₁₈, 2 μ m, 100 Å reversed-phase capillary chromatography column. The gradient elution profile consisted of 1% of mobile phase A for 5 min, then brought to 60% of mobile phase B over 90 min, and followed by 90 % of mobile phase B for 8 min. The total run time was 105 min. Mobile phase A was 0.1 % (v/v) formic acid in HPLC-grade ddH₂O, and the mobile phase B was 0.1 % (v/v) formic acid in HPLC-grade acetonitrile. Peptide detection was done using the positive information-dependent-acquisition (IDA) mode of AB Sciex QStar™ Elite Q-TOF mass spectrometer (AB Sciex, Foster City, CA, USA). Data acquisition was performed using AB Sciex Analyst QS (v. 2.0).

2.4.10 Plasmid construction and design

F2H-FAZ1 expressing *T.b. brucei* cells. *T.b. brucei* strains and plasmids: The *T.b. brucei* strains used in this study were derived from bloodstream-form Lister 427 cells that express VSG2, a T7 polymerase, and the Tet repressor (also known as the single marker or SM strain) [199]. The Bloodstream Form (BF.) *T.b. brucei* cells were cultured in an HMI-9 medium supplemented with 10% fetal bovine serum (FBS) and appropriate antibiotics. Insertion of N-terminal FLAG-HA-HA (F2H) tag into one endogenous allele of FAZ1 was performed in the SM strain. PCR amplified the N-terminal FLAG-HA-HA FAZ1 fragment with primers OBL-Tb3740-N-term-PURO-FW

(5'GGAAAAAATAAAAATAGCACTTCCGCAAGGATATAGGGATTCGCGAACTCC
GGATTAAGTCGCTTTAGAAGTGCTCCAATTATGACCGAGTACAAGCCCAC3")

and

OBL-Tb3740-Nterm-F2Hend-BW

(5'CTCCGTTTGCCAAATGATCGAATGCAATAACTTGGCCAGGCTGTAAAGTTA
GTGGGTTTTCACTGATAACATTCAGAAGAGCTCTAGATGCCTCGAGGGC)

using a plasmid containing FLAG-HA-HA and a Puro marker as the template. The PCR product was then purified and transfected into SM strain to generate F2H-TbFAZ1/+.

2.4.11 *T.b. brucei* cell lysate preparation and western blot assay

T.b. brucei cells were treated with 0.5% DMSO or different doses of compounds. Cell pellets were harvested by centrifugation at 1500 rpm for 10 mins at 4 °C, washed twice with 1X TDB buffer (5 mM KCl, 80 mM NaCl, 1 mM MgSO₄, 20 mM Na₂HPO₄, 2 mM NaH₂PO₄, 20 mM glucose, pH 7.4), and lysed with 300 µL of lysis buffer (80 mM Pipes, pH 6.8, 1 mM EGTA, 1 mM MgCl₂, 0.2% Triton X-100, 10% glycerol and protease inhibitors at 30 °C for 5 mins. The cell lysate was centrifuged at 12,000 rpm for 10 mins at 4 °C, and the supernatant was transferred into a fresh Eppendorf tube. Pellets were resuspended in 50 µL of lysis buffer and sonicated. 50 µL of 2× SDS buffer was subsequently added, and the sample was boiled at 95 °C for 5 min. Protein lysates from an equal number of cells were separated on 10% polyacrylamide gels by electrophoresis. Proteins were transferred onto polyvinylidene difluoride (PVDF) membranes. Then, the membrane was incubated in TBST containing 5% non-fat milk for 1 hr. Then, the membrane was incubated with primary antibody specific to F2H-TbFAZ1/+ overnight at 4°C. HRP-conjugated anti-mouse IgG (Cell signaling, MA) were used as secondary

antibody and incubated at room temperature for 1hr. Membrane was incubated in ECL plus reagent (GE health) and then exposed to hyper film.

2.4.12 Immunofluorescence assay

Immunofluorescence experiments were performed as described in other study.[176] Specifically, cells were fixed with 2% formaldehyde at room temperature for 10 mins, permeabilized in 0.2% NP-40 phosphate-buffered saline (PBS) at room temperature for 5 mins, and blocked by the use of PBS 0.2% cold fish gelatin 0.5% bovine serum albumin (BSA) at room temperature twice for 10 mins each time, followed by incubation with the primary antibody at room temperature for 2 hrs and the secondary antibody at room temperature for 1 hr. Cells were then washed with PBS followed by staining with 0.5 g/mL DAPI (4,6-diamidino-2-phenylindole) by mounting of coverslips on slides. A DeltaVision Elite deconvolution microscope was used to take images. Images were deconvolved using SoftWoRx.

Acknowledgments

Cody M. Orahoske was supported by Molecular Medicine graduate fellowship of Cleveland State University. This work was also supported by Center for Gene Regulation in Health and Disease (GRHD), Faculty Research Development (FRD) program, summer undergraduate research program of Cleveland State University, and National Institutes of Health instrumental grant (1S10OD025252-01)

CHAPTER III
DIMERIC SMALL MOLECULE AGONISTS OF EPHA2 RECEPTOR INHIBIT
GLIOBLASTOMA CELL GROWTH

3.1 Introduction

Glioblastoma multiforme (GBM) is the most common and malignant primary neurological brain tumor in adults [200-202]. Treatment options for GBM are still very limited, and the standard available chemotherapy agent for GBM is Temozolomide (TMZ), a DNA-alkylating reagent [203]. This current treatment has a major problem that it often fails due to resistance [204]. It is thus critical to identify new reagents targeting other pathways in GBM. Erythropoietin-producing hepatocellular receptor 2 (EphA2) is one of the receptor tyrosine kinases that regulate cancer cell migration [201, 202, 205]. It has been well documented that EphA2 is overexpressed in GBM, and the overexpression is correlated with malignant progression and poor prognosis [206, 207]. Studies indicate that EphA2 activation by its ligand, ephrin-A1, suppresses tumor progression, including induction of apoptosis, inhibition of cell proliferation, and suppression of cell migration [208-211]. In vivo studies demonstrate that EphA2 activation by systemically administered ephrin-A1 decreases tumorigenicity and invasiveness of carcinoma xenografts [212, 213].

Unfortunately, EphA2 overexpression is often accompanied by loss of expression or mis-localization of ephrin-A1 in tumor tissue [202, 205, 214]. The reduced ligand coupled with increased EphA2 expression results in frequent Akt activation, which promotes ligand-independent pro-invasive Akt-EphA2 crosstalk [202, 215, 216]. This interaction may be in part responsible for EphA2 overexpression during tumor progression and the positive correlation of EphA2 expression and unfavorable prognosis [200, 216]. From a therapeutic point of view, restoring the ligand for EphA2 could recover the tumor suppressing activity of EphA2, and provide a new approach for the treatment of EphA2 overexpressed tumor. Unfortunately, the endogenous ligand of EphA2, ephrin-A1, could not effectively pass blood brain barrier (BBB), which makes this endogenous ligand less useful for the treatment of glioblastoma with over expression of EphA2. This fact led us to hypothesize that a small molecule agonist for EphA2 can be exploited as novel cancer therapeutic [217, 218].

In previous studies, we identified a small molecule EphA2 agonist Doxazosin using a combination of structure-based virtual screening and cell-based assays.[218] Further lead optimization of Doxazosin to activate EphA2 resulted in one particular compound with a unique dimeric structure and superior activity compared to Doxazosin (Figure 12) [217]. Furthermore, this dimer also has the capability to cross BBB [219].

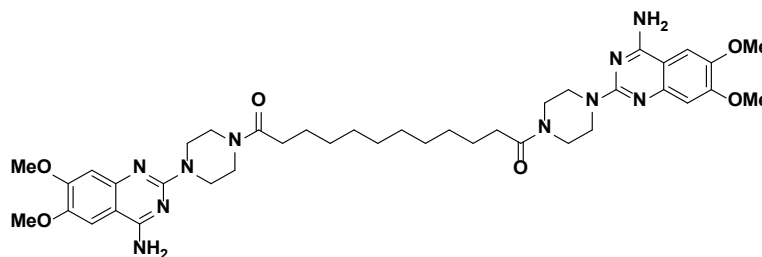


Figure 13. Dimer scaffold synthesized to target EphA2 receptor

In a current study, we performed optimization of the dimeric lead compound. 27 new derivatives were synthesized and examined with glioblastoma cell lines. Three new dimers 3d, 3e, and 6gd' showed similar activities compared to the lead compound. Dimer 3d is consistent of the same monomer of the lead compound but possesses a short polyethylene glycol linker, reducing the molecular weight allowing for a more favorable drug likeness profile. Dimer 6gd' has a longer polyethylene glycol chain compared to compound 3d, and the addition of a benzamide moiety increases the binding capacity to EphA2 receptor. Dimer 3e has a rigid aromatic linker, suggesting that flexibility of the linker is less critical for the activity. All three dimers showed better activity in EphA2 over-expressed cells verse wild type glioma cells, indicating the targeting effect is through EphA2 pathways. However, only 6gd' showed significant EphA2 activation, suggesting that the introduction of a benzamide moiety does increase the ligand binding potency due to the similar use of the polyethylene glycol linker. Compounds 3d and 3e failed to cause EphA2 activation as effectively as the lead compound indicating that the modification reduced the selectivity of the compounds.

3.2 Results and Discussion

3.2.1 Development of an EphA2 overexpressed glioblastoma cell line

Targeting EphA2 to induce cell apoptosis and inhibit cell growth has a lower toxicity compared to chemotherapy for GBM. The ideal drug candidates should selectively decrease the growth of EphA2 overexpressed cells. To examine the selectivity of the compounds, we constructed a GBM cell line with high expression of EphA2 based on U251 GBM cell line as the wild type.

The western blotting results indicate that the basal EphA2 expression in U251 cells is like the empty vector transfected cells, but much lower than the EphA2 transfected cells (Figure 13). In addition, the lead compound showed selectivity to the growth of the three cell lines: wild type with an IC₅₀ of 5.2 μ M, the empty vector with an IC₅₀ of 4.8 μ M, and the EphA2 overexpressed with an IC₅₀ of 2.1 μ M. The results are consistent to our previous study that the dimeric lead compound is a selective EphA2 ligand [217], and inhibits cell growth via activation of EphA2.

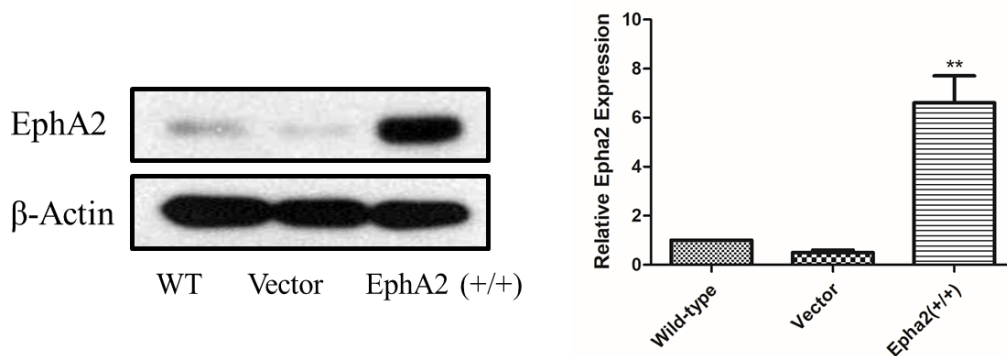


Figure 14. Construction of U251/EphA2 cell line based on U251 wild type cells
The intensities of the bands quantified with ImageJ (NIH) to generate the figure. The figures are representative of 3 experiments. ** $p < 0.001$ EphA2 vs. wild type by unpaired t-test

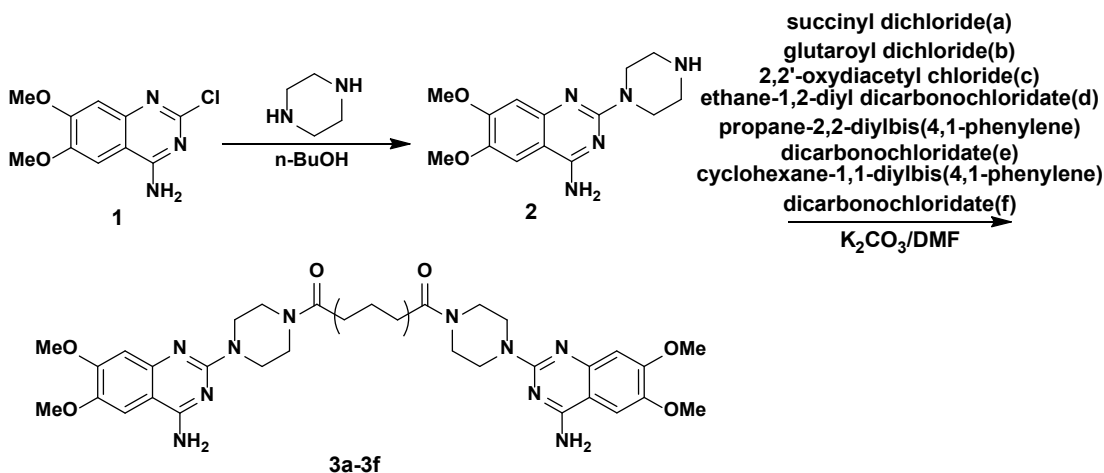
3.2.2 Lead optimization and biological evaluation

In this study, a total of 27 new derivatives were synthesized using combinatorial chemistry strategy, focused on the exploration of the dimeric structures (Figure 14-15).

First, we focused on the modification of the linker of this lead compound. The exceptionally long alkyl linker cannot serve as either hydrogen bond acceptor or donor and reduces the druggable characteristics of the compound. Therefore, we introduced various polyethylene glycol linkers to overcome the drawbacks (compound 3c and 3d). In addition,

we also generated analogs with short alkyl linkers and rigid linkers to explore the flexibility of the linker (compound 3a, 3b, 3e, 3f). We also tried to generate exceedingly long polyethylene glycol linkers, unfortunately, the synthesis was not successful. To examine the effects of the length of polyethylene glycol linker an additional modification was made to the original structure and resulted in one successfully synthesized compound.

Subsequently, we synthesized monomers with a benzamide moiety and an aromatic nitro group (4g-4l). These nitro groups were reduced to amino groups (5g-5l), which was used to generate new dimers. Unfortunately, with the additional benzamide moiety, the formed dimers have poor solubility in various solvents making the purification not practicable. Overall, 9 new dimers were generated with this process.



- 3a** 1,4-bis(4-(4-amino-6,7-dimethoxyquinazolin-2-yl)piperazin-1-yl)butane-1,4-dione (80%)
3b 1,5-bis(4-(4-amino-6,7-dimethoxyquinazolin-2-yl)piperazin-1-yl)pentane-1,5-dione (80%)
3c 2,2'-oxybis(1-(4-(4-amino-6,7-dimethoxyquinazolin-2-yl)piperazin-1-yl)ethanone) (57%)
3d ethane-1,2-diyl bis(4-(4-amino-6,7-dimethoxyquinazolin-2-yl)piperazine-1-carboxylate) (43%)
3e propane-2,2-diylbis(4,1-phenylene) bis(4-(4-amino-6,7-dimethoxyquinazolin-2-yl)piperazine-1-carboxylate) (31%)
3f cyclohexane-1,1-diylbis(4,1-phenylene) bis(4-(4-amino-6,7-dimethoxyquinazolin-2-yl)piperazine-1-carboxylate) (31%)

Figure 15. Synthesis of dimers based on 6,7-dimethoxy-2-(piperazin-1-yl) quinazolin-4-amine as the monomer

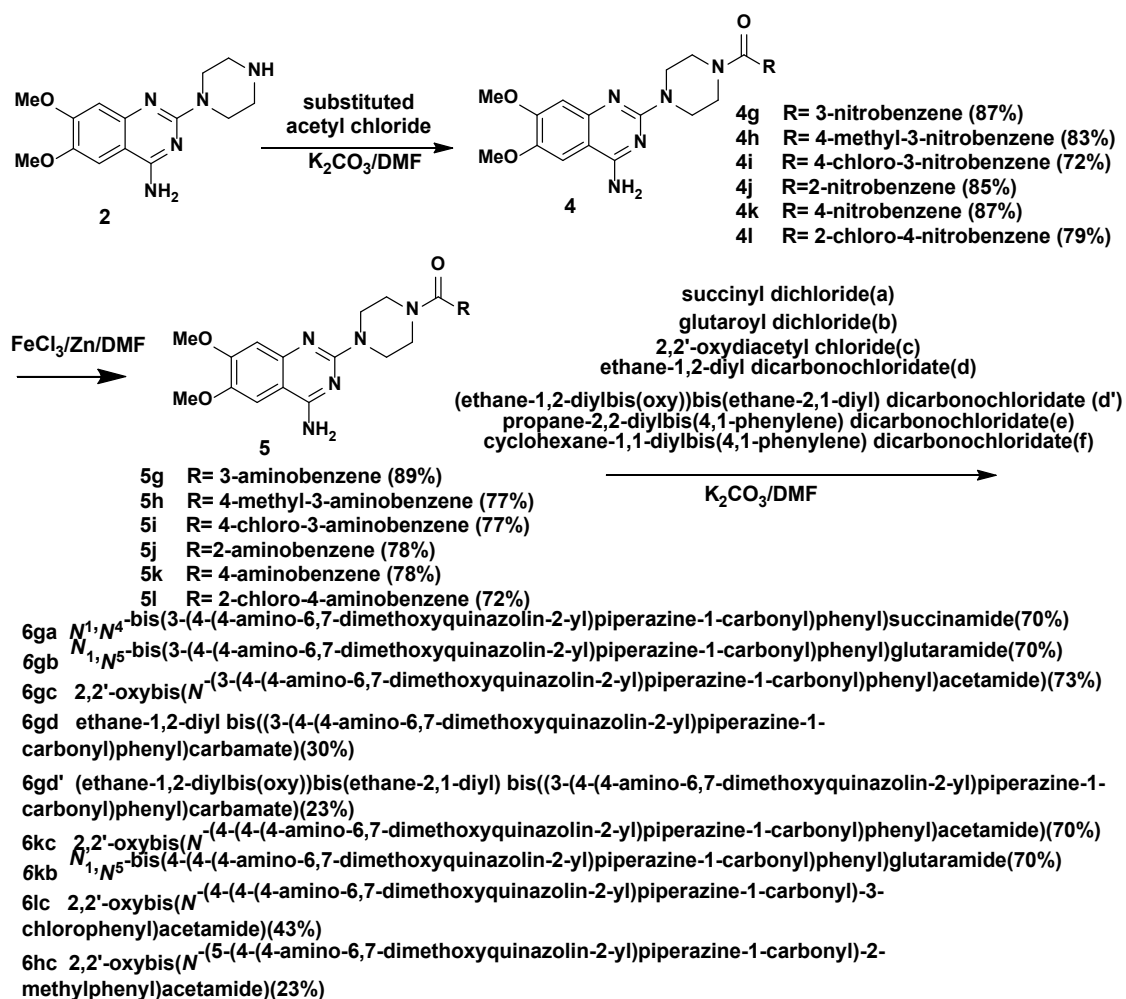


Figure 16. Monomers with a benzamide moiety form dimer

The 27 new analogs including 15 dimers and 12 monomers show diverse substitution on the linker, and the biological results of the compounds can provide us a detailed SAR to elucidate the structural requirement for the targeting of EphA2.

To evaluate the compounds, we utilized the above developed EphA2 overexpressed U251 cells. To verify the selectivity of the compounds, we also screened the compounds with wild type U251 cells with low EphA2 expression. The selective index is calculated based on the IC₅₀s of the two cell lines (Table 6).

All the compounds were examined with multiple doses, and the cells were treated with the compounds for 48 hr., and cell viability was determined after. We used the lead compound and 0.1% DMSO as the positive and negative control, respectively. Among the dimers 3a-3f, 3c showed the weakest activity. In fact, 3c and 3d have similar structures. The polyethylene glycol linkers seem contribute to the binding of the ligand to bind to EphA2. 3d has two oxygens in the linker that dramatically improves the activity. 3d also showed two-fold more selective to the EphA2 overexpressed cells than the wild type. 3e and 3f both have a rigid and aromatic linker, and both inhibited the growth of EphA2 overexpressed cells with IC50s in the low micro mole range, suggesting that keeping the two monomers far away from each other benefits the activity. Compounds 3a and 3b with a short alkyl linker showed decreased activity, which is consistent with our previous results and should be eliminated as an optimization direction in the future. For monomers 4g-5l, most of them have the IC50s above 10 μ M, regardless of if it is the nitro group or the amino group on the benzamide moiety. Only compounds 5j, 5k and 5l showed better activity, with an IC50 of 3.6, 3.0 and 2.7 μ M, respectively. Compound 5l had the largest selectivity index among all the compounds with a value of 17.78, suggesting the reduction of the nitro group to the amine plays a role in binding to the EphA2 receptor specifically to this 2-chloro-4-nitro-benzamide moiety. For the 9 dimers among this group, the activities of the majority were not appealing except for compound 6gd'. It showed an IC50 of 1.9 μ M for EphA2 overexpressed cells and 7.9 μ M for wild type of cells, which results in a selective index of 4.2. Overall, the dimers formed by monomers with benzamide moiety did not show better activity compared to dimers 3a-3f.

Considering both potency and selectivity, we narrow down to compounds 3d, 3e, 6gd' for further mechanism investigation.

Compound	U251 EphA2 Overexpressed	U251 Wild Type	Wild/ Overexpressed
3a	6.75 ± 2.40	12.62 ± 6.62	1.9
3b	7.47 ± 3.98	8.07 ± 4.37	1.1
3c	51.86 ± 26.07	160 ± 80.62	3.1
3d	1.60 ± 0.40	3.05 ± 0.82	1.9
3e	2.45 ± 1.11	9.22 ± 5.56	3.8
3f	3.18 ± 1.44	7.48 ± 4.03	2.4
4g	12.70 ± 8.72	12.23 ± 8.35	1.0
4h	27.41 ± 15.05	24.80 ± 16.01	0.9
4i	7.41 ± 2.98	8.34 ± 4.42	1.1
4j	12.06 ± 5.98	14.73 ± 9.20	1.2
4k	26.43 ± 11.8	53.01 ± 29.78	2.0
4l	4.41 ± 2.36	10.77 ± 7.23	2.4
5g	11.14 ± 7.26	8.98 ± 4.61	0.8
5h	16.50 ± 9.16	8.84 ± 4.36	0.5
5i	14.60 ± 8.67	35.29 ± 21.98	2.4
5j	5.15 ± 3.01	17.91 ± 12.66	3.5
5k	3.00 ± 1.26	16.49 ± 10.56	5.5
5l	2.70 ± 0.55	47.94 ± 21.13	17.8
6ga	41.41 ± 25.89	47.86 ± 26.93	1.2
6gb	122.30 ± 59.31	128.10 ± 53.59	1.0
6gc	9.92 ± 6.20	8.112 ± 4.42	0.8
6gd	4.99 ± 2.32	10.12 ± 6.11	2.0
6gd'	1.90 ± 0.55	3.134 ± 2.28	4.2
6kb	27.99 ± 14.87	45.72 ± 34.86	1.6
6kc	30.44 ± 12.63	174.01 ± 129.21	5.7

Compound	U251 EphA2 Overexpressed	U251 Wild Type	Wild/ Overexpressed
6lc	3.41 ± 1.50	2.59 ± 1.24	0.8
6hc	5.66 ± 2.94	11.69 ± 7.361	2.1

Table VI. Inhibition of the cell proliferation of U251/U251 EphA2 cells

IC₅₀ values reported in μM with mean ± SD (n=4), and the selectivity index is calculated with IC₅₀s from different cell lines.

3.2.3 EphA2 activation

EphA2 overexpression has been identified in various different malignant cells [201, 202, 205, 206, 211, 212, 216, 220-223]. Decreased levels of EphA2-ligand combined with the overexpression of EphA2 in cancer cells lead to the aggressive growth of the tumor, which can be overcome *in vitro* by using endogenous EphA2 ligand or a small molecule ligand [211, 217, 218, 221, 224]. Our lead compound could induce EphA2 phosphorylation just as the endogenous ligand ephrin-A1, and it is necessary to determine if the new analogs could cause EphA2 activation as well [217].

Dimers 3e and 6gd' showed better activity to induce EphA2 phosphorylation at 2μM, with only 6gd' showed statistical significance (Figure 17). To our surprise, dimer 3d did not show clear EphA2 activation. Even 3d showed great activity and selectivity to EphA2 overexpressed cells. It is possible that 3d targeting EphA2 with some unknown different mechanism, which needs further investigation.

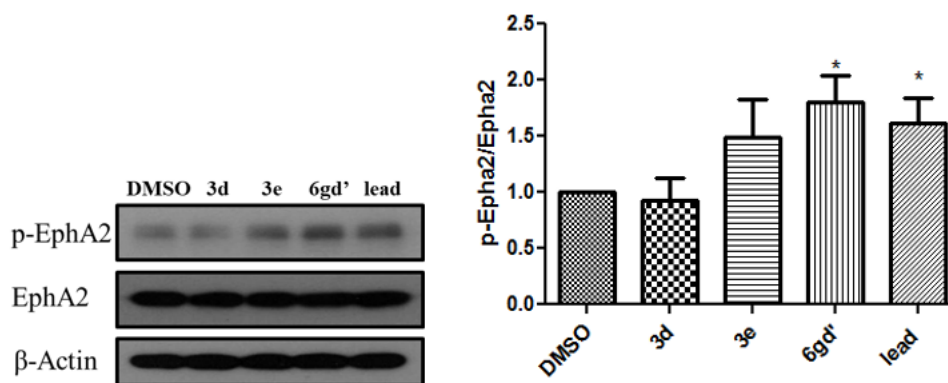


Figure 17. EphA2 activation of the new derivatives

U251 EphA2 cells were treated with the compounds with 2 μ M (in 0.1% DMSO) for 1hr and cell lysates were subject to immunoprecipitation and immunoblot for phosphorylated EphA/B kinases (pEphA/B) and total EphA2. Treatment with 2 μ M of lead was served as positive control. Treatment with 0.1% DMSO was served as vehicle control. The band intensities of the bands were quantified using ImageJ (NIH) to generate the figure. The figures are representative of 3 experiments. * $p < 0.05$ treatment vs. DMSO by unpaired t -test.

3.2.4 Log P value

Since the compounds are designed to be used for the treatment of GBM, whether they can cross BBB is critical for the potential application. Hansch and Leo found that blood-brain barrier penetration is optimal when the LogP values of the compounds are in the range of 1.5-2.7, with the mean value of 2.1 [225, 226]. Therefore, we measured LogP value of compounds 3d, 3e, and 6gd' to predict the potential capability of these compounds to cross BBB, and the lead compound was measured as a positive control. The results are listed in Table 7. The data reported here showed that dimers 3e and 6gd' showed similar LogP values to the lead compounds. Although the value is out of the range of the preferred LogP values indicated by Hansch, the lead compound can cross the BBB shown in our

previous study. We speculate that for these types of dimeric structures, may cross the BBB with an unknown mechanism instead of passive lipid penetration.

Compound	Log P (Mean±SD)
3d	1.28±0.03
3e	0.75±0.01
6gd'	0.78±0.03
Lead comp	0.71±0.02

Table VII. Log P values

The measurement was repeated three times with water and 1-octanol as the two solvents, and the results are presented as Mean±SD.

3.3 Conclusion

Based on the previous structure activity relationship, the dimeric structure of Doxazosin analog showed promising ligand binding activity to EphA2. To further study this unique structure a variety of structural moieties examined if they could further improve the activity, we synthesized 27 new derivatives and 15 which retain the dimeric structure. The dimers consist of different monomers and various linkers including alkyl, polyethylene glycol and aromatic or rigid structures. Two compounds 6gd' and 3d showed great potency and selectivity toward EphA2 overexpressed GBM cells. They also stimulated EphA2 phosphorylation, which demonstrated their targeting effect to EphA2 receptor. The LogP values of the two identified dimers are not in the ideal range for their capability to cross the BBB. However, the lead compound has a similar LogP value and does cross the BBB in our previous study [219], suggesting that these types of compounds may possess a novel

mechanism to cross the BBB other than passive lipid penetration, which will need further investigation.

3.4 Methods

3.4.1 Chemistry

Chemicals were commercially available and used as received without further purification unless otherwise noted. Moisture sensitive reactions were conducted under a dry argon atmosphere in flame-dried glassware. Solvents were distilled before use under argon. Thin-layer chromatography was performed on precoated silica gel F254 plates (Whatman). Silica gel column chromatography was performed using silica gel 60Å (Merck, 230-400 Mesh), and ethanol/dichloromethane was used as the elution solvent. Mass spectra were obtained on the electrospray mass spectrometer at Cleveland State University MS facility Center. The molecular weight of the compounds was examined with LC-MS. All the NMR spectra were recorded on a Bruker 400 MHz in DMSO-d₆. Chemical shifts (δ) for ¹H NMR spectra are reported in parts per million to residual solvent protons.

3.4.2 Organic compounds synthesis and identification

Compounds 3a-3f were prepared as the following procedure:

The dimethoxyquinazoline and piperazine were dissolved in n-BuOH with 1 to 5 mole ratio, and the mixture was heated to 100°C for 24 hours, then it was cooled down to room temperature. The precipitated white solid was collected via filtration and washed with n-BuOH. After it was dried, the solid was mixed with various linkers and K₂CO₃ in DMF. It was stirred until the reaction was completed. The reaction was quenched with Na₂CO₃

aqueous solution and stirred overnight, and the precipitated product was collected via filtration, washed with water, and dried to give the corresponding compounds.

1,4-bis(4-(4-amino-6,7-dimethoxyquinazolin-2-yl) piperazin-1-yl) butane-1,4-dione (3a) Light pink solid, 80% yield for the last step; ¹H-NMR (400MHz, DMSO-d₆) δ 7.44 (2H, s), 7.14 (4H, b), 6.76 (2H, s), 3.84 (6H, s), 3.81(10H, s) 3.70 (4H, s), 3.55-3.52 (4H, s), 2.63 (4H, s). ¹³C-NMR (400MHz, DMSO-d₆) δ 170.67, 161.62, 159.10, 158.82, 154.73, 149.35, 149.26, 145.50, 145.39, 105.73, 104.20, 103.44, 56.33, 55.89, 45.33, 44.25, 43.93, 41.73, 28.15. DUIS-MS calculated for C₃₂H₄₀N₁₀O₆ [M + H]⁺: 660.31, found: 661.

1,5-bis(4-(4-amino-6,7-dimethoxyquinazolin-2-yl) piperazin-1-yl) pentane-1,5-dione (3b). Light pink solid, 80% yield for the last step; ¹H-NMR (400MHz, DMSO-d₆) δ 7.43 (2H, s), 7.14 (4H, b), 6.75 (2H, s), 3.84 (6H, s), 3.80 (6H, s), 3.75 (4H, s), 3.70 (4H, s), 3.52 (8H, s), 2.43-2.40 (3H, t, J=7.1 Hz), 1.78 (2H, t, J= 14.0 Hz). ¹³C-NMR (400MHz, DMSO-d₆) δ 171.09, 161.62, 159.10, 158.79, 154.73, 149.35, 149.26, 145.50, 145.39, 105.72, 104.19, 103.44, 56.33, 55.89, 45.34, 44.33, 44.18, 43.94, 41.54, 32.41, 21.09. DUIS-MS calculated for C₃₃H₄₂N₁₀O₆ [M + H]⁺: 674.33, found: 675.

2,2'-oxybis(1-(4-(4-amino-6,7-dimethoxyquinazolin-2-yl)piperazin-1-yl) ethanone) (3c). Light pink solid, 72% yield for the last step; ¹H-NMR (400MHz, DMSO-d₆) δ 7.43 (2H, s), 7.15 (4H, b), 6.76 (4H, s), 4.31 (4H, s), 3.84 (6H, s), 3.79 (6H, s), 3.75(8H,s) 3.52 (8H, s) ¹³C-NMR (400MHz, DMSO-d₆)) δ 167.62, 161.63, 158.76, 154.73, 149.25, 145.52, 105.74, 104.18, 103.45, 69.64, 56.33, 55.89, 44.72, 44.28, 43.87, 41.66. DUIS-MS calculated for C₃₂H₄₀N₁₀O₇ [M + H]⁺: 676.31, found: 677.

Ethane-1,2-diyl bis(4-(4-amino-6,7-dimethoxyquinazolin-2-yl) piperazine-1-carboxylate) (3d) Light pink solid, 43% yield for the last step; ¹H-NMR (400MHz, DMSO-d₆) δ 7.43 (2H, s), 7.14 (4H, b), 6.75 (4H, s), 4.27 (4H, s), 3.83 (6H, s), 3.79 (6H, s), 3.78(8H, s), 3.45 (8H, s) ¹³C-NMR (400MHz, DMSO-d₆) δ 162.77, 161.63, 158.76, 155.00, 149.22, 145.52, 105.72, 104.19, 103.46, 63.67, 56.32, 55.87, 43.98, 43.80. DUIS-MS calculated for C₃₂H₄₀N₁₀O₈ [M + H]⁺: 692.30, found: 693.

Propane-2,2-diylbis(4,1-phenylene)bis(4-(4-amino-6,7-dimethoxyquinazolin-2-yl) piperazine-1-carboxylate) (3e). Light pink solid, 31% yield for the last step; ¹H-NMR (400MHz, DMSO-d₆) δ 7.45 (2H, s), 7.24-7.18 (8H, m), 7.07-7.06 (4H, m), 6.78(2H, s) 3.84 (9H, s), 3.80 (9H, s), 3.64 (4H, m) 3.50 (4H, m), 1.66 (6H, s). ¹³C-NMR (400MHz, DMSO-d₆) δ 161.67, 158.68, 154.77, 153.60, 149.51, 149.09, 147.45, 145.58, 127.75, 121.74. 105.66, 104.23, 103.48, 56.34, 55.91, 43.78, 42.38, 31.02. DUIS-MS calculated for C₄₅H₅₀N₁₀O₈ [M + H]⁺: 858.38, found: 859.

Cyclohexane-1,1-diylbis(4,1-phenylene)bis(4-(4-amino-6,7-dimethoxyquinazolin-2-yl) piperazine-1-carboxylate) (3f). Light pink solid, 31% yield for the last step; ¹H-NMR (400MHz, DMSO-d₆) δ 7.45 (2H, s), 7.31 (2H, s), 7.28 (2H, s), 7.18(4H, b) 7.06 (2H, s) , 7.04 (2H, s), 6.77 (2H, s) 3.84 (6H, s), 3.80 (13H, s), 3.63 (5H, m) 3.50 (6H, m), 2.25 (4H, s), 1.47 (6H, s). ¹³C-NMR (400MHz, DMSO-d₆) δ 161.66, 158.64, 154.78, 153.56, 149.26, 149.04, 145.59, 145.42, 128.04, 121.91, 105.64, 104.24, 103.47, 56.35, 55.92, 45.52, 43.78, 36.80, 26.17, 22.97. DUIS-MS calculated for C₄₈H₅₄N₁₀O₈ [M + H]⁺: 898.41, found: 899.

Compounds 4g-4l were prepared as the following procedure:

The dimethoxyquinazoline and piperazine product were mixed with various substituted acetyl chloride and K₂CO₃ in THF / H₂O one to one mixture. It was stirred until the reaction was completed. The reaction was quenched with Na₂CO₃ aqueous solution and stirred overnight, and the precipitated product was collected via filtration, washed with water, and dried to give the corresponding compounds.

(4-(4-amino-6,7-dimethoxyquinazolin-2-yl) piperazin-1-yl) (3-nitrophenyl) methanone (4g). Light yellow solid, 80% yield for the step; ¹H-NMR (400MHz, DMSO-d₆) δ 8.33-8.31 (1H, d, J= 8.2 Hz), 8.27 (1H, s), 7.92-7.90 (1H, d, J= 7.6 Hz), 7.79-7.75(1H, t, J= 15.9 Hz) 7.15(2H, b), 6.75 (1H, s), 3.84 (4H, s), 3.80 (4H, s), 3.74 (3H, m), 3.40 (1H, m). ¹³C-NMR (400MHz, DMSO-d₆) δ 167.39, 161.65, 158.78, 154.75, 149.22, 148.21, 145.58, 138.01, 133.92, 130.71, 124.72, 122.46, 105.73, 104.20, 103.50, 56.33, 55.89, 44.19, 42.23. DUIS-MS calculated for C₂₁H₂₂N₆O₅ [M + H]⁺: 438.17, found: 439.

(4-(4-amino-6,7-dimethoxyquinazolin-2-yl) piperazin-1-yl) (4-methyl-3-nitrophenyl) methanone (4h). Light yellow solid, 83% yield for the step; ¹H-NMR (400MHz, DMSO-d₆) δ 8.05, (1H, s), 7.70 (1H, s), 7.60 (1H, s), 7.44 (1H, s) 7.16 (2H, b), 6.74 (1H, s), 3.83 (4H, s), 3.80 (4H, s), 3.74 (4H, m), 3.42 (2H, m), 2.56(3H, s).¹³C-NMR (400MHz, DMSO-d₆) δ 167.37, 161.63, 158.76, 154.72, 149.28, 149.19, 145.55, 135.45, 134.52, 133.47, 132.12, 123.67, 105.70, 104.10, 103.48, 56.30, 55.88, 47.65, 44.19, 43.82, 42.23, 19.82. DUIS-MS calculated for C₂₂H₂₄N₆O₅ [M + H]⁺: 452.18, found: 453.

(4-(4-amino-6,7-dimethoxyquinazolin-2-yl) piperazin-1-yl) (4-chloro-3-nitrophenyl) methanone (4i). Light yellow solid, 72% yield for the step; ¹H-NMR (400MHz, DMSO-d₆) δ 8.18, (1H, s), 7.88-7.87 (1H, s), 7.80 (1H, s), 7.44 (1H, s) 7.17

(2H, b), 6.74 (1H, s), 3.83 (6H, s), 3.79 (5H, s), 3.73-3.60 (4H, m), 3.41 (2H, m.)¹³C-NMR (400MHz, DMSO-d₆) δ 166.45, 161.63, 158.71, 154.72, 149.12, 148.03, 145.56, 136.69, 132.76, 132.39, 126.40, 124.90, 105.66, 104.12, 103.46, 56.30, 55.89, 47.55, 44.18, 43.71, 42.32. DUIS-MS calculated for C₂₁H₂₁ClN₆O₅ [M + H]⁺: 472.13, found: 473.

(4-(4-amino-6,7-dimethoxyquinazolin-2-yl) piperazin-1-yl) (2-nitrophenyl) methanone (4j). Light yellow solid, 85% yield for the step; ¹H-NMR (400MHz, DMSO-d₆) δ 8.23-8.212, (1H, d, J= 8.0 Hz), 7.87 (1H, t, J= 6.9 Hz), 7.72 (1H, t, J= 7.3 Hz), 7.60-7.58 (1H, d, J= 7Hz) 7.44 (1H, s), 7.17 (2H, b) 6.74 (1H, s), 3.83 (5H, s), 3.79 (4H, s), 3.72 (3H, m), 3.26 (2H, m)-NMR (400MHz, DMSO-d₆) δ 166.02, 161.65, 158.77, 154.72, 149.16, 145.91, 145.59, 133.36, 132.89, 130.77, 128.62, 125.23, 105.71, 104.15, 103.51, 56.31, 55.89, 46.95, 43.95, 43.65, 41.88. DUIS-MS calculated for C₂₁H₂₂N₆O₅ [M + H]⁺: 438.17, found: 439.

(4-(4-amino-6,7-dimethoxyquinazolin-2-yl) piperazin-1-yl) (4-nitrophenyl) methanone (4k). Light yellow solid, 87% yield for the step; ¹H-NMR (400MHz, DMSO-d₆) 8.30, 8.28, (1H, d, J= 7.9 Hz), 8.25-8.23 (1H, d, J= 7.9), 8.13-8.11 (1H, d, J= 8.1Hz), 7.74-7.72 (1H, d, J = 8.0 Hz), 7.47-7.45 (1H, d, J= 7.0 Hz) 7.19 (2H, b), 6.76-6.75(1H, d, J= 5.9 Hz), 3.94 (2H, s), 3.83 (4H, s), 3.80 (3H, s), 3.73 (2H, s) 3.35 (1H, s), 3.12 (1H, s).¹³C-NMR (400MHz, DMSO-d₆) δ 167.73, 167.39, 161.74, 161.65, 158.66, 158.35, 154.78, 154.73, 149.38, 149.05, 148.95, 148.29, 145.78, 145.58, 142.80, 130.77, 128.86, 124.25, 123.64, 105.70, 105.64, 104.19, 103.61, 103.48, 56.33, 55.90, 47.43, 44.22, 43.77, 43.08, 42.16, 41.36. DUIS-MS calculated for C₂₁H₂₂N₆O₅ [M + H]⁺: 438.17, found: 439.

(4-(4-amino-6,7-dimethoxyquinazolin-2-yl) piperazin-1-yl) (2-chloro-4-nitrophenyl) methanone (4l). Light yellow solid, 79% yield for the step; ¹H-NMR (400MHz, DMSO-d₆) δ 8.42 (1H, s), 8.30-8.28 (1H, d, J= 7.5 Hz), 7.76-7.74 (1H, d, J= 7.8) 7.43 (1H, s), 7.17 (2H, b), 6.76-6.74 (1H, d, J= 7.0), 3.83 (4H, s), 3.79 (4H, s), 3.73 (3H, s), 3.22 (1H, s). ¹³C-NMR (400MHz, DMSO-d₆) δ 164.61, 161.64, 161.58, 159.09, 158.68, 154.72, 154.67, 149.33, 149.13, 148.60, 145.60, 145.37, 145.31, 130.86, 129.71, 125.15, 123.39, 105.70, 104.20, 104.12, 103.50, 103.39, 56.31, 55.89, 46.62, 44.21, 44.17, 43.76, 41.81. DUIS-MS calculated for C₂₁H₂₁ClN₆O₅ [M + H]⁺: 472.13, found: 473.

Compounds 5g- 5l was prepared as the following procedure:

Last step products with the nitro group were reduced by using NH₄Cl 5 molar equivalence and Zn 15 molar equivalence to the nitro compounds. This was monitored by TLC in DCM/MeOH until reaction was complete it was then stopped by using an Acid base extraction. Acid was added until all zinc was dissolved then filtered to remove any undissolved zinc or other contaminates. Follow by readjusting the pH to a basic 12 by adding sodium carbonate aqueous solution. This mixture was then extracted by DCM and ethyl acetate then was dried with MgSO₄ and washed with diethyl ether and hexane to give the corresponding compounds.

(4-(4-amino-6,7-dimethoxyquinazolin-2-yl) piperazin-1-yl) (3-aminophenyl) methanone (5g). Light yellow solid, 89% yield for the last step; ¹H-NMR (400MHz, DMSO-d₆) δ 7.43 (1H, s), 7.15 (2H, b), 7.10-7.06 (1H, t, J= 7.7 Hz), 6.74 (1H, s), 6.64-6.2 (1H, d, J= 8.0 Hz), 6.59 (1H, s), 6.53-6.51 (1H, d, J= 7.4 Hz), 3.83 (3H, s), 3.79 (3H, s), 3.75 (4H, m), 3.62-3.59 (2H, t, J= 16.5 Hz), 3.42 (2H, b). ¹³C-NMR (400MHz, DMSO-d₆) δ 170.30, 161.61, 158.80, 154.72, 149.20, 145.54, 137.13, 129.32, 115.25, 114.43,

112.63 105.71, 104.18, 103.47, 56.33, 55.89, 44.17. DUIS-MS calculated for C₂₁H₂₁N₆O₅ [M + H]⁺: 408.19, found: 409.

(3-amino-4-methylphenyl) (4-(4-amino-6,7-dimethoxyquinazolin-2-yl) piperazin-1-yl) methanone (5h). Light yellow solid, 77% yield for the step; ¹H-NMR (400MHz, DMSO-d₆) δ 7.43 (1H, s), 7.14 (2H, b), 6.99-6.97 (1H, d, J= 7.7 Hz), 6.74 (1H, s), 6.67 (1H, s), 6.50-6.49 (1H, s, J= 3 Hz), 5.02 (2H, b) 3.83 (3H, s), 3.80 (4H, m), 3.723-3.40 (8H, m), 2.08(3H, s). ¹³C-NMR (400MHz, DMSO-d₆) δ 170.41, 161.65, 154.82, 147.06, 145.76, 134.53, 130.16, 123.04, 1114.97, 112.95, 104.51, 103.31, 56.45, 56.10, 55.98, 44.37, 17.80. DUIS-MS calculated for C₂₂H₂₆N₆O₃ [M + H]⁺: 422.21, found: 423.

(3-amino-4-chlorophenyl) (4-(4-amino-6,7-dimethoxyquinazolin-2-yl) piperazin-1-yl) methanone (5i). Light yellow solid, 77% yield for the step; ¹H-NMR (400MHz, DMSO-d₆) δ 7.44 (1H, s), 7.25 (1H, s), 7.18, (2H, s), 6.84 (1H, s), 6.74 (1H, s), 6.57 (1H, s) 5.57 (2H, b), 3.83 (3H, s), 3.79 (5H, m), 3.64 (5H, m). ¹³C-NMR (400MHz, DMSO-d₆) δ 169.27, 161.62, 158.78, 154.69, 149.17, 145.52, 145.22, 135.92, 129.46, 118.40, 115.58, 114.29, 105.68, 104.12, 103.48, 56.30, 55.89, 47.59, 44.17, 42.17. DUIS-MS calculated for C₁₇H₂₃N₅O₃ [M + H]⁺: 442.15, found: 443.

(4-(4-amino-6,7-dimethoxyquinazolin-2-yl) piperazin-1-yl) (2-aminophenyl) methanone (5j). Light yellow solid, 78% yield for the step; ¹H-NMR (400MHz, DMSO-d₆) δ 7.43 (1H, s), 7.15-7.11 (3H, m), 7.04 (1H, s), 6.74 (2H, s) 6.58 (1H, b), 5.19 (2H, s), 3.83 (4H, s), 3.79 (7H, s), 3.53 (4H, m). ¹³C-NMR (400MHz, DMSO-d₆) δ 169.28, 161.61, 158.81, 154.70, 149.22, 146.32, 145.50, 130.50, 128.29, 119.80, 116.01, 105.70, 104.14, 103.45, 56.31, 55.88, 44.20, 30.89. DUIS-MS calculated for C₂₁H₂₄N₆O₃ [M + H]⁺: 408.19, found: 409.

(4-(4-amino-6,7-dimethoxyquinazolin-2-yl) piperazin-1-yl) (4-aminophenyl) methanone (5k). Light yellow solid, 78% yield for the step; ¹H-NMR (400MHz, DMSO-d₆) δ 7.43 (1H, s), 7.19-7.17 (3H, m), 6.74 (1H, s), 6.59 (1H, s) 6.56 (1H, d), 5.53 (2H, s), 3.83 (3H, s), 3.79 (3H, s), 3.76 (4H, s) 3.56 (4H, s). ¹³C-NMR (400MHz, DMSO-d₆) 170.55, 161.61, 158.82, 154.70, 150.99, 149.24, 145.48, 129.80, 122.44, 113.19, 105.70, 104.16, 103.44, 56.31, 55.88, 44.22. DUIS-MS calculated for C₂₁H₂₄N₆O₃ [M + H]⁺: 408.19, found: 409.

(4-amino-2-chlorophenyl) (4-(4-amino-6,7-dimethoxyquinazolin-2-yl) piperazin-1-yl) methanone (5l). Light yellow solid, 72% yield for the step; ¹H-NMR (400MHz, DMSO-d₆) δ 7.43 (1H, s), 7.14, (2H, b), 7.01-6.99, (1H, d, J= 7.5 Hz), 6.73 (1H, s) 6.63 (1H, s), 6.55- 6.53 (1H, d, J= 7.5 Hz), 5.63 (2H, s) 3.83 (4H, s) 3.79 (5H, s), 3.65-3.60 (8H, m), 3.25 (2H, s), 3.17(2H, s) ¹³C-NMR (400MHz, DMSO-d₆) δ 167.25, 161.61, 158.77, 154.70, 151.04, 149.17, 145.54, 130.48, 129.40, 122.63, 113.56, 112.90, 105.70, 104.13, 103.47, 56.32, 55.90, 49.07, 46.91, 44.34, 43.94, 41.83. DUIS-MS calculated for C₁₉H₂₁N₅O₄ [M + H]⁺: 442.15, found: 443.

Compounds 6ga-6hc were prepared as the following procedure:

The corresponding reduced benzamides 5g-5l were mixed with different dichloride linkers. They were dissolved in anhydrous DMF in a 2 to 1 ratio under argon protection. The dichloride linkers were diluted in anhydrous DMF and added slowly. It was stirred overnight and monitored by TLC after 24 hours. The reaction was stopped by reducing the solvent and purified with PTLC in DCM/EtOH.

N1, N4-bis(3-(4-(4-amino-6,7-dimethoxyquinazolin-2-yl) piperazine-1-carbonyl) phenyl) succinamide (6ga). Light yellow solid, 70% yield for the last step; ¹H-NMR

(400MHz, DMSO-d6) δ 10.32 (2H, s), 8.55 (4H, s), 7.83(2H, s), 7.70 (2H, s) 7.64-7.62 (2H, d, J= 7.0 Hz), 7.42-7.38(2H, t, J= 14 Hz), 7.12-7.10 (2H, d, J= 7.8 Hz), 3.92 (8H, m), 3.86 (8H, s), 3.84 (7H, s) 3.76 (4H, m) 3.53 (5H, m) 2.71 (4H, s). ¹³C-NMR (400MHz, DMSO-d6) δ 171.18, 169.60, 161.74, 155.59, 147.08, 139.91, 129.38, 121.93, 120.57, 118.05, 105.29, 102.39, 56.68, 56.43, 45.00, 31.68. DUIS-MS calculated for C₄₆H₅₀N₁₂O₈ [M + H]⁺: 898.39, found: 899.

N1, N5-bis(3-(4-(4-amino-6,7-dimethoxyquinazolin-2-yl) piperazine-1-carbonyl) phenyl) glutaramide (6gb). Light yellow solid, 70% yield for the last step; ¹H-NMR (400MHz, DMSO-d6) 10.09 (2H, s), 7.45 (2H, s), 7.64-7.62 (2H, m), 7.43 (2H, s) 7.40-7.38 (4H, m), 7.14-7.10(6H, m), 6.74 (2H, d), 3.92 (8H, m), 3.83 (9H, m), 3.79 (18H, m) 2.41 (4H, s) 1.93 (2H, s).¹³C-NMR (400MHz, DMSO-d6) δ 171.57, 169.44, 161.62, 158.79, 154.72, 149.18, 145.55, 139.77, 136.78, 129.33, 121.98, 120.50, 118.15, 105.71, 104.15, 103.48, 56.31, 55.89, 47.55, 44.06, 36.03, 21.28. DUIS-MS calculated for C₄₇H₅₂N₁₂O₈ [M + H]⁺: 912.40, found: 913.

2,2'-oxybis(N-(3-(4-(4-amino-6,7-dimethoxyquinazolin-2-yl)piperazine-1-carbonyl) phenyl) acetamide) (6gc). Light yellow solid, 73% yield for the last step; ¹H-NMR (400MHz, DMSO-d6) δ 10.26 (2H, s), 7.82 (2H, s), 7.74-7.73 (2H, d, J= 6.7 Hz), 7.44 (4H, m) 7.15 (5H, b), 6.74 (2H, d), 4.31 (3H, s) 3.82 (8H, s), 3.79 (9H, m).¹³C-NMR (400MHz, DMSO-d6) δ 169.30, 168.82, 162.78, 161.62, 158.80, 154.71, 149.19, 145.55, 138.83, 129.44, 122.71, 121.16, 118.79, 105.71, 104.17, 103.49, 71.31, 56.32, 55.88, 47.64, 44.18, 42.26, 36.24, 31.25. DUIS-MS calculated for C₄₆H₅₀N₁₂O₉ [M + H]⁺: 914.38, found: 915.

Ethane-1,2-diylbis((3-(4-(4-amino-6,7-dimethoxyquinazolin-2-yl)piperazine-1-carbonyl) phenyl) carbamate) (6gd). Light yellow solid, 30% yield for the last step; ¹H-NMR (400MHz, DMSO-d₆) δ 9.94 (2H, s), 7.57-7.54 (4H, m), 7.43 (3H, s), 7.37 (2H, s) 7.14 (5H, b), 7.07-7.05 (2H, d), 6.74 (3H, s) 4.37 (4H, s) 3.83 (11H, s), 3.79 (11H, m). ¹³C-NMR (400MHz, DMSO-d₆) δ 169.38, 161.62, 158.78, 154.71, 153.81, 149.18, 145.54, 139.58, 136.91, 129.44, 121.52, 119.75, 117.30, 105.70, 104.15, 103.47, 63.27, 62.49, 56.31, 55.88, 47.56, 44.12, 42.18, 25.95. DUIS-MS calculated for C₄₆H₅₀N₁₂O₁₀ [M + H]⁺: 930.38, found: 931.

(Ethane-1,2-diylbis(oxy))bis(ethane-2,1-diylbis((3-(4-(4-amino-6,7-dimethoxyquinazolin-2-yl) piperazine-1-carbonyl) phenyl) carbamate) (6gd'). Light yellow solid, 23% yield for the last step; ¹H-NMR (400MHz, DMSO-d₆) δ 9.92 (2H, s), 7.57-7.53 (4H, m), 7.43 (2H, s), 7.37-7.36 (2H, s) 7.14 (4H, b), 7.06-7.04 (2H, d), 6.74 (2H, s) 4.22 (3H, s) 3.83 (9H, s), 3.79 (10H, m), 3.67 (4H, s), 3.59 (4H, s). ¹³C-NMR (400MHz, DMSO-d₆) δ 169.41, 162.77, 161.62, 158.78, 154.70, 153.96, 149.19, 145.53, 139.70, 136.90, 129.41, 121.38, 119.61, 117.15, 105.71, 104.14, 103.47, 70.18, 69.15, 64.12, 60.69, 56.31, 55.88, 47.64, 44.17, 42.24, 36.24, 31.25. DUIS-MS calculated for C₅₀H₅₈N₁₂O₁₂ [M + H]⁺: 1018.43, found: 1019.

N1, N5-bis(4-(4-(4-amino-6,7-dimethoxyquinazolin-2-yl) piperazine-1-carbonyl) phenyl) glutaramide (6kb). Light yellow solid, 70% yield for the last step; ¹H-NMR (400MHz, DMSO-d₆) 10.15 (2H, s), 7.71-7.69 (4H, m), 7.44-7.40 (7H, d), 7.16 (6H, m), 6.74 (3H, d), 3.83 (10H, m), 3.79 (13H, m), 3.56 (9H, m) 2.44 (4H, s) 1.93 (2H, s). ¹³C-NMR (400MHz, DMSO-d₆) δ 171.61, 169.51, 161.62, 158.78, 154.70, 154.52, 149.20, 145.51, 140.99, 130.58, 128.94, 128.60, 120.88, 118.94, 105.69, 104.15, 103.45, 56.31,

55.88, 44.17, 36.06, 21.29. DUIS-MS calculated for C₄₇H₅₂N₁₂O₈ [M + H]⁺: 912.40, found: 913.

2,2'-oxybis(N-(4-(4-(4-amino-6,7-dimethoxyquinazolin-2-yl)piperazine-1-carbonyl) phenyl) acetamide) (6kc). Light yellow solid, 70% yield for the last step; ¹H-NMR (400MHz, DMSO-d₆) δ 10.27 (2H, s), 7.78 (2H, s), 7.77 (2H, s), 7.47 (2H, s), 7.45 (2H, s), 7.43 (2H, s), 7.15 (4H, m), 6.74 (2H, s), 4.33 (4H, s), 3.83 (10H, s), 3.79 (11H, m), 3.61-3.56 (8H, m). ¹³C-NMR (400MHz, DMSO-d₆) δ 169.40, 168.88, 161.62, 158.77, 154.71, 149.18, 145.52, 139.99, 131.34, 128.64, 119.61, 105.68, 104.15, 103.45, 71.33, 56.31, 55.88, 44.13. DUIS-MS calculated for C₄₆H₅₀N₁₂O₉ [M + H]⁺: 914.38, found: 915.

2,2'-oxybis(N-(4-(4-(4-amino-6,7-dimethoxyquinazolin-2-yl)piperazine-1-carbonyl)-3-chlorophenyl) acetamide) (6lc). Light yellow solid, 43% yield for the last step; ¹H-NMR (400MHz, DMSO-d₆) δ 10.32 (2H, s), 7.97 (2H, s), 7.68-7.66 (2H, d, J= 8.0 Hz), 7.44 (2H, s), 7.41-7.39 (2H, s), 7.18 (5H, m), 6.74 (3H, s), 4.33 (4H, s), 3.83 (13H, s), 3.75 (11H, s), 3.72 (11H, m), 3.24 (6H, m). ¹³C-NMR (400MHz, DMSO-d₆) δ 169.09, 166.09, 161.63, 158.64, 154.74, 148.97, 145.60, 145.48, 140.35, 131.20, 129.89, 129.02, 120.15, 118.86, 105.61, 105.42, 104.27, 104.16, 103.48, 103.35, 71.13, 56.32, 55.90, 46.78, 44.31, 44.16, 43.88, 41.79. DUIS-MS calculated for C₄₆H₄₈Cl₂N₁₂O₉ [M + H]⁺: 982.30, found: 983.

2,2'-oxybis(N-(5-(4-(4-amino-6,7-dimethoxyquinazolin-2-yl)piperazine-1-carbonyl)-2-methylphenyl) acetamide) (6hc). Light yellow solid, 23% yield for the last step; ¹H-NMR (400MHz, DMSO-d₆) δ 9.62 (2H, s), 7.60 (2H, s), 7.43 (2H, s), 7.34-7.32 (2H, d, J= 7.0 Hz), 7.21-7.19 (2H, d, J= 7.6 Hz), 7.15 (4H, b), 6.74 (2H, s), 4.33 (4H, s)

3.83 (9H, s), 3.79 (11H, s), 2.29 (6H, m) 1.36 (3H, s).¹³C-NMR (400MHz, DMSO-d₆) δ 169.16, 168.46, 161.62, 158.77, 154.71, 149.20, 145.52, 135.90, 134.08, 133.91, 130.91, 124.73, 124.29, 105.71, 104.15, 103.46, 71.09, 56.31, 55.88, 44.16, 34.85, 30.90, 18.09. DUIS-MS calculated for C₄₈H₅₄N₁₂O₉ [M + H]⁺: 942.41, found: 943.

3.4.3 Log P measurement

Compounds 3d, 3e, 6gd' and lead compound was used in the determination of their log P values. This method follows the OECD test guidelines for the slow stir method, with slight modification due to the data collection method. The data were collected on a UV-Vis spectrophotometer Shimadzu UV-1280 and standard UV Quartz 10 mm cuvette was used. The chemical was purchased from VWR brand EMPLURA 1-octanol 99% purity. The Flask was equipped with Teflon coated magnetic stirrers and Coring PC420D stir plates where used. The 1-octanol and DDH₂O were placed into two separate containers containing both phases to become mutually saturated by allowing them to stir for 48 h. Then the two phases were separated by a separation funnel. Compounds 3d, 3e, 6gd' and lead now were dissolved in 1-octanol pre-saturated with water. These stock solutions are then centrifuged at 5,000 rpm for 5 min. The supernatant was taken to be the working solution. Take 5 mL working solution of each into new clear flask, and add identical volume water saturated with 1-octanol, then stir at room temperature for 48 h. After that, stop stirring; take two-phase solution out, centrifuge at 5,000 rpm for 5 min to separate this two-phase system. Removal of the 1-octanol phase from the solution is then transferred for UV spectrophotometry to achieve absorbance at the correct wavelength. According to the procedure, concentrations were determined by UV measurement so, equation written as:

$$\text{Log P} = \log \frac{A_x}{A_0 - A_x}$$

Where A_0 and A_x are the initial and final absorbance values of organic layer.

3.4.4 Cell culture and antibodies

U251 cells were obtained from ATCC (Rockville, MD). The cells were maintained in Dulbecco's Modified Eagle Medium (DMEM) supplemented with 10% fetal bovine serum (FBS), 10 mg/ml L-Glutamine, 100 U/mL penicillin-streptomycin, and 0.1 mg/ml streptomycin. EphA2 overexpression cells were grown in the presence of 1 μ g/ml puromycin. Cell cultures were grown at 37 °C, in a humidified atmosphere of 5% CO₂ in a Thermo CO₂ incubator (Grand Island, NY). Antibodies used included rabbit polyclonal antibodies against pEphA/B (Santa Cruz, Santa Cruz, CA), as well as mouse monoclonal antibody to EphA2 (clone D7, Millipore, Billerica, MA).

3.4.5 Mammalian cell viability analysis

The MTT assay was used to examine the effect of the compounds on the growth of U251 and U251 over expression EphA2 cells in four replications. 3000 cells per well were seeded with RPMI1640 medium in 96-well flat-bottomed plates for 24 h and were then exposed to various concentrations of test compounds dissolved in DMSO (final concentration \leq 0.1%) in medium for 48 h. Controls received DMSO at a same concentration as that in drug-treated cells. Cells were incubated in 200 μ L of 0.5 mg/mL of MTT reagent diluted in fresh media at 37°C for 3 h. Supernatants were removed from the wells, and the reduced MTT dye was solubilized with 200 μ L/well DMSO. Absorbance at 570 nm was determined on a SpectraMax Plus384 spectrophotometer (Molecular

Devices). Data obtained with quadruplication were normalized and fitted to a dose–response curve using GraphPad Prism v.5 (GraphPad).

3.4.6 EphA2 activation.

U251 EphA2-overexpressing cells were plated in 6-well dishes at a density of 100,000 cells/well and grown for 24 hours prior to stimulation with appropriate compounds for 30 min. 0.1% DMSO was used as vehicle control. Following treatment, cells were washed and lysed in modified RIPA Buffer (20 mM Tris-HCl pH 7.4, 20 mM NaF, 150 mM NaCl, 10% glycerol, 0.1% SDS, 0.5% DCA, 2 mM EDTA, 1% Triton X-100, 2 mM Na₃VO₄, and protease inhibitors, including 1 mM phenylmethylsulphonyl fluoride, and 2 µg/ml each of aprotinin and leupeptin) for 20 min, followed by immunoprecipitation. Samples were boiled 5 min and run on 4-12% Bis-Tris Plus gels (Thermo Fisher), followed by transfer to Immobilon-P PVDF membranes (Millipore, Billerica, MA). Membranes were blocked 1 hr at room temperature in 3% BSA in TBS containing 0.05% Tween-20 (TBS-T) followed by overnight incubation with pEphA/B (1:500) and EphA2 (Santa Cruz) (1:1000) primary antibodies. Membranes were washed in TBS-T and incubated with goat anti-rabbit-HRP (1:5000) secondary antibody 1 hr at room temperature, followed by washing and developing with Luminol Reagent (Santa Cruz). Band intensities were quantified using ImageJ (NIH) to generate the figure.

Acknowledgements

This work was supported by grants from the National Institutes of Health to BW (1R01NS096956-01) and National Science Foundation Major Research Instrumentation Grants (CHE-0923398 and CHE-1126384).

CHAPTER IV

CONCLUSION AND FUTURE DIRECTION

The first study focuses on the identification of Flagellum attachment zone 1 (FAZ1) filament within *T.b. brucei* as a unique target for new drug development. The research initiated at a high throughput screen of the library of pharmaceutical active compounds to identify lead compounds Prazosin and Doxazosin with a core 6,7 dimethoxyquinazoline pharmacophore. A biotin-conjugated molecular probe was designed to capture interacting binding partners in a pulldown assay. FAZ1 filament was identified and further confirmed via western blot to be an interacting partner of the probe. Furthermore, A FAZ1 F2H HA HA tagged cell line was generated to explore FAZ1 via immunofluorescence and it showed slight co-localization of the 6,7 dimethoxyquinazoline pharmacophore. The study built a foundation for potential FAZ1 inhibitor development selectively targeting trypanosome cells.

The second project focused on the EphA2 agonist development based on 6,7 dimethoxyquinazoline pharmacophore derivatives. Overexpression of EphA2, a receptor tyrosine kinase that regulates cancer cell migration, has been well documented in GBM and is correlated with malignant progression and poor prognosis [201, 202, 205, 206, 211,

212, 216, 220-223]. EphA2 activation by its ligand, ephrin-A1, has been shown to suppress tumor progression, including inducing apoptosis, inhibiting cell proliferation, and suppressing cell migration. However, EphA2 overexpression is often accompanied by a reduced expression or mis-localization of ephrin-A1, resulting in frequent Akt activation, which promotes ligand-independent pro-invasive Akt-EphA2 crosstalk. However, the endogenous ligand of EphA2, ephrin-A1, cannot effectively pass the blood-brain barrier (BBB), making it less useful for treating GBM with overexpression of EphA2. Our research led to small molecule agonists for EphA2, which have demonstrated superior activity and the capability to cross the BBB.

In conclusion, my research demonstrated the potential of 6,7 dimethoxyquinazoline pharmacophore as a core structure to design promising small molecule drugs for the treatment of HAT and EphA2 overexpressed cancer. The SAR summarized in the study provides good rationale for further lead optimization. The potential orally activity of these type of compounds particularly makes it valuable since oral form of drugs are much easy to be administered.

As a continuing part of the project, Figure 18 has three schemes which will be fundamental in designing the new libraries. These compounds could be screened using either trypanosome cells or EphA2 overexpressed cancer cells to identify new candidates for HAT or cancer.

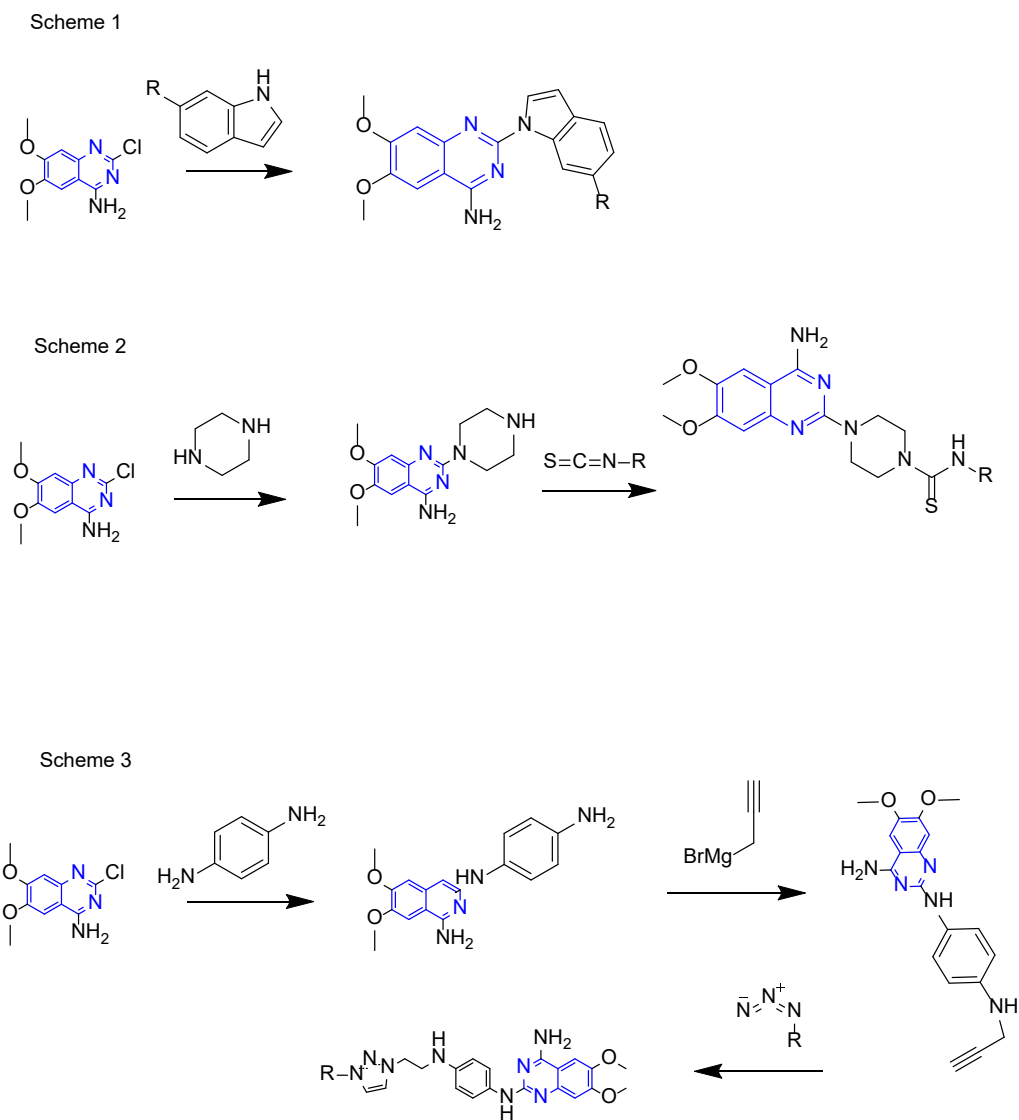


Figure 18. Schemes for drug discovery based on 6,7 dimethoxyquinazoline

BIBLIOGRAPHY

- [1] C. G. Wermuth, D. Aldous, P. Raboisson, and D. Rognan, “the practice of medicinal chemistry,” in *The Practice of Medicinal Chemistry*, Elsevier, 2015, pp. i–iii. doi: 10.1016/b978-0-12-417205-0.00036-5.
- [2] G. Sittampalam *et al.*, “Assay Guidance Manual,” *Assay Guidance Manual*, no. Md, pp. 305–336, 2016, doi: PMID:22553881.
- [3] T. L. Riss *et al.*, “Cell Viability Assays,” *Assay Guidance Manual*, no. Md, pp. 1–25, 2004, [Online]. Available: <http://www.ncbi.nlm.nih.gov/pubmed/23805433>
- [4] J. Hou, X. Liu, J. Shen, G. Zhao, and P. G. Wang, “The impact of click chemistry in medicinal chemistry,” *Expert Opin Drug Discov*, vol. 7, no. 6, pp. 489–501, 2012, doi: 10.1517/17460441.2012.682725.
- [5] J. J. TOPCZEWSKI and E.-C. LIU, “Chemical libraries from a double click,” *Nature*, vol. 574, pp. 42–43, 2019.
- [6] J. Song, S. Jang, J. W. Lee, D. Jung, S. Lee, and K. H. Min, “Click chemistry for improvement in selectivity of quinazoline-based kinase inhibitors for mutant epidermal growth factor receptors,” *Bioorg Med Chem Lett*, vol. 29, no. 3, pp. 477–480, 2019, doi: 10.1016/j.bmcl.2018.12.020.
- [7] X. Jiang *et al.*, “Recent applications of click chemistry in drug discovery,” *Expert Opin Drug Discov*, vol. 14, no. 8, pp. 779–789, 2019, doi: 10.1080/17460441.2019.1614910.
- [8] E. Bonandi, M. S. Christodoulou, G. Fumagalli, D. Perdicchia, G. Rastelli, and D. Passarella, “The 1,2,3-triazole ring as a bioisostere in medicinal chemistry,” *Drug*

- Discov Today*, vol. 22, no. 10, pp. 1572–1581, 2017, doi: 10.1016/j.drudis.2017.05.014.
- [9] R. Kharb, P. C. Sharma, and M. S. Yar, “Pharmacological significance of triazole scaffold,” *J Enzyme Inhib Med Chem*, vol. 26, no. 1, pp. 1–21, 2011, doi: 10.3109/14756360903524304.
- [10] Y. Chen and Z. R. Tong, *Click chemistry: Approaches, applications and challenges*. 2017.
- [11] H. Chen, X. Zhou, A. Wang, Y. Zheng, Y. Gao, and J. Zhou, “Evolutions in fragment-based drug design: The deconstruction-reconstruction approach,” *Drug Discovery Today*, vol. 20, no. 1. Elsevier Ltd, pp. 105–113, 2015. doi: 10.1016/j.drudis.2014.09.015.
- [12] P. Kirsch, A. M. Hartman, A. K. H. Hirsch, and M. Empting, “Concepts and core principles of fragment-based drug design,” *Molecules*, vol. 24, no. 23. MDPI AG, Nov. 26, 2019. doi: 10.3390/molecules24234309.
- [13] B. C. Doak, R. S. Norton, and M. J. Scanlon, “The ways and means of fragment-based drug design,” *Pharmacol Ther*, vol. 167, pp. 28–37, Nov. 2016, doi: 10.1016/j.pharmthera.2016.07.003.
- [14] C. W. Murray and T. L. Blundell, “Structural biology in fragment-based drug design,” *Current Opinion in Structural Biology*, vol. 20, no. 4. pp. 497–507, Aug. 2010. doi: 10.1016/j.sbi.2010.04.003.
- [15] P. J. Hajduk and J. Greer, “A decade of fragment-based drug design: Strategic advances and lessons learned,” *Nature Reviews Drug Discovery*, vol. 6, no. 3. pp. 211–219, Mar. 2007. doi: 10.1038/nrd2220.

- [16] A. Kumar, A. Voet, and K. Y. J. Zhang, "Send Orders of Reprints at reprints@benthamscience.org Fragment Based Drug Design: From Experimental to Computational Approaches," 2012. [Online]. Available: <http://fbdd-lit.blogspot.com/>].
- [17] Y. Bian and X. Q. (Sean) Xie, "Computational Fragment-Based Drug Design: Current Trends, Strategies, and Applications," *AAPS Journal*, vol. 20, no. 3. Springer New York LLC, May 01, 2018. doi: 10.1208/s12248-018-0216-7.
- [18] Paul. Leff, *Receptor-based drug design*. M. Dekker, 1998.
- [19] P. Kirsch, A. M. Hartman, A. K. H. Hirsch, and M. Empting, "Concepts and core principles of fragment-based drug design," *Molecules*, vol. 24, no. 23. MDPI AG, Nov. 26, 2019. doi: 10.3390/molecules24234309.
- [20] C. W. Murray and T. L. Blundell, "Structural biology in fragment-based drug design," *Current Opinion in Structural Biology*, vol. 20, no. 4. pp. 497–507, Aug. 2010. doi: 10.1016/j.sbi.2010.04.003.
- [21] A. A. LANDS ARNOLD J P McAULIFF F P LUDUENA T G BROWN, "Chemical Constitution and Pharmaco-dynamic Action," Marcel Dekker, Inc, 1948.
- [22] P. J. Hajduk and J. Greer, "A decade of fragment-based drug design: Strategic advances and lessons learned," *Nature Reviews Drug Discovery*, vol. 6, no. 3. pp. 211–219, Mar. 2007. doi: 10.1038/nrd2220.
- [23] H. Chen, X. Zhou, A. Wang, Y. Zheng, Y. Gao, and J. Zhou, "Evolutions in fragment-based drug design: The deconstruction-reconstruction approach," *Drug*

- Discovery Today*, vol. 20, no. 1. Elsevier Ltd, pp. 105–113, 2015. doi: 10.1016/j.drudis.2014.09.015.
- [24] B. C. Doak, R. S. Norton, and M. J. Scanlon, “The ways and means of fragment-based drug design,” *Pharmacol Ther*, vol. 167, pp. 28–37, Nov. 2016, doi: 10.1016/j.pharmthera.2016.07.003.
- [25] A. Kumar, A. Voet, and K. Y. J. Zhang, “Send Orders of Reprints at reprints@benthamscience.org Fragment Based Drug Design: From Experimental to Computational Approaches,” 2012. [Online]. Available: <http://fbdd-lit.blogspot.com/>].
- [26] P. J. Hajduk and J. Greer, “A decade of fragment-based drug design: Strategic advances and lessons learned,” *Nature Reviews Drug Discovery*, vol. 6, no. 3. pp. 211–219, Mar. 2007. doi: 10.1038/nrd2220.
- [27] H. Chen, X. Zhou, A. Wang, Y. Zheng, Y. Gao, and J. Zhou, “Evolutions in fragment-based drug design: The deconstruction-reconstruction approach,” *Drug Discovery Today*, vol. 20, no. 1. Elsevier Ltd, pp. 105–113, 2015. doi: 10.1016/j.drudis.2014.09.015.
- [28] “quinazolines-an-illustrated-review”.
- [29] T. P. Selvam and P. V. Kumar, “Quinazoline Marketed drugs-A Review,” 2011. [Online]. Available: www.researchinpharmacy.com
- [30] G. A. Khodarahmi, E. Jafari, M. R. Khajouei, F. Hassanzadeh, G. H. Hakimelahi, and G. A. Khodarahmi, “Quinazolinone and quinazoline derivatives: recent structures with potent antimicrobial and cytotoxic activities,” 2016.

- [31] D. J. Connolly, D. Cusack, T. P. O'Sullivan, and P. J. Guiry, "Synthesis of quinazolinones and quinazolines," *Tetrahedron*, vol. 61, no. 43. pp. 10153–10202, Oct. 24, 2005. doi: 10.1016/j.tet.2005.07.010.
- [32] D. Wang and F. Gao, "Quinazoline derivatives: Synthesis and bioactivities," *Chemistry Central Journal*, vol. 7, no. 1. Jun. 03, 2013. doi: 10.1186/1752-153X-7-95.
- [33] R. Karan, P. Agarwal, M. Sinha, and N. Mahato, "Recent advances on quinazoline derivatives: A potential bioactive scaffold in medicinal chemistry," *ChemEngineering*, vol. 5, no. 4. MDPI, Dec. 01, 2021. doi: 10.3390/chemengineering5040073.
- [34] M. Asif, "Chemical Characteristics, Synthetic Methods, and Biological Potential of Quinazoline and Quinazolinone Derivatives," *Int J Med Chem*, vol. 2014, pp. 1–27, Nov. 2014, doi: 10.1155/2014/395637.
- [35] R. Rezaeinasab, E. Jafari, and G. Khodarahmi, "Quinazolinone-based hybrids with diverse biological activities: A mini-review," *Journal of Research in Medical Sciences*, vol. 27, no. 1. Wolters Kluwer Medknow Publications, p. 68, Jan. 01, 2022. doi: 10.4103/jrms.jrms_1025_21.
- [36] J. Alam, O. Alam, J. Naim, and P. Alam, "A review: Recent investigations on Quinazoline Scaffold," 2015. [Online]. Available: <http://www.journalijar.com>
- [37] R. Rezaeinasab, E. Jafari, and G. Khodarahmi, "Quinazolinone-based hybrids with diverse biological activities: A mini-review," *Journal of Research in Medical Sciences*, vol. 27, no. 1. Wolters Kluwer Medknow Publications, p. 68, Jan. 01, 2022. doi: 10.4103/jrms.jrms_1025_21.

- [38] C. W. Murray and T. L. Blundell, "Structural biology in fragment-based drug design," *Current Opinion in Structural Biology*, vol. 20, no. 4. pp. 497–507, Aug. 2010. doi: 10.1016/j.sbi.2010.04.003.
- [39] P. Kirsch, A. M. Hartman, A. K. H. Hirsch, and M. Empting, "Concepts and core principles of fragment-based drug design," *Molecules*, vol. 24, no. 23. MDPI AG, Nov. 26, 2019. doi: 10.3390/molecules24234309.
- [40] J. F. Meyer and E. C. Wagner, "THE NIEMENTOWSKI REACTION. THE USE OF METHYL AN-THRANILATE OR ISATOIC ANHYDRIDE WITH SUBSTITUTED AMIDES OR AMIDINES IN THE FORMATION OF 3-SUBSTITUTED-4-KETO-3,4-DIHYDROQUINAZOLINES. THE COURSE OF THE REACTION The formation of substituted 4-keto-3,4-dihydroquinazolines by interaction of Janthranilic acid or substituted anthranilic acids and amides may be designated as the," UTC, 2023. [Online]. Available: <https://pubs.acs.org/sharingguidelines>
- [41] R. Rezaeinasab, E. Jafari, and G. Khodarahmi, "Quinazolinone-based hybrids with diverse biological activities: A mini-review," *Journal of Research in Medical Sciences*, vol. 27, no. 1. Wolters Kluwer Medknow Publications, p. 68, Jan. 01, 2022. doi: 10.4103/jrms.jrms_1025_21.
- [42] J. Alam, O. Alam, J. Naim, and P. Alam, "A review: Recent investigations on Quinazoline Scaffold," 2015. [Online]. Available: <http://www.journalijar.com>
- [43] R. Karan, P. Agarwal, M. Sinha, and N. Mahato, "Recent advances on quinazoline derivatives: A potential bioactive scaffold in medicinal chemistry,"

- ChemEngineering*, vol. 5, no. 4. MDPI, Dec. 01, 2021. doi: 10.3390/chemengineering5040073.
- [44] Paul. Leff, *Receptor-based drug design*. M. Dekker, 1998.
- [45] D. J. Connolly, D. Cusack, T. P. O’Sullivan, and P. J. Guiry, “Synthesis of quinazolinones and quinazolines,” *Tetrahedron*, vol. 61, no. 43. pp. 10153–10202, Oct. 24, 2005. doi: 10.1016/j.tet.2005.07.010.
- [46] A. P. Nicholas Tomas Htikfelt and V. A. Pieri bone, “The distribution and significance of eNS adrenoceptors examined with in situ hybridization,” 1996.
- [47] P. Kirsch, A. M. Hartman, A. K. H. Hirsch, and M. Empting, “Concepts and core principles of fragment-based drug design,” *Molecules*, vol. 24, no. 23. MDPI AG, Nov. 26, 2019. doi: 10.3390/molecules24234309.
- [48] A. P. Nicholas Tomas Htikfelt and V. A. Pieri bone, “The distribution and significance of eNS adrenoceptors examined with in situ hybridization,” 1996.
- [49] B. C. Doak, R. S. Norton, and M. J. Scanlon, “The ways and means of fragment-based drug design,” *Pharmacol Ther*, vol. 167, pp. 28–37, Nov. 2016, doi: 10.1016/j.pharmthera.2016.07.003.
- [50] Y. Bian and X. Q. (Sean) Xie, “Computational Fragment-Based Drug Design: Current Trends, Strategies, and Applications,” *AAPS Journal*, vol. 20, no. 3. Springer New York LLC, May 01, 2018. doi: 10.1208/s12248-018-0216-7.
- [51] H. Chen, X. Zhou, A. Wang, Y. Zheng, Y. Gao, and J. Zhou, “Evolutions in fragment-based drug design: The deconstruction-reconstruction approach,” *Drug Discovery Today*, vol. 20, no. 1. Elsevier Ltd, pp. 105–113, 2015. doi: 10.1016/j.drudis.2014.09.015.

- [52] B. Civantos Calzada and A. Aleixandre De Artiñano, "Alpha-adrenoceptor subtypes," *Pharmacol Res*, vol. 44, no. 3, pp. 195–208, 2001, doi: 10.1006/phrs.2001.0857.
- [53] D. Wang and F. Gao, "Quinazoline derivatives: Synthesis and bioactivities," *Chemistry Central Journal*, vol. 7, no. 1. Jun. 03, 2013. doi: 10.1186/1752-153X-7-95.
- [54] D. Wang and F. Gao, "Quinazoline derivatives: Synthesis and bioactivities," *Chemistry Central Journal*, vol. 7, no. 1. Jun. 03, 2013. doi: 10.1186/1752-153X-7-95.
- [55] D. J. Connolly, D. Cusack, T. P. O'Sullivan, and P. J. Guiry, "Synthesis of quinazolinones and quinazolines," *Tetrahedron*, vol. 61, no. 43. pp. 10153–10202, Oct. 24, 2005. doi: 10.1016/j.tet.2005.07.010.
- [56] T. P. Selvam and P. V. Kumar, "Quinazoline Marketed drugs-A Review," 2011. [Online]. Available: www.researchinpharmacy.com
- [57] R. Rezaeinasab, E. Jafari, and G. Khodarahmi, "Quinazolinone-based hybrids with diverse biological activities: A mini-review," *Journal of Research in Medical Sciences*, vol. 27, no. 1. Wolters Kluwer Medknow Publications, p. 68, Jan. 01, 2022. doi: 10.4103/jrms.jrms_1025_21.
- [58] R. Karan, P. Agarwal, M. Sinha, and N. Mahato, "Recent advances on quinazoline derivatives: A potential bioactive scaffold in medicinal chemistry," *ChemEngineering*, vol. 5, no. 4. MDPI, Dec. 01, 2021. doi: 10.3390/chemengineering5040073.

- [59] D. Wang and F. Gao, "Quinazoline derivatives: Synthesis and bioactivities," *Chemistry Central Journal*, vol. 7, no. 1. Jun. 03, 2013. doi: 10.1186/1752-153X-7-95.
- [60] R. Karan, P. Agarwal, M. Sinha, and N. Mahato, "Recent advances on quinazoline derivatives: A potential bioactive scaffold in medicinal chemistry," *ChemEngineering*, vol. 5, no. 4. MDPI, Dec. 01, 2021. doi: 10.3390/chemengineering5040073.
- [61] A. A. LANDS ARNOLD J P McAuLIFF F P LUDUENA T G BROWN, "Chemical Constitution and Pharmaco-dynamic Action," Marcel Dekker, Inc, 1948.
- [62] D. J. Connolly, D. Cusack, T. P. O'Sullivan, and P. J. Guiry, "Synthesis of quinazolinones and quinazolines," *Tetrahedron*, vol. 61, no. 43. pp. 10153–10202, Oct. 24, 2005. doi: 10.1016/j.tet.2005.07.010.
- [63] D. Wang and F. Gao, "Quinazoline derivatives: Synthesis and bioactivities," *Chemistry Central Journal*, vol. 7, no. 1. Jun. 03, 2013. doi: 10.1186/1752-153X-7-95.
- [64] M. Asif, "Chemical Characteristics, Synthetic Methods, and Biological Potential of Quinazoline and Quinazolinone Derivatives," *Int J Med Chem*, vol. 2014, pp. 1–27, Nov. 2014, doi: 10.1155/2014/395637.
- [65] N. M. Kogan *et al.*, "Synthesis and antitumor activity of quinonoid derivatives of cannabinoids," *J Med Chem*, vol. 47, no. 15, pp. 3800–3806, Jul. 2004, doi: 10.1021/jm040042o.

- [66] A. Cavalli, F. Lizzi, S. Bongarzone, R. Brun, R. Luise Krauth-Siegel, and M. L. Bolognesi, "Privileged structure-guided synthesis of quinazoline derivatives as inhibitors of trypanothione reductase," *Bioorg Med Chem Lett*, vol. 19, no. 11, pp. 3031–3035, Jun. 2009, doi: 10.1016/j.bmcl.2009.04.060.
- [67] A. Cavalli, F. Lizzi, S. Bongarzone, R. Brun, R. Luise Krauth-Siegel, and M. L. Bolognesi, "Privileged structure-guided synthesis of quinazoline derivatives as inhibitors of trypanothione reductase," *Bioorg Med Chem Lett*, vol. 19, no. 11, pp. 3031–3035, 2009, doi: 10.1016/j.bmcl.2009.04.060.
- [68] J. Baselga and S. M. Swain, "Novel anticancer targets: Revisiting ERBB2 and discovering ERBB3," *Nature Reviews Cancer*, vol. 9, no. 7, pp. 463–475, Jul. 2009. doi: 10.1038/nrc2656.
- [69] J. F. Meyer and E. C. Wagner, "THE NIEMENTOWSKI REACTION. THE USE OF METHYL AN-THRANILATE OR ISATOIC ANHYDRIDE WITH SUBSTITUTED AMIDES OR AMIDINES IN THE FORMATION OF 3-SUBSTITUTED-4-KETO-3,4-DIHYDROQUINAZOLINES. THE COURSE OF THE REACTION The formation of substituted 4-keto-3,4-dihydroquinazolines by interaction of Janthranilic acid or substituted anthranilic acids and amides may be designated as the," UTC, 2023. [Online]. Available: <https://pubs.acs.org/sharingguidelines>
- [70] Z. Y. Ibrahim, A. Uzairu, G. A. Shallangwa, S. E. Abechi, and S. Isyaku, "Computer-aided molecular design of 2-anilino 4-amino substituted quinazolines derivatives as malarial inhibitors," *SN Appl Sci*, vol. 3, no. 9, Sep. 2021, doi: 10.1007/s42452-021-04748-5.

- [71] S. Lü *et al.*, “Synthesis, characterization, screening and docking analysis of 4-anilinoquinazoline derivatives as tyrosine kinase inhibitors,” *Eur J Med Chem*, vol. 61, pp. 84–94, Mar. 2013, doi: 10.1016/j.ejmech.2012.07.036.
- [72] A. E. Kassab, E. M. Gedawy, Z. Mahmoud, and R. A. Khattab, “Design, synthesis, antitumor and antimicrobial activity of novel 6,7-dimethoxyquinazoline derivatives,” *Heterocycles*, vol. 92, no. 2, pp. 272–290, 2016, doi: 10.3987/COM-15-13329.
- [73] K. M. Alzaydi and T. S. Saleh, “2-Aryl hydrazonopropanal pharmacophores as potent cytotoxic agents against human hepatocellular carcinoma cell line,” *Medicinal Chemistry Research*, vol. 29, no. 2, pp. 199–205, Feb. 2020, doi: 10.1007/s00044-019-02473-8.
- [74] N. Srimongkolpithak, S. Sundriyal, F. Li, M. Vedadi, and M. J. Fuchter, “Identification of 2,4-diamino-6,7-dimethoxyquinoline derivatives as G9a inhibitors,” *Medchemcomm*, vol. 5, no. 12, pp. 1821–1828, Dec. 2014, doi: 10.1039/c4md00274a.
- [75] A. Garofalo *et al.*, “Design, synthesis, and DNA-binding of N-alkyl(anilino)quinazoline derivatives,” *J Med Chem*, vol. 53, no. 22, pp. 8089–8103, Nov. 2010, doi: 10.1021/jm1009605.
- [76] N. Agrawal *et al.*, “Exploration of 6,7-dimethoxyquinazoline derivatives as dual acting a₁ - and AT₁ -receptor antagonists: Synthesis, evaluation, pharmacophore & 3D-QSAR modeling and receptor docking studies,” *RSC Adv*, vol. 6, no. 36, pp. 30661–30682, 2016, doi: 10.1039/c6ra00589f.

- [77] S. Tasler *et al.*, “N-substituted 2'-(aminoaryl)benzothiazoles as kinase inhibitors: Hit identification and scaffold hopping,” *Bioorg Med Chem Lett*, vol. 19, no. 5, pp. 1349–1356, Mar. 2009, doi: 10.1016/j.bmcl.2009.01.054.
- [78] D. Goff *et al.*, “Discovery of dual Axl/VEGF-R2 inhibitors as potential anti-angiogenic and anti-metastatic drugs for cancer chemotherapy,” *Bioorg Med Chem Lett*, vol. 27, no. 16, pp. 3766–3771, 2017, doi: 10.1016/j.bmcl.2017.06.071.
- [79] L. Ji *et al.*, “Novel ruthenium complexes ligated with 4-anilinoquinazoline derivatives: Synthesis, characterisation and preliminary evaluation of biological activity,” *Eur J Med Chem*, vol. 77, pp. 110–120, Apr. 2014, doi: 10.1016/j.ejmech.2014.02.062.
- [80] M. R. Yadav, P. P. Naik, H. P. Gandhi, B. S. Chauhan, and R. Giridhar, “Design and synthesis of 6,7-dimethoxyquinazoline analogs as multi-targeted ligands for α 1- and AII-receptors antagonism,” *Bioorg Med Chem Lett*, vol. 23, no. 13, pp. 3959–3966, Jul. 2013, doi: 10.1016/j.bmcl.2013.04.054.
- [81] A. Ashok, K. Thanukrishnan, H. S. Bhojya Naik, and A. G. Shaik, “6,7-Dimethoxy-quinazolin-4-yl-amino-thiophene-2-carboxamides as Potent Inhibitors of VEGF Receptors 1 and 2,” *J Heterocycl Chem*, vol. 54, no. 2, pp. 1065–1070, Mar. 2017, doi: 10.1002/jhet.2675.
- [82] S. A. Rocco, J. E. Barbarini, and R. Rittner, “Syntheses of Some 4-Anilinoquinazoline Derivatives,” *Synthesis (Stuttg)*, no. 3, pp. 429–435, Feb. 2004, doi: 10.1055/s-2004-815949.

- [83] A. E. Kassab, E. M. Gedawy, Z. Mahmoud, and R. A. Khattab, "Design, synthesis, antitumor and antimicrobial activity of novel 6,7-dimethoxyquinazoline derivatives," *Heterocycles*, vol. 92, no. 2, pp. 272–290, 2016, doi: 10.3987/COM-15-13329.
- [84] S. A. Rocco, J. E. Barbarini, and R. Rittner, "Syntheses of Some 4-Anilinoquinazoline Derivatives," *Synthesis (Stuttg)*, no. 3, pp. 429–435, Feb. 2004, doi: 10.1055/s-2004-815949.
- [85] T. A. Chappie *et al.*, "Discovery of a series of 6,7-dimethoxy-4-pyrrolidylquinazoline PDE10A inhibitors," *J Med Chem*, vol. 50, no. 2, pp. 182–185, Jan. 2007, doi: 10.1021/jm060653b.
- [86] N. Srimongkolpithak, S. Sundriyal, F. Li, M. Vedadi, and M. J. Fuchter, "Identification of 2,4-diamino-6,7-dimethoxyquinoline derivatives as G9a inhibitors," *Medchemcomm*, vol. 5, no. 12, pp. 1821–1828, Dec. 2014, doi: 10.1039/c4md00274a.
- [87] Y. J. Shaw, Y. T. Yang, J. B. Garrison, N. Kyprianou, and C. S. Chen, "Pharmacological exploitation of the α 1-adrenoreceptor antagonist doxazosin to develop a novel class of antitumor agents that block intracellular protein kinase B/Akt activation," *J Med Chem*, vol. 47, no. 18, pp. 4453–4462, Aug. 2004, doi: 10.1021/jm049752k.
- [88] M. Rosini *et al.*, "Prazosin-Related Compounds. Effect of Transforming the Piperazinylquinazoline Moiety into an Aminomethyltetrahydroacridine System on the Affinity for α 1-Adrenoreceptors," *J Med Chem*, vol. 46, no. 23, pp. 4895–4903, Nov. 2003, doi: 10.1021/jm030952q.

- [89] I. J. A. MacDougall and R. Griffith, "Selective pharmacophore design for α 1-adrenoceptor subtypes," *J Mol Graph Model*, vol. 25, no. 1, pp. 146–157, Sep. 2006, doi: 10.1016/j.jmgm.2005.12.001.
- [90] Dianne M. Perez, *The Adrenergic Receptors*, 1st ed. humana press, 2006.
- [91] P. A. Zunszain, C. Federico, M. Sechi, S. Al-Damluji, and C. R. Ganellin, "Search for the pharmacophore in prazosin for Transport-P," *Bioorg Med Chem*, vol. 13, no. 11, pp. 3681–3689, Jun. 2005, doi: 10.1016/j.bmc.2005.03.030.
- [92] M. R. Yadav, P. P. Naik, H. P. Gandhi, B. S. Chauhan, and R. Giridhar, "Design and synthesis of 6,7-dimethoxyquinazoline analogs as multi-targeted ligands for α 1- and AII-receptors antagonism," *Bioorg Med Chem Lett*, vol. 23, no. 13, pp. 3959–3966, Jul. 2013, doi: 10.1016/j.bmcl.2013.04.054.
- [93] M. Ishiguro, Y. Futabayashi, T. Ohnuki, M. Ahmed, I. Muramatsu, and T. Nagatomo, "Identification of binding sites of prazosin, tamsulosin and KMD-3213 with a 1-adrenergic receptor subtypes by molecular modeling," 2002. [Online]. Available: www.elsevier.com/locate/lifescieLifeSciences71
- [94] A. A. LANDS ARNOLD J P McAuLIFF F P LUDUENA T G BROWN, "Chemical Constitution and Pharmaco-dynamic Action," Marcel Dekker, Inc, 1948.
- [95] Paul. Leff, *Receptor-based drug design*. M. Dekker, 1998.
- [96] M. K. Srivastav and S. M. Shantakumar, "Design , Synthesis and Characterization of Novel Anxiolytic and Antidepressant Agents," vol. 3, no. 1, pp. 14–22, 2013, doi: 10.5923/j.chemistry.20130301.04.

- [97] B. R. Keeshin, Q. Ding, A. P. Presson, S. J. Berkowitz, and J. R. Strawn, "Use of Prazosin for Pediatric PTSD-Associated Nightmares and Sleep Disturbances: A Retrospective Chart Review," *Neurol Ther*, vol. 6, no. 2, pp. 247–257, Dec. 2017, doi: 10.1007/s40120-017-0078-4.
- [98] D. Giardina *et al.*, "Structure—Activity Relationships in Prazosin-related Compounds. Effect of Replacing a Piperazine Ring with an Alkanediamine Moiety on α 1-Adrenoreceptor Blocking Activity.," *J Med Chem*, vol. 32, no. 1, pp. 50–55, 1989, doi: 10.1021/jm00121a011.
- [99] S. Kung, Z. Espinel, and M. I. Lapid, "Treatment of nightmares with prazosin: A systematic review," *Mayo Clinic Proceedings*. 2012. doi: 10.1016/j.mayocp.2012.05.015.
- [100] M. Ishiguro, Y. Futabayashi, T. Ohnuki, M. Ahmed, I. Muramatsu, and T. Nagatomo, "Identification of binding sites of prazosin, tamsulosin and KMD-3213 with a 1-adrenergic receptor subtypes by molecular modeling," 2002. [Online]. Available: www.elsevier.com/locate/lifescieLifeSciences71
- [101] A. Minarini, M. L. Bolognesi, and V. Vincenzo, "Recent advances in the design and synthesis of prazosin derivatives," *Expert Opinion on Drug Discovery*, vol. 1, no. 5, pp. 395–407, Oct. 2006. doi: 10.1517/17460441.1.5.395.
- [102] A. Minarini, M. L. Bolognesi, and V. Vincenzo, "Recent advances in the design and synthesis of prazosin derivatives," *Expert Opinion on Drug Discovery*, vol. 1, no. 5, pp. 395–407, Oct. 2006. doi: 10.1517/17460441.1.5.395.

- [103] P. A. Zunszain, C. Federico, M. Sechi, S. Al-Damluji, and C. R. Ganellin, "Search for the pharmacophore in prazosin for Transport-P," *Bioorg Med Chem*, vol. 13, no. 11, pp. 3681–3689, Jun. 2005, doi: 10.1016/j.bmc.2005.03.030.
- [104] A. Minarini, M. L. Bolognesi, and V. Vincenzo, "Recent advances in the design and synthesis of prazosin derivatives," *Expert Opinion on Drug Discovery*, vol. 1, no. 5, pp. 395–407, Oct. 2006. doi: 10.1517/17460441.1.5.395.
- [105] B. Gzyl-Malcher, J. Handzlik, and E. Klekowska, "Temperature dependence of the interaction of prazosin with lipid Langmuir monolayers," *Colloids Surf B Biointerfaces*, vol. 112, pp. 171–176, Dec. 2013, doi: 10.1016/j.colsurfb.2013.07.030.
- [106] D. B. Menkes, J. M. Baraban, and G. K. Aghajanian, "Prazosin selectively antagonizes neuronal responses mediated by α 1-adrenoceptors in brain," *Naunyn Schmiedebergs Arch Pharmacol*, vol. 317, no. 3, pp. 273–275, Nov. 1981, doi: 10.1007/BF00503830.
- [107] D. B. Menkes, J. M. Baraban, and G. K. Aghajanian, "Prazosin selectively antagonizes neuronal responses mediated by α 1-adrenoceptors in brain," *Naunyn Schmiedebergs Arch Pharmacol*, 1981, doi: 10.1007/BF00503830.
- [108] D. Giardina, R. Bertini, E. Brancia, L. Brasili, and C. Melchiorre, "Structure-Activity Relationships for Prazosin and WB 4101 Analogues as α 1-Adrenoreceptor Antagonists," *J Med Chem*, 1985, doi: 10.1021/jm00147a042.
- [109] B. R. Keeshin, Q. Ding, A. P. Presson, S. J. Berkowitz, and J. R. Strawn, "Use of Prazosin for Pediatric PTSD-Associated Nightmares and Sleep Disturbances: A

- Retrospective Chart Review,” *Neurol Ther*, vol. 6, no. 2, pp. 247–257, Dec. 2017, doi: 10.1007/s40120-017-0078-4.
- [110] M. L. Bolognesi *et al.*, “Analogues of prazosin that bear a benextramine-related polyamine backbone exhibit different antagonism toward α 1-adrenoreceptor subtypes,” *J Med Chem*, vol. 44, no. 3, pp. 362–371, 2001, doi: 10.1021/jm000995w.
- [111] B. Civantos Calzada and A. Aleixandre De Artiñano, “Alpha-adrenoreceptor subtypes,” *Pharmacol Res*, vol. 44, no. 3, pp. 195–208, 2001, doi: 10.1006/phrs.2001.0857.
- [112] J. C. McGrath, C. M. Brown, and V. G. Wilson, “Alpha-adrenoceptors: a critical review.,” *Med Res Rev*, vol. 9, no. 4, pp. 407–533, Oct. 1989, doi: 10.1002/med.2610090403.
- [113] M. Xing and P. A. Insel, “Protein kinase C-dependent activation of cytosolic phospholipase A2 and mitogen-activated protein kinase by alpha1-adrenergic receptors in Madin- Darby canine kidney cells,” *Journal of Clinical Investigation*, vol. 97, no. 5, pp. 1302–1310, 1996, doi: 10.1172/JCI118546.
- [114] R. H. Grimm Jr and J. M. Flack, “Alpha 1 Adrenoreceptor Antagonists,” *The Journal of Clinical Hypertension*, vol. 13, no. 9, pp. 654–657, Sep. 2011, doi: 10.1111/j.1751-7176.2011.00510.x.
- [115] D. T. Nash, “Alpha-adrenergic blockers: Mechanism of action, blood pressure control, and effects on lipoprotein metabolism,” *Clinical Cardiology*, vol. 13, no. 11, pp. 764–772, 1990. doi: 10.1002/clc.4960131104.

- [116] R. P. Mathur, S. Nayak, R. Sivaramakrishnan, and V. Jain, "Role of alpha blockers in hypertension with benign prostatic hyperplasia," *Journal of Association of Physicians of India*, 2014.
- [117] B. Rorabaugh, "Prazosin*," in *xPharm: The Comprehensive Pharmacology Reference*, Elsevier, 2007, pp. 1–6. doi: 10.1016/B978-008055232-3.62453-5.
- [118] R. Roskoski, "ErbB/HER protein-tyrosine kinases: Structures and small molecule inhibitors," *Pharmacological Research*, vol. 87. Academic Press, pp. 42–59, 2014. doi: 10.1016/j.phrs.2014.06.001.
- [119] R. Roskoski, "ErbB/HER protein-tyrosine kinases: Structures and small molecule inhibitors," *Pharmacological Research*, vol. 87. Academic Press, pp. 42–59, 2014. doi: 10.1016/j.phrs.2014.06.001.
- [120] C. L. Arteaga and J. A. Engelman, "ERBB receptors: From oncogene discovery to basic science to mechanism-based cancer therapeutics," *Cancer Cell*, vol. 25, no. 3. Cell Press, pp. 282–303, Mar. 17, 2014. doi: 10.1016/j.ccr.2014.02.025.
- [121] "Signal Transduction by Receptors with Tyrosine Kinase Activity Review Axel Ullrich' and Joseph Schlessingert," 1990.
- [122] Y. Yarden and G. Pines, "The ERBB network: At last, cancer therapy meets systems biology," *Nature Reviews Cancer*, vol. 12, no. 8. pp. 553–563, Aug. 2012. doi: 10.1038/nrc3309.
- [123] "Signal Transduction by Receptors with Tyrosine Kinase Activity Review Axel Ullrich' and Joseph Schlessingert," 1990.

- [124] R. Roskoski, “ErbB/HER protein-tyrosine kinases: Structures and small molecule inhibitors,” *Pharmacological Research*, vol. 87. Academic Press, pp. 42–59, 2014. doi: 10.1016/j.phrs.2014.06.001.
- [125] C. L. Arteaga and J. A. Engelman, “ERBB receptors: From oncogene discovery to basic science to mechanism-based cancer therapeutics,” *Cancer Cell*, vol. 25, no. 3. Cell Press, pp. 282–303, Mar. 17, 2014. doi: 10.1016/j.ccr.2014.02.025.
- [126] Y. Yarden and G. Pines, “The ERBB network: At last, cancer therapy meets systems biology,” *Nature Reviews Cancer*, vol. 12, no. 8. pp. 553–563, Aug. 2012. doi: 10.1038/nrc3309.
- [127] J. Baselga and S. M. Swain, “Novel anticancer targets: Revisiting ERBB2 and discovering ERBB3,” *Nature Reviews Cancer*, vol. 9, no. 7. pp. 463–475, Jul. 2009. doi: 10.1038/nrc2656.
- [128] R. Roskoski, “ErbB/HER protein-tyrosine kinases: Structures and small molecule inhibitors,” *Pharmacological Research*, vol. 87. Academic Press, pp. 42–59, 2014. doi: 10.1016/j.phrs.2014.06.001.
- [129] “Signal Transduction by Receptors with Tyrosine Kinase Activity Review Axel Ullrich’ and Joseph Schlessingert,” 1990.
- [130] J. Telleria and M. Tibayrenc, *American Trypanosomiasis, 100 Years of Research Chagas Disease*. 2017. doi: 9780128010693.
- [131] C. Halliday *et al.*, “Cellular landmarks of *Trypanosoma brucei* and *Leishmania mexicana*,” *Mol Biochem Parasitol*, vol. 230, pp. 24–36, 2019, doi: 10.1016/j.molbiopara.2018.12.003.

- [132] S. Krishna, C. Kleine, and A. Stich, “African Trypanosomiasis,” in *Hunter’s Tropical Medicine and Emerging Infectious Diseases*, Tenth Edit. Elsevier, 2020, pp. 755–761. doi: 10.1016/B978-0-323-55512-8.00102-2.
- [133] G. M. Attardo *et al.*, “Comparative genomic analysis of six *Glossina* genomes, vectors of African trypanosomes,” *Genome Biol*, vol. 20, no. 1, pp. 1–31, 2019, doi: 10.1186/s13059-019-1768-2.
- [134] R. Brun, J. Blum, F. Chappuis, and C. Burri, “Human African trypanosomiasis,” *The Lancet*, vol. 375, no. 9709, pp. 148–159, 2010, doi: 10.1016/S0140-6736(09)60829-1.
- [135] K. Stuart *et al.*, “Kinetoplastids: related protozoan pathogens, different diseases,” *Journal of Clinical Investigation*, vol. 118, no. 4, pp. 1301–1310, Apr. 2008, doi: 10.1172/JCI33945.
- [136] N. M. El-Sayed *et al.*, “Comparative genomics of trypanosomatid parasitic protozoa,” *Science (1979)*, vol. 309, no. 5733, pp. 404–410, 2005, doi: 10.1126/science.1112181.
- [137] W. Gibson, “Kinetoplastea,” in *Handbook of the Protists*, Cham: Springer International Publishing, 2017, pp. 1089–1138. doi: 10.1007/978-3-319-28149-0_7.
- [138] A. Kaufer, D. Stark, and J. Ellis, “Evolutionary insight into the trypanosomatidae using alignment-free phylogenomics of the kinetoplast,” *Pathogens*, vol. 8, no. 3, Sep. 2019, doi: 10.3390/pathogens8030157.

- [139] A. P. Jackson *et al.*, “Kinetoplastid Phylogenomics Reveals the Evolutionary Innovations Associated with the Origins of Parasitism,” *Current Biology*, vol. 26, no. 2, pp. 161–172, Jan. 2016, doi: 10.1016/j.cub.2015.11.055.
- [140] “Stefann Magez · Magdalena Radwanska Editors Trypanosomes and Trypanosomiasis.”
- [141] C. M. Morel *et al.*, “Health innovation networks to help developing countries address neglected diseases,” *Science*, vol. 309, no. 5733, pp. 401–404, Jul. 15, 2005. doi: 10.1126/science.1115538.
- [142] C. S. Sutherland, J. Yukich, R. Goeree, and F. Tediosi, “A Literature Review of Economic Evaluations for a Neglected Tropical Disease: Human African Trypanosomiasis (‘Sleeping Sickness’),” *PLoS Negl Trop Dis*, vol. 9, no. 2, pp. 1–22, 2015, doi: 10.1371/journal.pntd.0003397.
- [143] E. DeJesus, R. Kieft, B. Albright, N. A. Stephens, and S. L. Hajduk, “A Single Amino Acid Substitution in the Group 1 Trypanosoma brucei gambiense Haptoglobin-Hemoglobin Receptor Abolishes TLF-1 Binding,” *PLoS Pathog*, vol. 9, no. 4, p. e1003317, Apr. 2013, doi: 10.1371/journal.ppat.1003317.
- [144] J. M. Harrington, S. Howell, and S. L. Hajduk, “Membrane Permeabilization by Trypanosome Lytic Factor, a Cytolytic Human High Density Lipoprotein,” *Journal of Biological Chemistry*, vol. 284, no. 20, pp. 13505–13512, May 2009, doi: 10.1074/jbc.M900151200.
- [145] R. Kieft, P. Capewell, C. M. R. Turner, N. J. Veitch, A. MacLeod, and S. Hajduk, “Mechanism of Trypanosoma brucei gambiense (group 1) resistance to human

- trypanosome lytic factor,” *Proceedings of the National Academy of Sciences*, vol. 107, no. 37, pp. 16137–16141, Sep. 2010, doi: 10.1073/pnas.1007074107.
- [146] J. R. Bishop, M. Shimamura, and S. L. Hajduk, “Insight into the mechanism of trypanosome lytic factor-1 killing of *Trypanosoma brucei brucei*,” *Mol Biochem Parasitol*, vol. 118, no. 1, pp. 33–40, Nov. 2001, doi: 10.1016/S0166-6851(01)00361-9.
- [147] M. D. Urbaniak, M. L. S. Guther, and M. A. J. Ferguson, “Comparative SILAC proteomic analysis of trypanosoma brucei bloodstream and procyclic lifecycle stages,” *PLoS One*, vol. 7, no. 5, 2012, doi: 10.1371/journal.pone.0036619.
- [148] V. H. Gazestani *et al.*, “A Protein Complex Map of *Trypanosoma brucei*,” *PLoS Negl Trop Dis*, vol. 10, no. 3, pp. 1–32, 2016, doi: 10.1371/journal.pntd.0004533.
- [149] D. Steverding, “The development of drugs for treatment of sleeping sickness: a historical review,” *Parasit Vectors*, vol. 3, no. 1, p. 15, 2010, doi: 10.1186/1756-3305-3-15.
- [150] P. G. E. Kennedy and J. Rodgers, “Clinical and Neuropathogenetic Aspects of Human African Trypanosomiasis,” *Front Immunol*, vol. 10, Jan. 2019, doi: 10.3389/fimmu.2019.00039.
- [151] V. K. B. K. Mesu *et al.*, “Oral fexinidazole for late-stage African *Trypanosoma brucei gambiense* trypanosomiasis: a pivotal multicentre, randomised, non-inferiority trial,” *The Lancet*, vol. 391, no. 10116, pp. 144–154, Jan. 2018, doi: 10.1016/S0140-6736(17)32758-7.

- [152] P. G. E. Kennedy and J. Rodgers, “Clinical and neuropathogenetic aspects of human African trypanosomiasis,” *Front Immunol*, vol. 10, no. JAN, pp. 1–11, 2019, doi: 10.3389/fimmu.2019.00039.
- [153] D. Steverding, “The development of drugs for treatment of sleeping sickness: a historical review,” *Parasit Vectors*, vol. 3, no. 1, p. 15, 2010, doi: 10.1186/1756-3305-3-15.
- [154] B. M. Anene, D. N. Onah, and Y. Nawa, “Drug resistance in pathogenic African trypanosomes: What hopes for the future?,” *Vet Parasitol*, vol. 96, no. 2, pp. 83–100, 2001, doi: 10.1016/S0304-4017(00)00427-1.
- [155] M. Kaiser, M. A. Bray, M. Cal, B. B. Trunz, E. Torrele, and R. Brun, “Antitrypanosomal activity of fexinidazole, a new oral nitroimidazole drug candidate for treatment of sleeping sickness,” *Antimicrob Agents Chemother*, vol. 55, no. 12, pp. 5602–5608, 2011, doi: 10.1128/AAC.00246-11.
- [156] E. Torrele *et al.*, “Fexinidazole - a new oral nitroimidazole drug candidate entering clinical development for the treatment of sleeping sickness,” *PLoS Negl Trop Dis*, vol. 4, no. 12, pp. 1–15, 2010, doi: 10.1371/journal.pntd.0000923.
- [157] S. Geerts, P. H. Holmes, O. Diall, and M. C. Eisler, “African bovine trypanosomiasis: The problem of drug resistance,” *Parasitology Today*, vol. 17, no. 1, pp. 25–28, 2001, doi: 10.1016/S0169-4758(00)01827-5.
- [158] WHO, “Ending the neglect to attain the Sustainable Development Goals (A road map for neglected tropical disease 2021-2030) Overview,” in *World Health Organization*, 2021.

- [159] S. Smith, “Trypanosome Infection in Cattle and African Sleeping Sickness,” *International Journal of Global Health and Health Disparities*, vol. 5, no. 1, p. 90, 2007.
- [160] M. Wéry, “Drug used in the treatment of sleeping sickness (human African trypanosomiasis: HAT),” *Int J Antimicrob Agents*, 1994, doi: 10.1016/0924-8579(94)90012-4.
- [161] WHO, “Ending the neglect to attain the Sustainable Development Goals (A road map for neglected tropical disease 2021-2030) Overview,” in *World Health Organization*, 2021.
- [162] E. D. Deeks and K. A. Lyseng-Williamson, “Fexinidazole in human African trypanosomiasis: a profile of its use,” *Drugs and Therapy Perspectives*, 2019, doi: 10.1007/s40267-019-00672-2.
- [163] J. R. Franco *et al.*, “Monitoring the elimination of human African trypanosomiasis at continental and country level: Update to 2018,” *PLoS Negl Trop Dis*, vol. 14, no. 5, 2020, doi: 10.1371/journal.pntd.0008261.
- [164] F. Njiokou *et al.*, “Domestic animals as potential reservoir hosts of trypanosoma brucei gambiense in sleeping sickness foci in Cameroon,” *Parasite*, 2010, doi: 10.1051/parasite/2010171061.
- [165] S. Krishna, C. Kleine, and A. Stich, “African Trypanosomiasis,” in *Hunter’s Tropical Medicine and Emerging Infectious Diseases*, Tenth Edit.Elsevier, 2020, pp. 755–761. doi: 10.1016/B978-0-323-55512-8.00102-2.

- [166] R. Brun, J. Blum, F. Chappuis, and C. Burri, "Human African trypanosomiasis," *The Lancet*, vol. 375, no. 9709, pp. 148–159, 2010, doi: 10.1016/S0140-6736(09)60829-1.
- [167] C. G. Wermuth, "Selective optimization of side activities: The SOSA approach," *Drug Discovery Today*. 2006. doi: 10.1016/S1359-6446(05)03686-X.
- [168] S. Choudhary, Y. S. Malik, and S. Tomar, "Identification of SARS-CoV-2 Cell Entry Inhibitors by Drug Repurposing Using in silico Structure-Based Virtual Screening Approach," *Front Immunol*, vol. 11, 2020, doi: 10.3389/fimmu.2020.01664.
- [169] W. Huang *et al.*, "Small molecule inhibitors of phospholipase C from a novel high-throughput screen," *Journal of Biological Chemistry*, vol. 288, no. 8, 2013, doi: 10.1074/jbc.M112.422501.
- [170] E. Pays and D. P. Nolan, "Expression and function of surface proteins in *Trypanosoma brucei*," *Mol Biochem Parasitol*, vol. 91, no. 1, Mar. 1998, doi: 10.1016/S0166-6851(97)00183-7.
- [171] A. P. Jackson, H. C. Allison, J. D. Barry, M. C. Field, C. Hertz-Fowler, and M. Berriman, "A Cell-surface Phylome for African Trypanosomes," *PLoS Negl Trop Dis*, vol. 7, no. 3, 2013, doi: 10.1371/JOURNAL.PNTD.0002121.
- [172] D. J. Bridges *et al.*, "Characterisation of the plasma membrane subproteome of bloodstream form *Trypanosoma brucei*," *Proteomics*, vol. 8, no. 1, pp. 83–99, Jan. 2008, doi: 10.1002/PMIC.200700607.
- [173] M. D. Urbaniak, M. L. S. Guther, and M. A. J. Ferguson, "Comparative SILAC proteomic analysis of *trypanosoma brucei* bloodstream and procyclic lifecycle

- stages,” *PLoS One*, vol. 7, no. 5, May 2012, doi: 10.1371/JOURNAL.PONE.0036619.
- [174] P. Borst and A. H. Fairlamb, “Surface receptors and transporters of *Trypanosoma brucei*,” *Annu Rev Microbiol*, vol. 52, pp. 745–778, 1998, doi: 10.1146/ANNUREV.MICRO.52.1.745.
- [175] M. M. Shimogawa, E. A. Saada, A. A. Vashisht, W. D. Barshop, J. A. Wohlschlegel, and K. L. Hill, “Cell Surface Proteomics Provides Insight into Stage-Specific Remodeling of the Host-Parasite Interface in *Trypanosoma brucei**,” *Molecular & Cellular Proteomics*, vol. 14, no. 7, pp. 1977–1988, Jul. 2015, doi: 10.1074/MCP.M114.045146.
- [176] S. E. Jehi, F. Wu, and B. Li, “*Trypanosoma brucei* TIF2 suppresses VSG switching by maintaining subtelomere integrity,” *Cell Res*, vol. 24, no. 7, 2014, doi: 10.1038/cr.2014.60.
- [177] H. Lepor, A. Kazzazi, and B. Djavan, “ α -Blockers for benign prostatic hyperplasia: The new era,” *Curr Opin Urol*, vol. 22, no. 1, pp. 7–15, Jan. 2012, doi: 10.1097/MOU.0B013E32834D9BFD.
- [178] “Quinazoline-derived α 1-Adrenoceptor Antagonists Induce Prostate Cancer Cell Apoptosis Via an α 1-Adrenoceptor-independent Action1 | Cancer Research | American Association for Cancer Research.” <https://aacrjournals.org/cancerres/article/62/2/597/509197/Quinazoline-derived-1-Adrenoceptor-Antagonists> (accessed May 28, 2022).

- [179] A. Petty *et al.*, “Design and synthesis of small molecule agonists of EphA2 receptor,” *Eur J Med Chem*, vol. 143, pp. 1261–1276, Jan. 2018, doi: 10.1016/j.ejmech.2017.10.026.
- [180] C. E. Stebeck *et al.*, “Kinetoplastid membrane protein-11 (KMP-11) is differentially expressed during the life cycle of African trypanosomes and is found in a wide variety of kinetoplastid parasites,” *Mol Biochem Parasitol*, vol. 71, no. 1, pp. 1–13, 1995, doi: 10.1016/0166-6851(95)00022-S.
- [181] Z. Li and C. C. Wang, “KMP-11, a basal body and flagellar protein, is required for cell division in *Trypanosoma brucei*,” *Eukaryot Cell*, vol. 7, no. 11, pp. 1941–1950, Nov. 2008, doi: 10.1128/EC.00249-08/ASSET/DAA17F87-64D8-4419-8BDB-F627E05E3D79/ASSETS/GRAPHIC/ZEK0110832360007.JPEG.
- [182] J. D. Sunter and K. Gull, “The Flagellum Attachment Zone: ‘The Cellular Ruler’ of Trypanosome Morphology,” *Trends Parasitol*, vol. 32, no. 4, pp. 309–324, 2016, doi: 10.1016/j.pt.2015.12.010.
- [183] M. Affolter, A. Hemphill, I. Roditi, N. Müller, and T. Seebeck, “The Repetitive Microtubule-Associated Proteins MARP-1 and MARP-2 of *Trypanosoma brucei*,” *J Struct Biol*, vol. 112, no. 3, pp. 241–251, May 1994, doi: 10.1006/jsbi.1994.1024.
- [184] C. Vedrenne *et al.*, “Two related subpellicular cytoskeleton-associated proteins in *Trypanosoma brucei* stabilize microtubules,” *Mol Biol Cell*, vol. 13, no. 3, pp. 1058–1070, Mar. 2002, doi: 10.1091/mbc.01-06-0298.
- [185] K. S. Ralston, Z. P. Kabututu, J. H. Melehani, M. Oberholzer, and K. L. Hill, “The *Trypanosoma brucei* flagellum: Moving parasites in new directions,” *Annu Rev*

- Microbiol*, vol. 63, pp. 335–362, 2009, doi: 10.1146/annurev.micro.091208.073353.
- [186] R. Broadhead *et al.*, “Flagellar motility is required for the viability of the bloodstream trypanosome,” *Nature*, vol. 440, no. 7081, pp. 224–227, 2006, doi: 10.1038/nature04541.
- [187] K. S. Ralston and K. L. Hill, “The flagellum of *Trypanosoma brucei*: New tricks from an old dog,” *Int J Parasitol*, vol. 38, no. 8–9, pp. 869–884, Jul. 2008, doi: 10.1016/J.IJPARA.2008.03.003.
- [188] M. Okuno, D. J. Asai, K. Ogawa, and C. J. Brokaw, “Effects of antibodies against dynein and tubulin on the stiffness of flagellar axonemes,” *Journal of Cell Biology*, vol. 91, no. 3, pp. 689–694, Dec. 1981, doi: 10.1083/JCB.91.3.689.
- [189] S. Vaughan, L. Kohl, I. Ngai, R. J. Wheeler, and K. Gull, “A Repetitive Protein Essential for the Flagellum Attachment Zone Filament Structure and Function in *Trypanosoma brucei*,” *Protist*, vol. 159, no. 1, pp. 127–136, 2008, doi: 10.1016/j.protis.2007.08.005.
- [190] S. Vaughan, L. Kohl, I. Ngai, R. J. Wheeler, and K. Gull, “A Repetitive Protein Essential for the Flagellum Attachment Zone Filament Structure and Function in *Trypanosoma brucei*,” *Protist*, vol. 159, no. 1, pp. 127–136, 2008, doi: 10.1016/j.protis.2007.08.005.
- [191] Q. Zhou, H. Hu, C. Y. He, and Z. Li, “Assembly and maintenance of the flagellum attachment zone filament in *Trypanosoma brucei*,” *J Cell Sci*, vol. 128, no. 13, pp. 2361–2372, Jul. 2015, doi: 10.1242/jcs.168377.

- [192] W. Zhang *et al.*, “Discovery of Quinazoline-Based Fluorescent Probes to α 1 Adrenergic Receptors,” 2015, doi: 10.1021/ml5004298.
- [193] Z.-W. Hu, “Contrasting Signaling Pathways of 1A- and 1B-Adrenergic Receptor Subtype Activation of Phosphatidylinositol 3-Kinase and Ras in Transfected NIH3T3 Cells,” *Molecular Endocrinology*, vol. 13, no. 1, pp. 3–14, Jan. 1999, doi: 10.1210/me.13.1.3.
- [194] T. Shi *et al.*, “Novel α 1 -Adrenergic Receptor Signaling Pathways: Secreted Factors and Interactions with the Extracellular Matrix,” *Mol Pharmacol*, vol. 70, no. 1, pp. 129–142, Jul. 2006, doi: 10.1124/mol.105.020735.
- [195] K. Milde-Langosch *et al.*, “Role of Fra-2 in breast cancer: Influence on tumor cell invasion and motility,” *Breast Cancer Res Treat*, 2008, doi: 10.1007/s10549-007-9559-y.
- [196] B. Zhong, R. Lama, K. M. Smith, Y. Xu, and B. Su, “Design and synthesis of a biotinylated probe of COX-2 inhibitor nimesulide analog JCC76,” *Bioorg Med Chem Lett*, 2011, doi: 10.1016/j.bmcl.2011.07.025.
- [197] W. Zhang *et al.*, “Discovery of Quinazoline-Based Fluorescent Probes to α 1 Adrenergic Receptors,” 2015, doi: 10.1021/ml5004298.
- [198] G. Candiano *et al.*, “Blue silver: A very sensitive colloidal Coomassie G-250 staining for proteome analysis,” *Electrophoresis*, vol. 25, no. 9, pp. 1327–1333, 2004, doi: 10.1002/elps.200305844.
- [199] E. Wirtz, S. Leal, C. Ochatt, and G. A. M. Cross, “A tightly regulated inducible expression system for conditional gene knock-outs and dominant-negative

- genetics in *Trypanosoma brucei*,” *Mol Biochem Parasitol*, vol. 99, no. 1, 1999, doi: 10.1016/S0166-6851(99)00002-X.
- [200] H. Miao and B. Wang, “EphA receptor signaling-Complexity and emerging themes,” *Seminars in Cell and Developmental Biology*, vol. 23, no. 1. pp. 16–25, 2012. doi: 10.1016/j.semcdb.2011.10.013.
- [201] J. K. McCarron, B. W. Stringer, B. W. Day, and A. W. Boyd, “Ephrin expression and function in cancer,” *Future Oncol*, vol. 6, no. 1, pp. 165–176, 2010, doi: 10.2217/fon.09.146.
- [202] H. Miao *et al.*, “EphA2 Mediates Ligand-Dependent Inhibition and Ligand-Independent Promotion of Cell Migration and Invasion via a Reciprocal Regulatory Loop with Akt,” *Cancer Cell*, vol. 16, no. 1, pp. 9–20, 2009, doi: 10.1016/j.ccr.2009.04.009.
- [203] R. Stupp *et al.*, “Effect of Tumor-Treating Fields Plus Maintenance Temozolomide vs Maintenance Temozolomide Alone on Survival in Patients With Glioblastoma,” *JAMA*, vol. 318, no. 23, p. 2306, Dec. 2017, doi: 10.1001/jama.2017.18718.
- [204] S. Y. Lee, “Temozolomide resistance in glioblastoma multiforme,” *Genes Dis*, vol. 3, no. 3, pp. 198–210, Sep. 2016, doi: 10.1016/j.gendis.2016.04.007.
- [205] X. Li *et al.*, “Up-regulation of EphA2 and down-regulation of EphrinA1 are associated with the aggressive phenotype and poor prognosis of malignant glioma,” *Tumour Biol*, vol. 31, no. 5, pp. 477–488, 2010, doi: 10.1007/s13277-010-0060-6.

- [206] J. Wykosky, “EphA2 as a Novel Molecular Marker and Target in Glioblastoma Multiforme,” *Molecular Cancer Research*, vol. 3, no. 10, pp. 541–551, Oct. 2005, doi: 10.1158/1541-7786.MCR-05-0056.
- [207] F. Liu *et al.*, “A Genome-Wide Screen Reveals Functional Gene Clusters in the Cancer Genome and Identifies EphA2 as a Mitogen in Glioblastoma,” *Cancer Res*, vol. 66, no. 22, pp. 10815–10823, Nov. 2006, doi: 10.1158/0008-5472.CAN-06-1408.
- [208] H. Miao, E. Burnett, M. Kinch, E. Simon, and B. Wang, “Activation of EphA2 kinase suppresses integrin function and causes focal-adhesion-kinase dephosphorylation,” *Nat Cell Biol*, vol. 2, no. 2, pp. 62–69, 2000, doi: 10.1038/35000008.
- [209] K. Carles-Kinch, K. E. Kilpatrick, J. C. Stewart, and M. S. Kinch, “Antibody targeting of the EphA2 tyrosine kinase inhibits malignant cell behavior,” *Cancer Res*, vol. 62, no. 10, pp. 2840–2847, 2002, doi: 12019162.
- [210] L. W. Noblitt *et al.*, “Decreased tumorigenic potential of EphA2-overexpressing breast cancer cells following treatment with adenoviral vectors that express EphrinA1,” *Cancer Gene Ther*, vol. 11, no. 11, pp. 757–66, 2004, doi: 10.1038/sj.cgt.7700761.
- [211] M. S. Duxbury, H. Ito, M. J. Zinner, S. W. Ashley, and E. E. Whang, “Ligation of EphA2 by Ephrin A1-Fc inhibits pancreatic adenocarcinoma cellular invasiveness,” *Biochem Biophys Res Commun*, vol. 320, no. 4, pp. 1096–1102, 2004, doi: 10.1016/j.bbrc.2004.06.054.

- [212] H. Guo *et al.*, “Disruption of EphA2 receptor tyrosine kinase leads to increased susceptibility to carcinogenesis in mouse skin,” *Cancer Res*, vol. 66, no. 14, pp. 7050–7058, 2006, doi: 10.1158/0008-5472.CAN-06-0004.
- [213] D. Jackson *et al.*, “A human antibody-drug conjugate targeting EphA2 inhibits tumor growth in vivo,” *Cancer Res*, vol. 68, no. 22, pp. 9367–9374, 2008, doi: 10.1158/0008-5472.CAN-08-1933.
- [214] E. B. Pasquale, “Eph-Ephrin Bidirectional Signaling in Physiology and Disease,” *Cell*, vol. 133, no. 1, pp. 38–52, 2008. doi: 10.1016/j.cell.2008.03.011.
- [215] J. W. Astin *et al.*, “Competition amongst Eph receptors regulates contact inhibition of locomotion and invasiveness in prostate cancer cells,” *Nat Cell Biol*, vol. 12, no. 12, pp. 1194–1204, 2010, doi: 10.1038/ncb2122.
- [216] E. B. Pasquale, “Eph receptors and ephrins in cancer: bidirectional signalling and beyond,” *Nat Rev Cancer*, vol. 10, no. 3, pp. 165–80, 2010, doi: 10.1038/nrc2806.
- [217] A. Petty *et al.*, “Design and synthesis of small molecule agonists of EphA2 receptor,” *Eur J Med Chem*, vol. 143, pp. 1261–1276, Jan. 2018, doi: 10.1016/j.ejmech.2017.10.026.
- [218] A. Petty *et al.*, “A Small Molecule Agonist of EphA2 Receptor Tyrosine Kinase Inhibits Tumor Cell Migration In Vitro and Prostate Cancer Metastasis In Vivo,” *PLoS One*, vol. 7, no. 8, p. e42120, Aug. 2012, doi: 10.1371/journal.pone.0042120.
- [219] B. Zhong, Y. Li, N. Idippily, A. Petty, B. Su, and B. Wang, “A quantitative LC-MS/MS method for determination of a small molecule agonist of EphA2 in mouse

- plasma and brain tissue,” *Biomedical Chromatography*, p. e4461, Dec. 2018, doi: 10.1002/bmc.4461.
- [220] A. Barquilla, I. Lamberto, R. Noberini, S. Heynen-Genel, L. M. Brill, and E. B. Pasquale, “Protein kinase A can block EphA2 receptor-mediated cell repulsion by increasing EphA2 S897 phosphorylation,” *Mol Biol Cell*, vol. 27, no. 17, pp. 2757–2770, 2016, doi: 10.1091/mbc.E16-01-0048.
- [221] J. W. Lee *et al.*, “EphA2 immunoconjugate as molecularly targeted chemotherapy for ovarian carcinoma,” *J Natl Cancer Inst*, vol. 101, no. 17, pp. 1193–1205, 2009, doi: 10.1093/jnci/djp231.
- [222] B. Wang, “Cancer cells exploit the Eph-ephrin system to promote invasion and metastasis: tales of unwitting partners,” *Sci Signal*, vol. 4, no. 175, p. pe28, 2011, doi: 10.1126/scisignal.2002153.
- [223] H. Miao *et al.*, “EphA2 promotes infiltrative invasion of glioma stem cells in vivo through cross-talk with Akt and regulates stem cell properties,” *Oncogene*, vol. 34, no. 5, pp. 558–567, 2015, doi: 10.1038/onc.2013.590.
- [224] S. Duggineni *et al.*, “Design and synthesis of potent bivalent peptide agonists targeting the EphA2 receptor,” *ACS Med Chem Lett*, vol. 4, no. 3, pp. 344–348, 2013, doi: 10.1021/ml3004523.
- [225] K. Mertsch and J. Maas, “Blood-Brain Barrier Penetration and Drug Development from an Industrial Point of View,” *Current Medicinal Chemistry-Central Nervous System Agents*, vol. 2, no. 3, pp. 187–201, Sep. 2002, doi: 10.2174/1568015023358067.

- [226] A. Leo, C. Hansch, and D. Elkins, "Partition coefficients and their uses," *Chem Rev*, vol. 71, no. 6, pp. 525–616, Dec. 1971, doi: 10.1021/cr60274a001.